Universidad Autónoma de San Luis Potosí

Instituto de Física

Quantum Entanglement in Bose-Hubbard Models with Light-Mediated Synthetic Long-Range Interactions

TESIS PARA OBTENER EL GRADO DE

Maestro en Ciencias Física

PRESENTA

Lic. Humberto Emiliano Hernández López

Directores de Tesis

Dr. Santiago Francisco Caballero Benítez

Dr. John Alexander Franco Villafañe

San Luis Potosí, S.L.P.

Junio 2026

A mi madre, por sembrar en mí una forma de ver el mundo...

"Árbol, hoja, salto, luz..."
— Luis Alberto Spinetta

Acknowledgements

English

First, I want to express my gratitude to my advisors: Dr. Santiago Francisco Caballero Benítez, who guided me through every obstacle that at first seemed insurmountable and repeatedly reminded me how fascinating it is to work in this field of infinite possibilities; and Dr. John Alexander Franco Villafañe, whose personal mentorship provided me with valuable tools for both life and science.

I am infinitely grateful to my family, the true reason behind everything I pursue. To my mother, Dr. Rufina, my inspiration in life and my best friend. To my sister, Emillie, of whom I am proud to be the brother. To my father, Humberto, who has always shown confidence in me, supported me unconditionally, and allowed me to build my own path.

To my friends, my fellow undergraduates, and my fellow graduate students: may the pursuit of knowledge continue to move us forward.

To my brothers in all but blood, Sergio, Daniel, and Arturo.

A special thanks to Alabel, my life partner and my great love, whose support has been ever-present through conversations, sleepless nights, opinions, and advice. Without Alabel, I wouldn't be anywhere near where I am. She is my motivation.

Finally, to my beloved pets: Masha, Cosita, Galileo, and Milán.

Español

En primer lugar, quisiera expresar mi gratitud hacia mis asesores: el Dr. Santiago Francisco Caballero Benítez, quien fue capaz de orientarme ante cada obstáculo que al principio parecía insuperable y de recordarme repetidamente lo fascinante que es trabajar en este campo de infinitas posibilidades; y el Dr. John Alexander Franco Villafañe, por sus asesorías personales, en las que me enseñó herramientas valiosas para la vida y para la ciencia.

Agradezco infinitamente a mi familia, la verdadera razón detrás de todo lo que persigo. A mi madre, la Dra. Rufina, mi inspiración de vida y mi mejor amiga. A mi hermana,

Emillie, de quien me enorgullece ser hermano. A mi padre, Humberto, quien siempre ha demostrado su confianza en mí, me ha apoyado incondicionalmente y me ha permitido construir mi propio camino.

A mis amigos, compañeros de carrera y compañeros de posgrado: que la búsqueda del conocimiento siga moviéndonos.

A mis casi hermanos, Sergio, Daniel y Arturo.

Un agradecimiento especial a Alabel, mi compañera de vida y mi gran amor, cuya ayuda estuvo siempre presente en forma de pláticas, desvelos, opiniones y consejos. Sin Alabel no estaría ni cerca de donde me encuentro hoy. Ella es mi motivación.

Finalmente, a mis adorables mascotas: Masha, Cosita, Galileo y Milán.

Funding. This work was partially supported by the grants UNAM–DGAPA–PAPIIT IN118823, UNAM–DGAPA–PAPIIT IG101826, UNAM–CIC Apoyo a Laboratorios Nacionales 2025, and CONAHCYT/SECIHTI LNC–2023–51.

Abstract

This thesis studies the bipartite entanglement entropy S_A as a parameter to diagnose quantum phases and transitions in extended Bose-Hubbard models (EBHM) with light mediated synthetic interactions with long range. This interactions arise from the coupling of ultracold bosons in optical lattices to quantum modes of a high-finesse cavity. In particular we analyse the (J_D) extended model, where the global interaction acts as a density coupling, generating an even/odd sublattice structure.

We obtain the solutions for the (J_D) extended model in agreement with the established literature by implementing the slave-boson formalism around the mean-field solutions and validating the results through exact diagonalization. The entropy S_A proves to be a sensitive indicator of the transition points and of the internal structure of the phases present in the model: superfluid, Mott insulator, supersolid and density waves. The main contribution of this work is to create a unified description and application of the methodology, to compute S_A at fixed average density using a variatonal approach, and to lay the groundwork for its future applicability to related extended models.

Contents

Chapter 1

Introduction

1.1 State of the art

This section does a review of the origin, derivations and experimental realizations of the Bose-Hubbard Model (BHM) on ultracold bosons in optical lattices. The advances on methods of treatment and contemporary extensions of the model will be mentioned. We begin from the microscopic derivation, then describe the main experimental platforms, the usual theoretical methods of treatment and how to incorporate extensions with long-range interactions. Finally, we will discuss how are quantum measurements made today.

The BHM has become the paradigmatic model for studying strongly correlated bosonic matter in a lattice, in close analogy with the fermionic Hubbard model in condensed matter physics, derived in 1963 [1]. Theoretically, it provides one of the cleanest examples of quantum phase transitions arising from the interplay between hopping and interaction energy; experimentally, ultracold bosonic lattices realize with a high degree of control an almost ideal implementation of the model [2, 3, 4]. With the advent of new technologies that allow working with atomic quantum simulators at ultra-low temperatures, many proposals have been made to experimentally realize non-standard BHM's. Implementations including interactions beyond on-site and nearest neighbour interactions are often referred as extended Bose Hubbard models (EBHM's).

Before discussing the EBHM's, let us first derive the BHM.

Derivation of the BHM

The physics for the Mott insulator phase and superfluid phase on bosons in a lattice was formalized in the context of the BHM and the analysis of its phase transitions [5, 6]. For dilute gases in periodic optical potentials, the ab-initio derivation of the BH was consolidated in [2], and supported by exhaustive reviews [7, 3].

Typically, we start from the description of a weakly interacting bosonic gas inside a periodic potential, introducing Hamiltonian in second quantization for a many-mody system, describing N bosonic particles with atom-atom interaction V_{aa} and an external

potential V_{ext}.

$$\hat{H} = \int d^3\mathbf{r}\, \hat{\Psi}^\dagger(\mathbf{r}) \left[-\frac{\hbar^2}{2m}\nabla^2 + V_{\text{ext}}(\mathbf{r})\right] \hat{\Psi}(\mathbf{r}) + \frac{1}{2}\int d\mathbf{r}\, d\mathbf{r}'\, \hat{\Psi}^\dagger(\mathbf{r})\hat{\Psi}^\dagger(\mathbf{r}')V_{aa}(\mathbf{r}-\mathbf{r}')\hat{\Psi}(\mathbf{r})\hat{\Psi}(\mathbf{r}'), \tag{1.1}$$

$\hat{\Psi}$ ($\hat{\Psi}^\dagger$) being the annihilation (creation) bosonic operators satisfying the canonical commutation relations

$$\left[\hat{\Psi}(\mathbf{r}), \hat{\Psi}^\dagger(\mathbf{r}')\right] = \delta(\mathbf{r}-\mathbf{r}'), \qquad \left[\hat{\Psi}(\mathbf{r}), \hat{\Psi}(\mathbf{r}')\right] = \left[\hat{\Psi}^\dagger(\mathbf{r}), \hat{\Psi}^\dagger(\mathbf{r}')\right] = 0, \tag{1.2}$$

Interactions between atoms typically consider a short-range pseudo-potential of s-wave interactions

$$V_{aa}(\mathbf{r}-\mathbf{r}') = \frac{4\pi\hbar a_s}{m}\delta(\mathbf{r}-\mathbf{r}')\frac{\partial}{\partial|\mathbf{r}-\mathbf{r}'|}(|\mathbf{r}-\mathbf{r}'|\cdot) \tag{1.3}$$

where m is the atomic mass and a_s the scattering length (s-wave) [8].

Assuming no long-range interactions and non-singular $\hat{\Psi}$, this becomes a contact potential

$$V_{aa}(\mathbf{r}-\mathbf{r}') = \frac{4\pi\hbar a_s}{m}\delta(\mathbf{r}-\mathbf{r}') = g\delta(\mathbf{r}-\mathbf{r}') \tag{1.4}$$

On a typical 3D square lattice, the external potential has the form

$$V_{\text{ext}}(\mathbf{r}) = \sum_{\alpha=x,y,z} V_{0,\alpha}\, \sin^2\Big(k_\alpha r_\alpha\Big), \qquad k_\alpha = \frac{2\pi}{\lambda_\alpha}, \qquad E_R = \frac{\hbar^2 k^2}{2m}, \tag{1.5}$$

with E_R the recoil energy and $s_\alpha \equiv V_{0,\alpha}/E_R$ the dimensionless depth of the optical potential defining the lattice. This is proportional to the dynamic polarizability of the atoms and the intensity of the laser[3, 7].

The Bloch functions $\phi_{n,k}$ are the eigenfunctions of a Hamiltonian with an external potential with periodicity, with band number n and momentum k. In general, one can expand the operators in terms of Bloch functions

$$\hat{\Psi}(\mathbf{r}) = \sum_{n,k} b_{n,k}\phi_{n,k}, \tag{1.6}$$

For a sufficiently deep potential and low temperature, the lowest band and first excitation have a large gap, so we can apply the lowest band approximation, so that we can expand the field into Wannier functions $w(\mathbf{r}-\mathbf{R}_i)$, localized around the lattice sites.

$$\hat{\Psi}(\mathbf{r}) = \sum_i \hat{b}_i w(\mathbf{r} - \mathbf{R}_i), \tag{1.7}$$

where R_i corresponds to the minima of the lattice potential (these are the lattice sites).

Introducing this expansion into (1.1) and keeping only the tunneling between nearest neighbours, leads to

$$\hat{H}_{\text{BH}} = -\sum_{\langle i,j \rangle} t_{ij} \left(\hat{b}_i^\dagger \hat{b}_j + \text{h.c.} \right) + \frac{U}{2} \sum_i \hat{n}_i \left(\hat{n}_i - 1 \right) - \mu \sum_i \hat{n}_i, \tag{1.8}$$

with $\hat{n}_i = \hat{b}_i^\dagger \hat{b}_i$, hopping energy t_{ij} and local interaction energy U given by [2, 3, 9]

$$t_{ij} = -\int d\mathbf{r}\, w^*(\mathbf{r} - \mathbf{R}_i) \left[-\frac{\hbar^2}{2m} \nabla^2 + V_{\text{ext}}(\mathbf{r}) \right] w(\mathbf{r} - \mathbf{R}_j), \quad (i, j \text{ neighbors}), \tag{1.9}$$

$$U = g \int d\mathbf{r}\, |w(\mathbf{r})|^4. \tag{1.10}$$

On deep lattices ($s \gtrsim 5$) these analytic approximations are commonly used [9, 3]:

$$\frac{t_{i,j}}{E_R} \approx \frac{4}{\sqrt{\pi}}\, s^{3/4}\, e^{-2\sqrt{s}}, \tag{1.11}$$

$$\frac{U}{E_R} \approx \sqrt{\frac{8}{\pi}}\, k a_s\, s^{3/4}, \tag{1.12}$$

Explaining the exponential control over t with respect to the deepness s and the independent control over U through a_s (Feshbach resonances)[8]. The lowest band approximation requires low occupation by site, $U,\ t \ll \Delta_{\text{gap}}$ and $k_B T \ll \Delta_{\text{gap}}$, where Δ_{gap} is the gap of the first and second Bloch energy bands [3].

If the external potential V_{ext} also consider a trapping potential V_T, then the potential energy term appears in the Hamiltonian

$$\hat{H}_{\text{ext}} = \sum_i \epsilon_i \hat{n}_i \tag{1.13}$$

with

$$\epsilon_i = \int d\mathbf{r}\, V_T |w(\mathbf{r})|^2 = V_T(\mathbf{R}_i). \tag{1.14}$$

This is an energy offset, and can be absorbed as a site-dependant chemical potential $\mu_i = \mu + \epsilon_i$.

The competition between the hopping and local interactions result in two quantum phases for this system:

- Superfluid (SF). When the dominant term is the tunneling $t_{i,j}$ the system becomes

compressible and gapless.

- Mott Insulator (MI). If the dominant term in the local interaction U, the system becomes incompressible. This phase has a fixed average density.

At $T = 0$, the phase diagram shows a MI-SF quantum transition for dimension $d \geq 2$ and integer filling [6]. Quantum Monte Carlo simulations find the critical point at $(t_0/U)_c = 0.05974(3)$ for a 2D square lattice [10, 11], and $(t_0/U)_c \simeq 0.034(2)$ for a 3D cubic lattice [10]. The Gutzwiller mean-field treatment can qualitatively capture the Mott lobes [12, 13]. These critical points will serve as benchmarks to check the validity of our numerical methods.

The single-band condition $U, t_0 \ll \Delta_{\text{gap}}$ can be made more quantitative by approximating each lattice minimum as a harmonic oscillator. For a separable sinusoidal lattice, the local trapping frequency in direction α is $\omega_\alpha = 2\sqrt{s_\alpha}\, E_R/\hbar$, and the band gap is of order

$$\Delta_{\text{gap}} \sim \hbar\omega_\alpha = 2\sqrt{s_\alpha} E_R, \tag{1.15}$$

so that the requirement $U, t_0 \ll \Delta_{\text{gap}}$ is automatically satisfied for sufficiently deep lattices $s_\alpha \gg 1$ and moderate a_s [9, 3]. In addition, low filling factors $\langle \hat{n}_i \rangle \lesssim 1$ are typically imposed to suppress three-body losses and occupation of higher on-site vibrational modes.

The transition MI-SF for the BHM belongs, at commensurate filling, to the XY model (dimension $(d+1)$) universality class, with dynamic critical exponent $z = 1$ for the particle-hole symmetric transition [6, 14]. In $d = 2$, this implies a 3-dimensional XY critical point, in agreement with the QMC results quoted above for lattices of dimensions 2 and 3. In mean-field theory, obtained by decoupling the hopping term as

$$\hat{b}_i^\dagger \hat{b}_j \approx \hat{b}_i^\dagger \psi_j + \psi_i^* \hat{b}_j - \psi_i^* \psi_j, \qquad \psi_i = \langle \hat{b}_i \rangle, \tag{1.16}$$

one finds analytic expressions for the Mott lobe boundaries, e.g. for a homogeneous system and coordination number z,

$$\left(\frac{U}{zt_0}\right)_c = 2\rho + 1 \pm 2\sqrt{\rho(\rho+1)}, \tag{1.17}$$

for the transition between Mott lobes with ρ and $\rho + 1$ particles per site [12, 15]. Although this overestimates the stability of the Mott phase compared with QMC, it captures qualitatively the lobe structure and provides a useful first estimate for experimental parameters.

Experimental realizations

Quantum optical latices are implemented through counter-propagating lasers creating sinusoidal stationary potentials. The first experimental milestone for BHM's with ultracold atoms was the observation of the transition MI-SF using ^{87}Rb bosonic atoms in a 3D cubic lattice [16], deduced through the long-range loss of coherence in time-of-flight distributions. Detailed reviews on physics of condensates in optical lattices and their dynamics are found on [7, 3].

The independent control over t and U, as stated, is achieved by varying s and the Zeeman shift with respect to a Feschbach resonance to tune a_s [8]. Experimentally, it is common to calibrate using E_R, band spectroscopy and matter interference [7, 3]. Another important advance in that respect was quantum gas microscopy, achieving in-situ imaging with single-site resolutions and even the reconstruction of parity/occupation [17, 18].

Beyond static realizations of BH systems, thanks to light-matter coupling, it is possible now to engineer diverse interaction Hamiltonians: synthetic gauge fields, spin-orbit coupling, t tuning, effective signs and band topology by periodic conduction [19, 20].

In more detail, optical lattices are typically generated by counter-propagating laser beams with a wavelength λ_α along the desired spatial direction, producing the standing-wave potential described above. By adjusting the laser intensities I_α and polarizations, one can realize 1D, 2D or 3D lattices, superlattices with additional periodicities, or more complex geometries (e.g. honeycomb, triangular, kagome) using multiple interfering beams or spatial light modulators [4, 3]. The lattice spacing is fixed by the optical wavelength, $a_\alpha = \lambda_\alpha/2$, providing a clean and defect-free periodic structure in contrast to solid-state crystals.

A typical experimental protocol to realize the BHM begins from a weakly trapped Bose-Einstein condensate. Then the lattice depth s is ramped up adiabatically on a timescale slow compared with the inverse band gap, so that atoms stay within the lowest band, but fast compared with typical heating mechanisms [3]. For small s the atoms form a superfluid with long-range phase coherence, which manifests as pronounced peaks in absortion images of time of flight (TOF) experiments. As s is increased and t_0/U decreases, these peaks gradually vanish, signalling the loss of global coherence for the phase and the onset of a Mott insulating state with localized atoms and an gap for particle-hole excitation energies [16]. The dependence of the interference pattern visibility with s has been used as a quantitative probe of the MI-SF transition and compared successfully with QMC and Gutzwiller calculations including the effects of harmonic confinement [3, 21].

Feshbach resonances provide an additional powerful knob: by adjusting the external magnetic field, almost at resonance, one can vary the length a_s over orders of magnitude, including changes of its sign [8]. This allows experiments not only to reach the strongly interacting regime (large U) at fixed lattice depth, but also to perform interaction quenches, revealing coherent matter-field collapse and revival dynamics in deep lattices [22]. Such experiments are sensitive to higher-order interaction terms and have been used to benchmark the microscopic derivation of U, the local interaction energy.

The advent of quantum gas microscopes represented a qualitative leap in the experimental study of BHM physics. Using high-numerical-aperture objectives and fluorescence imaging in deep lattices, it is possible to detect the occupation of each lattice site with single-atom resolution [17, 18, 23]. This has enabled in situ measurements of local density profiles, direct observation of Mott shells in trapped systems, reconstruction of parity and occupation statistics, and measurements of spatial correlations across the MI-SF transition [17, 24]. Furthermore, single-site addressing with focused light beams or digital micromirror devices has allowed the engineering of programmable potential landscapes and the implementation of local quenches and defect dynamics, directly probing the microscopic processes described by the BH Hamiltonian.

Methods of treatment

Some typical quantitative methods to treat the BH model are: Gutzwiller mean-field, strong coupling expansions, Density Matrix Renormalization Group (DMRG), Quantum Monte Carlo (QMC). These frameworks have been validated directly against experiments [3].

From a many-body perspective, the BH Hamiltonian is non integrable in dimensions $d \geq 2$, and only a few limiting cases admit exact solutions. A variety of numerical methods have therefore been developed to compute its properties, both stationary and dynamic, each with its own regime of validity. In the following we concisely review the main approaches that are relevant for this work.

Gutzwiller mean-field theory. The simplest non trivial variational description for the BHM is captured by the Gutzwiller product state

$$|\Psi_{\mathrm{GW}}\rangle = \prod_i \left(\sum_{n=0}^{n_{\max}} f_n^{(i)} \, |n\rangle_i \right), \tag{1.18}$$

where $|n\rangle_i$ denotes a Fock state containing exactly n bosons for the site i and with coefficients $f_n^{(i)}$ satisfy $\sum_n |f_n^{(i)}|^2 = 1$ [12, 2]. Inserting this ansatz into $\langle \Psi_{\mathrm{GW}} | \hat{H}_{\mathrm{BH}} | \Psi_{\mathrm{GW}} \rangle$

and minimizing with respect to $f_n^{(i)}$ result in a set of nonlinear coupled equations that are equivalent to the self-consistent mean-field decoupling of the hopping part, as the discussion above shows. The local superfluid parameter is then

$$\psi_i = \langle \hat{b}_i \rangle = \sum_{n=0}^{n_{\max}-1} \sqrt{n+1}\, f_n^{(i)*} f_{n+1}^{(i)}. \tag{1.19}$$

In homogeneous systems, $f_n^{(i)} \equiv f_n$ and $\psi_i \equiv \psi$ are site independent, reducing the problem to a single-site non linear eigenvalue equation. The Gutzwiller recovers the exact results when taking the limit of infinite coordination number $z \to \infty$ and provides a qualitatively accurate description of the MI-SF transition and dynamics in high dimensions [15, 25]. Time-dependent Gutzwiller theory, obtained by applying a time-dependent variational principle to $|\Psi_{\mathrm{GW}}(t)\rangle$, allows one to study quench dynamics, collective modes and response to periodic driving [19, 25].

Strong-coupling expansions. In the deep MI limit $t_0/U \ll 1$, perturbative expansions around the atomic limit provide systematic corrections to energies and correlation functions. Using Rayleigh-Schrödinger perturbation theory or linked-cluster expansions, one can compute the ground-state energy, excitation gaps and critical values of $(t_0/U)_c$ as series in t_0/U [26, 27]. Alternatively, starting from the path-integral representation, one may eliminate high-energy degrees of freedom and derive effective actions for the low-energy particle and hole excitations, obtaining a field-theoretical description of the critical behaviour [14, 25]. These methods are particularly useful for benchmarking numerical approaches and for understanding universal scaling near the transition.

Quantum Monte Carlo. For bosonic BHM's without frustration or sign problems, QMC methods yield numerically exact results for thermodynamic quantities, correlation functions and critical properties in equilibrium. Worldline algorithms in discrete imaginary time, stochastic series expansion (SSE) in continuous time, and worm algorithms are among the most widely used techniques [28, 29, 10]. Finite-size scaling of QMC data near the MI-SF transition allows accurate determination of critical points and exponents, as in the results quoted earlier for 2D and 3D lattices [10]. QMC has been used also to study disordered BHM's, systems with harmonic confinement, and extended BH models with nearest-neighbour interactions, as long as the resulting Hamiltonian remains stochastic [30, 31].

Density Matrix Renormalization Group and other tensor approaches. In 1D, the BH model and its extensions can be treated very efficiently using DMRG and more

generally matrix product states (MPS) [32, 33]. These methods exploit the entanglement structure of low-energy eigenstates, which obey an area law in gapped phases and only weakly violate it at criticality, to represent the many-body wavefunction in a compressed form. DMRG provides essentially exact results for ground states and low-lying excitations, as well as access to entanglement entropies and spectra. Time-dependent variants (tDMRG, TEBD) allow one to simulate real-time dynamics following quenches or ramps of the parameters t_0, U or external potentials, up to times limited by entanglement growth [34]. For higher dimensions, related tensor network proposal like projected entangled pair states (PEPS) extend these ideas, though at significantly higher computational cost [35, 36].

Other approaches. Additional methods include cluster mean-field theories, which partially restore correlations by treating small clusters exactly and coupling them in mean field [37, 38]; dynamical mean-field theory (DMFT), and its versions adapted for bosons, for capturing local quantum fluctuations in high dimensions [39, 40]; and field-theoretic renormalization-group approaches near criticality [14]. In driven or dissipative BH models, Keldysh functional integral techniques have been developed to describe non-equilibrium steady states and quantum criticality beyond detailed balance [41]. Together, these methods form a toolbox that will be used and explained in the following chapters to analyse models with cavity-mediated interactions.

1.2 Extended Bose-Hubbard Models (EBHM's)

The standard BHM was derived under this considerations: lowest Bloch band approximation, tight-binding approximation resulting in localized Wannier functions, and hopping restricted to nearest neighbour.

However, relaxing this approximations or including external interactions give rise to the commonly known as Extended Bose-Hubbard Models (EBHM's) [42, 43]. These new extravagant models can include long-range interactions, density-dependent tunneling and effective couplings induced by higher bands or mediated by external components like optical cavities.

Microscopic derivation for the extended terms

We start again from the continuous second quantization Hamiltonian

$$\hat{H} = \int d^3\mathbf{r}\, \hat{\Psi}^\dagger(\mathbf{r}) \left[-\frac{\hbar^2}{2m}\nabla^2 + V_{\text{ext}}(\mathbf{r}) \right] \hat{\Psi}(\mathbf{r}) + \frac{1}{2} \int d^3\mathbf{r} d^3\mathbf{r}'\, \hat{\Psi}^\dagger(\mathbf{r}) \hat{\Psi}^\dagger(\mathbf{r}') V_{aa}(\mathbf{r}-\mathbf{r}') \hat{\Psi}(\mathbf{r}') \hat{\Psi}(\mathbf{r}). \tag{1.20}$$

Expanding the field operator in the lowest band Wannier basis

$$\hat{\Psi}(\mathbf{r}) = \sum_i w(\mathbf{r} - \mathbf{R}_i)\hat{b}_i, \tag{1.21}$$

and substituting in the interaction term, we obtain in general

$$\hat{H}_{\text{int}} = \frac{1}{2}\sum_{ijkl} U_{ijkl}\, \hat{b}_i^\dagger \hat{b}_j^\dagger \hat{b}_k \hat{b}_l, \tag{1.22}$$

where

$$U_{ijkl} = \int d^3\mathbf{r} d^3\mathbf{r}' w_i^*(\mathbf{r}) w_j^*(\mathbf{r}') V_{aa}(\mathbf{r} - \mathbf{r}') w_k(\mathbf{r}') w_l(\mathbf{r}). \tag{1.23}$$

For the standard BHM we only keep the term U_{iiii}, which results in the local interaction U. However, in general there are additional contributions:

- density-density interactions between different sites: U_{ijji}.
- density-induced tunneling: U_{iiij}.
- pairwise tunneling processes: U_{iijj}.

Long-range Interactions

On systems with dipolar magnetic or electric interactions, the microscopic potential has the form

$$V_{\text{dipolar}}(\mathbf{r}) = \frac{C_{dd}(1 - 3\cos^2\theta)}{4\pi r^3}, \tag{1.24}$$

Which generates density-density long-range couplings $V_{|i-j|}$. They tend to decay algebraically [42]. In this regime, new phases appear, for example, charge density waves (CDW), supersolids (SS) and topological Haldane phases in 1D.

The extended model with next-nearest-neighbour interaction already presents a rich phase structure, including topological symmetry-protected insulators.

Interaction-induced tunneling

An important advance in the last decade was the experimental identification for the density-induced tunneling [43].

Physically, this term emerges due to the local modification of the Wannier functions by the contact interaction. The repulsion widens the local state, and increases the overlap between neighbours. This produces a correction to the hopping parameter

with amplitude t_1:

$$t_{\text{eff}} = t_0 + t_1\langle\hat{n}\rangle. \tag{1.25}$$

This mechanism displaces the critical point of the transition MI-SF and induces new phases with bond order (coupling between neighbour sites).

Higher bands effects

For a sufficiently strong interaction, the lowest band approximation is no longer valid even for deep lattices. The virtual occupation for higher bands leads to effective models with density-dependent renormalized parameters [42].

In this regime, the effective Hamiltonian is modified as

$$U \to U(n), \qquad t \to t(n), \tag{1.26}$$

which introduces additional non-linearities on the collective dynamic.

Cavity-mediated interactions

One of the most notable extensions of the BHM in the last decade has arisen by coupling the ultracold bosonic lattices to quantized modes of a high finesse cavity. In this regime, the electromagnetic field no longer acts as a classical external potential, but as a dynamic quantum degree of freedom that entangles with the collective state of the matter [44, 45, 46].

Microscopic light-matter model Let us consider bosonic atoms trapped in a classical optical potential and illuminated by one or more pump laser beams scattering the light to one or more cavity modes. In the dispersive regime ($|\Delta_a| \gg g, \Gamma$), where Δ_a is the detuning between the light and the atoms, we can perform adiabatic elimination to the excited atomic level. Then the effective Hamiltonian reads

$$\hat{H} = \hat{H}_{\text{BH}} + \sum_c \omega_c \hat{a}_c^\dagger \hat{a}_c + \sum_{c,p} \left(\frac{g_{cp}}{\sqrt{N_s}} \hat{a}_c^\dagger \hat{F}_{cp} + \text{h.c.} \right), \tag{1.27}$$

where $\hat{H}_{\text{BH}}$ is the standard BH Hamiltonian and the collective operator

$$\hat{F}_{cp} = \sum_i J_{ii}^{cp} \hat{n}_i + \sum_{\langle i,j \rangle} J_{ij}^{cp} \left(\hat{b}_i^\dagger \hat{b}_j + \text{h.c.} \right) \tag{1.28}$$

moderates the spatially structured coupling experimented by the bosons and the

scattered light.

The term proportional to J_{ii} corresponds to the density coupling, while J_{ij} describes a coupling to coherences between neighbouring sites (bond coupling), meaning, it couples with the phase of the matter [45]. This distinction is crucial, as it allows for the design of synthetic interactions not only on density, but also on superfluid order.

Adiabatic elimination of the photonic field For a well behaved cavity ($|\Delta_{pc}| \gg \kappa$ while $|\Delta_{pc}| \gg |U|$ and $|\Delta_{pc}| \gg |t_0|$), one can perform adiabatic elimination to the inter-cavity field. The result is a purely atomic Hamiltonian [44]

$$\hat{H}_{\text{eff}} = \hat{H}_{\text{BH}} + \sum_{c,p,q} \frac{g_{pc} g_{qc}^*}{N(\Delta_{pc} + i\kappa_c)} \frac{1}{2} \left(\hat{F}_{pc}^\dagger \hat{F}_{qc} + h.c. \right). \tag{1.29}$$

This term is the origin for the synthetic light-mediated interaction. An atom scatters one photon to the cavity mode, and it gets reabsorbed collectively by the whole system, generating a global interaction.

For the simplest case (one cavity mode, one pump beam and only density coupling), the additional term reduces to

$$\hat{H}_{\text{cav}} = \frac{g_{\text{eff}}}{N_s} \left(\sum_i J_i \hat{n}_i \right)^2, \tag{1.30}$$

where $g_{\text{eff}} \propto \Delta_{pc}/(\Delta_{pc}^2 + \kappa^2)$ is the effective coupling, tunable through the frequency of the pump and parameters of the cavity.

The quadratic term implies that the energy depends on the collective density pattern projected onto the spatial profile of the light. The interaction, formally, is of infinite range, but its spatial structure is determined by the coefficients J_i, that can alter sign or repeat periodically depending on the optical geometry.

For example, if the scattering occurs in a diffraction minima (when the cavity axis and the pump beam are at $90°$), one obtains

$$\hat{H}_{\text{cav}} = \frac{g_{\text{eff}}}{N_s} \left(\sum_i (-1)^i \hat{n}_i \right)^2, \tag{1.31}$$

which favours a density wave (DW) ordering and allows the emergence of supersolid phases, already observed experimentally [47].

One notable result shown in [45] is that, although the light-matter interaction is global, it can be structured in sublattices (atomic modes) through the geometry of the optical arrangement. Grouping sites that scatter with the same phase, the Hamiltonian reads

$$\hat{H}_{\text{cav}} = \sum_{\varphi,\varphi'} \tilde{\gamma}_{\varphi,\varphi'} \hat{N}_{\varphi} \hat{N}_{\varphi'} + \tilde{\gamma}'_{\varphi,\varphi'} \hat{S}_{\varphi} \hat{S}_{\varphi'}, \tag{1.32}$$

where $\hat{N}_{\varphi}$ are the collective density operators by mode, and $\hat{S}_{\varphi}$ bond operators and $\tilde{\gamma}'_{\varphi,\varphi'} = \left[g_{\text{eff}} J_D^* J_B + c.c\right] / (2\sqrt{N_s})$.

This allows to simulate effective interactions of finite range using a few optical modes, combining properties from short-range and global interactions.

The balance between the local hopping t_0, the interaction U and the global term g_{eff} generates an enriched phase landscape, including supersolids, bond order, dimerized and trimerized states and phases where global order and local quantum fluctuations coexist.

The collective nature for the coupling implies a global order parameter, modifying the critical nature of the transition and allowing for the study of the BHM beyond the purely local paradigm.

The conceptual development for this system began with the study of quantum scattering and QND measurements on quantum gases [44], then moved to the understanding of quantum optical lattices and collective back-action, and concluding with the formulation of synthetic global Hamiltonians capable of simulating any desired structured interactions [45].

1.3 Quantum measurements: the role of entanglement

Among the most attractive features of quantum simulators is their ability to reproduce, with high fidelity and control, the physics of many-body Hamiltonians typically hard to manage by classical methods in strongly correlated regimes. For ultracold bosons in optical lattices the paradigmatic systems to do so are Bose-Hubbard-like models. The experimental state of the art allows for the adjustment almost in-situ of the parameters for lattice depth, interactions via Feshbach resonances, the geometry and the dimensionality, and then measuring observables with spatial or momentum resolution, or even quantum gas microscopy.

However, the complete complex quantum behaviour of a many-body state is not always captured entirely by local observables or two-point correlations. In this context, quantum entanglement has consolidated as the natural language to characterize this systems, quantifying purely quantum correlations between partitions of the systems, serving both as a measure and as a probe. In particular, the entanglement entropy (EE) allows to diagnose the quantum phase transitions, distinguish phases with non-trivial orders and stablish limits for numerical simulations based on the validation of the

area laws.

A state composed by two subsystems A and B is called entangled if it cannot be expressed as a product $|\Psi\rangle_{AB} \neq |\psi\rangle_A \otimes |\phi\rangle_B$. This non-separability means there is no way to completely describe each part independently.

For many-body systems, the entanglement acquires also a geometrical interpretation: if we cut a system in a subsystem A and its complement subsystem B, the entanglement measures how much information crosses the frontier $A|B$. For local Hamiltonians this typically leads to an area law, where the entanglement increases along with the frontier (area law) not with the volume of the system. Nonetheless, for highly excited or out-of-equilibrium dynamical systems, a volumetric scaling law may emerge.

From the quantum simulation point of view, this ideas explain why it is relevant to advance in mechanisms to measure and calculate the entanglement. Not only it identifies the quantum phases and their transitions, it also characterizes how the quantum correlations are distributed through the whole system, which is specially essential when we have non-local interactions.

A convenient way to measure quantitatively how much entangled is a system is via the entanglement entropy (EE). For bipartite systems it takes the form of the Von Neumann bipartite entropy. If the global state is pure, then all the mixture found by observing A comes exclusively from the entanglement with B, not from temperature or classical ignorance.

For example, in the standard BHM, the behaviour of the EE while crossing the MI-SF transition gives complementary information on top of the compressibility. In fact, studies such as [48] show that it presents a singularity at the transition point, associated with the nature of the bosonic criticality and the structure of the entanglement spectrum.

Definition of the von Neumann bipartite entropy

Consider a system in a global state described by the density matrix ρ_{AB} in the Hilbert space subdivided into regios A and B: $\mathcal{H} = \mathcal{H}_A \otimes \mathcal{H}_B$.

Observing A, the reduced density matrix encodes the accessible information

$$\rho_A = \mathrm{Tr}_B(\rho_{AB}). \tag{1.33}$$

The von Neumann entropy associated with A is defined as

$$S_A \equiv S(\rho_A) = -\mathrm{Tr}(\rho_A \log \rho_A)\,, \tag{1.34}$$

here the units are fixed by the base of the logarithm. In that sense $\log_2$ gives a bits description.

For a total pure state, $\rho_{AB} = |\Psi\rangle\langle\Psi|$, it follows $S(\rho_{AB}) = 0$, but in general it satisfies

$$S(\rho_A) = S(\rho_B). \tag{1.35}$$

The EE S_A measures how much information on the global state is lost by constraining to observables of A. On many-body systems, the comparison between the scaling with the subsystem size and the geometry of the cut contains universal information and, therefore, it serves as a diagnosis for quantum phases and transitions.

The definition of the bipartite EE requires a choice of bipartition of the Hilbert space. This is not unique, it depends on the physical problem being addressed, the subdivision could be, for instance, by separating sets of modes, internal degrees of freedom or, convenient for this work, by spatial regions (lattice sites). A typical choice would be

$$A = \{\text{first half}\}, \qquad B = \{\text{second half}\}, \tag{1.36}$$

as shown in Fig. 1.1a. In extended models with synthetic long-range interactions, the relevant degree of freedom may not be strictly local. The light couples collective modes with a spatial shape depending on the optical geometry. For example, as mentioned in Section 1.2, for the diffraction minima regime, it can emerge an odd/even sublattice structure. This motivates a direct and privileged bipartition

$$A = \{\text{even sublattice}\}, \qquad B = \{\text{odd sublattice}\}, \tag{1.37}$$

as shown in Fig. 1.1b.

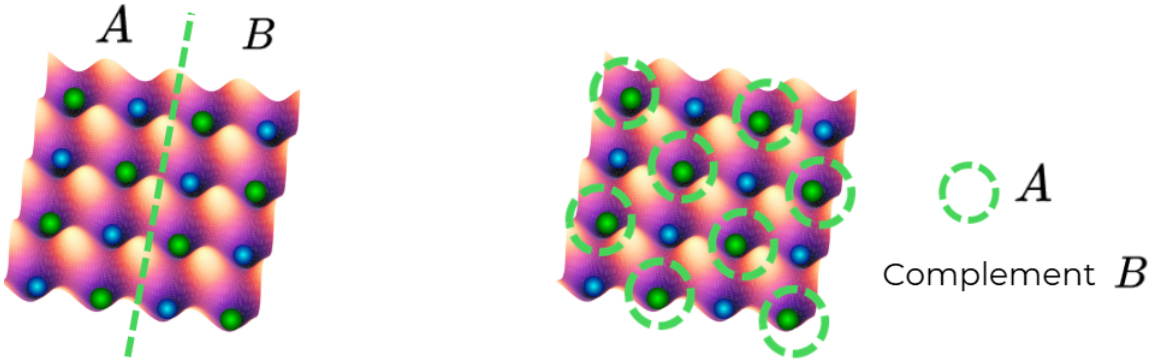

(a) Half-half spatial bipartition.

(b) Even-odd spatial bipartition.

Figure 1.1. Schematic of different bipartitions.

Chapter 2

The models

On this chapter we will present, and explicitly construct, the effective models that constitute the nucleus for this work: extensions to the Bose-Hubbard model where synthetic global interactions emerge from the coupling of a system of ultracold bosons in a lattice with one or many modes of an optical cavity. The central motivation is two-sided. On one hand, these non-standard systems allow to implement non-local interactions with a highly configurable spatial structure determined by the optical geometry. On the other hand, the collective behaviour of the light-matter coupling introduces new kinds of correlations (density and coherence), enriching the classical phase diagram and emerging sublattice odd/even structures, extremely relevant for the study of quantum entanglement [45].

We start from the standard BHM, contributing with the already known local processes of neighbouring sites hopping and on-site repulsion. Then we add the contributions of the quantized optical field and the light-matter interactions due to the addition of the optical cavity. We will derive, step by step, the effective Hamiltonians.

The structure will be the following. In Section 2.1 the full microscopic model is presented from the BHM with the addition of the cavity interactions to the Hamiltonian. Then in Section 2.2 we will define a specific geometry to obtain an effective coupling to the atomic density, and then derive explicitly the effective Hamiltonian for that regime, explaining the interplay between the local processes and the synthetic collective interaction, and how it is expected to modify the landscape for the phase diagram. In Section 2.3 we'll do an analogue description but for the geometry that selects the inter-site coherences, coupling on the bonds. Finally, on Section 2.4 we provide a natural extension with a geometry consisting on multiple pump beams at different angles, and how that modifies the effective model and the phase diagram.

2.1 Extended Bose-Hubbard: light-matter Hamiltonian

Here we'll stablish the general model used for this work, describing bosons in a lattice coupled with one cavity mode. The objective is to present a step-by-step derivation of a purely atomic effective Hamiltonian incorporating the effects of the cavity interaction. The result is a family of extended Bose-Hubbard models, with a structure given by

the geometry of the light-field.

The derivarion begins with the already discussed BHM

$$\hat{H}_b = -t_0 \sum_{\langle i,j \rangle} \left(\hat{b}_i^\dagger \hat{b}_j + \text{h.c.} \right) - \mu \sum_i \hat{n}_i + \frac{U}{2} \sum_i \hat{n}_i (\hat{n}_i - 1), \tag{2.1}$$

where $\hat{b}_i$ ($\hat{b}_i^\dagger$) are the annihilation (creation) operators at site i. $\hat{n}_i = \hat{b}_i^\dagger \hat{b}_i$, t_0 is the hopping amplitude, U the local repulsion and μ the chemical potential. We've established that the models parameters are obtained by the Wannier integrals using the correspondent optical lattice potential:

$$t_0 = -\int d^3\mathbf{r}\; w(\mathbf{r} - \mathbf{R}_i) \left[-\frac{\hbar^2 \nabla^2}{2m} + V_{\text{OL}}(\mathbf{r}) \right] w(\mathbf{r} - \mathbf{R}_j), \tag{2.2}$$

Considering one or many cavity light modes labelled by c, with operators $\hat{a}_c$ and frequencies ω_c, we have the light field Hamiltonian

$$\hat{H}_a = \sum_c \hbar \omega_c \, \hat{a}_c^\dagger \hat{a}_c. \tag{2.3}$$

In practice, one illuminates the system with one or many classical pump beams labelled by p, with frequencies ω_p and complex amplitude Ω_p (in Rabi units). For convenience, we work in the rotating frame of the pump frequency, where the detuning appear naturally:

$$\Delta_a = \omega_p - \omega_a, \qquad \Delta_{pc} = \omega_p - \omega_c, \tag{2.4}$$

knowing ω_a is the atomic resonance frequency.

Now, let's suppose off-resonant scattering, where $|\Delta_a| \gg \kappa$, κ being the spontaneous emission rate, and $|\Delta_{pc}| \gg |U|$ and $|\Delta_{pc}| \gg |t_0|$, In this regime we can perform adiabatic elimination the excited atomic state, and the the interaction between light and matter is given by an effective dispersive coupling [44].

The cavity selects and enhances the pump light that the atoms scatter to the cavity modes. For the lowest band approximation (with localized Wannier states) the interaction can be written as [45]

$$\hat{H}_{ab} = \sum_{c,p} \frac{1}{\sqrt{N_s}} \left(g_{pc}^* \, \hat{a}_c \, \hat{F}_{pc}^\dagger + g_{pc} \, \hat{a}_c^\dagger \, \hat{F}_{pc} \right), \tag{2.5}$$

where the effective coupling

$$g_{pc} = \frac{g_c \, \Omega_p}{2\Delta_a} \tag{2.6}$$

depends on the atom-cavity coupling g_c, the pump amplitude Ω_p and the atomic

detuning Δ_a.

The collective operator $\hat{F}_{pc}$ is composed of two different contributions

$$\hat{F}_{pc} = \hat{D}_{pc} + \hat{B}_{pc}, \tag{2.7}$$

where the density coupling occurs due to

$$\hat{D}_{pc} = \sum_j J_{jj}^{pc}\, \hat{n}_j, \tag{2.8}$$

and the bond coupling occurs due to

$$\hat{B}_{pc} = \sum_{\langle i,j \rangle} J_{ij}^{pc} \left(\hat{b}_i^\dagger \hat{b}_j + \text{h.c.} \right). \tag{2.9}$$

Here the coefficients J_{ij}^{pc} are overlap integrals over the Wannier functions and the optical mode functions,

$$J_{ij}^{pc} = \int d^3\mathbf{r}\; w(\mathbf{r} - \mathbf{R}_i)\, u_c^*(\mathbf{r})\, u_p(\mathbf{r})\, w(\mathbf{r} - \mathbf{R}_j), \tag{2.10}$$

with $u_c(\mathbf{r})$ and $u_p(\mathbf{r})$ are respectively the cavity mode and pump functions. This expression explicitly contains the optical geometry determining how the light couples (to density or coherence).

The equations (2.8)-(2.9) show that the light can couple to the diagonal ($\hat{n}_j$) or off-diagonal part ($\hat{b}_i^\dagger \hat{b}_j + \text{h.c.}$). This will become important in the following sections, as it determines the cases J_D and J_B respectively.

Inside the cavity, there is a loss of photons with rate κ_c, leaking through the mirrors. A complete description includes that dissipative term in the Heisenberg–Langevin equations for $\hat{a}_c$

$$\dot{\hat{a}}_c = -i[\hat{a}_c, \hat{H}_a + \hat{H}_{ab}] - \kappa_c \hat{a}_c \; (+ \text{noise}), \tag{2.11}$$

where, for this purpose, we omit the noise operator because we only care for the effective mean dynamic. In the 'good' cavity regime it is used as an approximation for work

$$|\Delta_{pc}| \gg \kappa_c, \qquad |\Delta_{pc}| \gg t_0,\, U, \tag{2.12}$$

The first condition assures the cavity field is quasi-coherent (high finesse); the second guarantees the optical field gets relaxed to the stationary state way faster than the atomic dynamic. Under this conditions, the cavity field follows adiabatically the state of the matter, hence it can be adiabatically eliminated [44, 45]. Formally, this corresponds to imposing $\dot{\hat{a}}_c \approx 0$, giving the time-independent solution to the field, as

a function of $\hat{F}$

$$\hat{a}_c \simeq \frac{1}{\sqrt{N_s}} \frac{\sum_p g_{pc} \hat{F}_{pc}}{\Delta_{pc} + i\kappa_c}. \tag{2.13}$$

this is the cavity backaction mechanism. The field inside the optical cavity is determined by the collective quantum state through $\hat{F}_{pc}$, and it acts on the atoms through $\hat{H}_{ab}$. In consequence, the resulting interaction is non-local, because the sites are coupled due to the cavity.

Substituting (2.13) into the full Hamiltonian $\hat{H} = \hat{H}_b + \hat{H}_a + \hat{H}_{ab}$, and performing the adiabatic elimination, leads to a purely atomic Hamiltonian [44, 45]:

$$\hat{H}_{\text{eff}} = \hat{H}_b + \frac{1}{N_s} \sum_c \sum_{p,q} \left[\frac{g_{\text{eff}}^{qc}}{2} \hat{F}_{pc}^\dagger \hat{F}_{qc} + \frac{\left(g_{\text{eff}}^{qc}\right)^*}{2} \hat{F}_{pc} \hat{F}_{qc}^\dagger \right], \tag{2.14}$$

with an effective coupling

$$g_{\text{eff}}^{qc} = \frac{g_c^* g_q}{\Delta_{qc} + i\kappa_c}. \tag{2.15}$$

The real part of g_{eff}^{qc} controls the coherent coupling, while the imaginary part contains the dissipative effects, in other words, the leaking of photons. For now on, we will use (2.14) as a starting point for the following models.

This general EBHM represent an effective long-range interaction induced by the light. This interaction is, in principle, of infinite range (global), as the cavity field couples to all the simultaneously illuminated sites. However, as will be discussed later, the spatial structure of the coupling can be designed through the coefficients J_{ij}^{pc}, allowing effective short-range or medium-range interactions with a designable profile [45].

The general expression (2.14) can be reorganized in terms of the operators for collective modes. Given that the coefficients J_{ij}^{pc} can have a spatial periodicity according to the optical geometry, it is convenient to define atomic modes φ as sets of sites coupling light with the same J_{ij}^{pc}. On this terms, the collective operator (2.7) can be rewritten as

$$\hat{F}_{pc} = \sum_{\varphi} J_{D,\varphi}^{pc} \hat{N}_\varphi + \sum_{\varphi'} J_{B,\varphi'}^{pc} \hat{S}_{\varphi'}, \tag{2.16}$$

where the density and bond modes are, respectively

$$\hat{N}_\varphi = \sum_{i \in \varphi} \hat{n}_i, \qquad \hat{S}_{\varphi'} = \sum_{\langle i,j \rangle \in \varphi'} \left(\hat{b}_i^\dagger \hat{b}_j + \hat{b}_j^\dagger \hat{b}_i \right). \tag{2.17}$$

Here $J_{D,\varphi}^{pc}$ and $J_{B,\varphi'}^{pc}$ are the common values resulting from the overlap integrals

for all sites of the specific mode φ. Substituting (2.16) on (2.14), the new terms of the Hamiltonian take the form

$$\hat{H}_{\text{eff}} - \hat{H}_b = \sum_{\varphi,\varphi'} \sum_{c,p,q} \left[\tilde{\gamma}^{D,D}_{\varphi,\varphi'} \hat{N}_\varphi \hat{N}_{\varphi'} + \tilde{\gamma}^{B,B}_{\varphi,\varphi'} \hat{S}_\varphi \hat{S}_{\varphi'} + \tilde{\gamma}^{D,B}_{\varphi,\varphi'} \left(\hat{N}_\varphi \hat{S}_{\varphi'} + \hat{N}_{\varphi'} \hat{S}_\varphi \right) \right], \tag{2.18}$$

with coefficients $\tilde{\gamma}_{\varphi,\varphi'} = [g^{qc}_{\text{eff}} (J^{pc}_{\mu,\varphi})^* J^{qc}_{\nu,\varphi'} + \text{c.c.}]/2$, with superscripts D or B [45].

Here the term $\hat{N}_\varphi \hat{N}_{\varphi'}$ is analogous to a density-density interaction between spatial modes; the term $\hat{S}_\varphi \hat{S}_{\varphi'}$ is analogous to a coherent interchange interaction; and the crossed term $\hat{N}_\varphi \hat{S}_{\varphi'}$ couples both density and coherence. The competence between these are modulated by the coefficients $\tilde{\gamma}^{\mu,\nu}_{\varphi,\varphi'}$, determining the possible rich phase diagram.

Depending on which term is dominant, controlled by the optical geometry through J^{pc}_{ij}, quantitatively different effective models can be obtained. In particular:

- If the light couples predominantly with density ($J^{pc}_{jj} \gg J^{pc}_{ij}$, for $i \neq j$), the relevant interaction is density-density. This leads to the effective density coupling model of Section 2.2.
- If the light predominantly couples with the bonds ($J^{pc}_{ij} \gg J^{pc}_{jj}$, for $i \neq j$), the relevant interaction is between coherences. This leads to the effective bond coupling model of Section 2.3.
- In the general case, both couplings coexist, and the model also includes the crossed density-bond interaction term.

The following sections will explicitly derive the particular cases for each proposed geometry.

2.2 Density coupling (J_D)

Here we will derive the EBHM Hamiltonian resulting when the optical geometry is such that the light couples predominantly with the atomic density. This is the most widely studied case in the literature of optical cavities with ultracold bosons [47, 49, 45, 46].

Remembering the light-matter coupling is codified in the overlaps J^{pc}_{ij}

$$J^{pc}_{ij} = \int d^3\mathbf{r}\, w(\mathbf{r} - \mathbf{R}_i)\, u^*_c(\mathbf{r})\, u_p(\mathbf{r})\, w(\mathbf{r} - \mathbf{R}_j). \tag{2.19}$$

For a deep lattice, these w functions are strongly localized on each site (around $\mathbf{R}_i$).

For this case, the on-site overlap ($i = j$) dominates over the inter-site overlaps ($i \neq j$)

$$|J_{ii}^{pc}| \gg |J_{ij}^{pc}| \quad (i \neq j), \tag{2.20}$$

Physically, this occurs when the peaks of the pump field $u_p(\mathbf{r})$ coincide with the positions of the atoms (the sites), so that the light mainly sees the atomic density on each site, and not the coherence. For this regime, the site coefficients can be expressed as

$$J_{jj}^{pc} \simeq u_c^*(\mathbf{R}_j)\, u_p(\mathbf{R}_j) \equiv J_j, \tag{2.21}$$

where J_j can be constant for homogeneous coupling or have a periodic modulation. This spatial structure determines which collective combination of densities contributes to the effective Hamiltonian.

Then, starting from the general result of the previous section

$$\hat{H}_{\text{eff}} = \hat{H}_b + \frac{1}{N_s} \sum_c \sum_{p,q} \left[\frac{g_{\text{eff}}^{qc}}{2}\, \hat{F}_{pc}^\dagger \hat{F}_{qc} + \frac{\left(g_{\text{eff}}^{qc}\right)^*}{2}\, \hat{F}_{pc} \hat{F}_{qc}^\dagger \right]. \tag{2.22}$$

considering only one c and one p modes

$$\hat{H}_{\text{eff}} \simeq \hat{H}_b + \frac{g_{\text{eff}}}{2N_s} \left(\hat{F}^\dagger \hat{F} + \hat{F} \hat{F}^\dagger \right), \qquad \hat{F} \approx \hat{D} = \sum_j J_j\, \hat{n}_j, \tag{2.23}$$

with an effective real coupling amplitude, i.e. assuming no leaking,

$$g_{\text{eff}} = \frac{|g|^2\, \Delta_{pc}}{\Delta_{pc}^2 + \kappa^2}. \tag{2.24}$$

The sign of g_{eff} is controllable experimentally through the cavity-pump detuning Δ_{pc}. For $\Delta_{pc} > 0$ we have $g_{\text{eff}} > 0$; for $\Delta_{pc} < 0$ we have $g_{\text{eff}} < 0$. This has important physical consequences, as we will discuss on Chapter 3.

Given an adequate phase selection for the pump, J_j can be taken as real , and $\hat{D}$ is hermitic, then it simplifies to

$$\frac{1}{2} \left(\hat{D}^\dagger \hat{D} + \hat{D} \hat{D}^\dagger \right) = \hat{D}^2, \tag{2.25}$$

Therefore the term induced by the cavity is reduced to

$$\hat{H}_{\text{cav}}^{(D)} = \frac{g_{\text{eff}}}{N_s}\, \hat{D}^2 = \frac{g_{\text{eff}}}{N_s} \left(\sum_j J_j \hat{n}_j \right)^2. \tag{2.26}$$

Expanding (2.26) one obtains a long-range interaction, structured by the geometric coefficients J_j

$$\hat{H}^{(D)}_{\text{cav}} = \frac{g_{\text{eff}}}{N_s}\sum_{i,j} J_i J_j\, \hat{n}_i\hat{n}_j = \frac{g_{\text{eff}}}{N_s}\sum_i J_i^2\, \hat{n}_i^2 + \frac{g_{\text{eff}}}{N_s}\sum_{i\neq j} J_i J_j\, \hat{n}_i\hat{n}_j. \tag{2.27}$$

As we can see, the first term is local, but the second is global, connecting whichever pair of sites, independent of their separation.

To interpret the local term, we can use the identity

$$\hat{n}_i^2 = \hat{n}_i(\hat{n}_i - 1) + \hat{n}_i. \tag{2.28}$$

substituting (2.28) on (2.27) we obtain

$$\hat{H}^{(D)}_{\text{cav}} = \frac{g_{\text{eff}}}{N_s}\sum_i J_i^2\, \hat{n}_i(\hat{n}_i - 1) + \frac{g_{\text{eff}}}{N_s}\sum_i J_i^2\, \hat{n}_i + \frac{g_{\text{eff}}}{N_s}\sum_{i\neq j} J_i J_j\, \hat{n}_i\hat{n}_j. \tag{2.29}$$

which allows a direct interpretation: the first term is a renormalization of U, spatially dependent thanks to J_i^2; then μ suffers a shift; the third term introduces a density-density infinite-range interaction, modulating the collective configurations depending on the sign of g_{eff} and the spatial pattern of J_i.

Adding this (2.29) to $\hat{H}_b$ gives an effective Hamiltonian

$$\begin{aligned}\hat{H}^{(D)}_{\text{eff}} =& -t_0\sum_{\langle i,j\rangle}\left(\hat{b}_i^\dagger\hat{b}_j + \text{h.c.}\right) - \mu\sum_i \hat{n}_i + \frac{U}{2}\sum_i \hat{n}_i(\hat{n}_i - 1)\\ &+ \frac{g_{\text{eff}}}{N_s}\sum_i J_i^2\, \hat{n}_i(\hat{n}_i - 1) + \frac{g_{\text{eff}}}{N_s}\sum_i J_i^2\, \hat{n}_i + \frac{g_{\text{eff}}}{N_s}\sum_{i\neq j} J_i J_j\, \hat{n}_i\hat{n}_j.\end{aligned} \tag{2.30}$$

With an equivalent form, obtained by grouping the terms in renormalized parameters, of

$$\frac{U}{2}\sum_i \hat{n}_i(\hat{n}_i{-}1) + \frac{g_{\text{eff}}}{N_s}\sum_i J_i^2\, \hat{n}_i(\hat{n}_i{-}1) = \sum_i \frac{U_i^{\text{eff}}}{2}\,\hat{n}_i(\hat{n}_i{-}1), \qquad U_i^{\text{eff}} = U + 2\frac{g_{\text{eff}}}{N_s}J_i^2, \tag{2.31}$$

and

$$-\mu\sum_i \hat{n}_i + \frac{g_{\text{eff}}}{N_s}\sum_i J_i^2\, \hat{n}_i = -\sum_i \mu_i^{\text{eff}}\,\hat{n}_i, \qquad \mu_i^{\text{eff}} = \mu - \frac{g_{\text{eff}}}{N_s}J_i^2, \tag{2.32}$$

Then we can rewrite (2.30) as

$$\hat{H}^{(D)}_{\text{eff}} = -t_0\sum_{\langle i,j\rangle}\left(\hat{b}_i^\dagger\hat{b}_j + \text{h.c.}\right) - \sum_i \mu_i^{\text{eff}}\,\hat{n}_i + \sum_i \frac{U_i^{\text{eff}}}{2}\,\hat{n}_i(\hat{n}_i - 1) + \frac{g_{\text{eff}}}{N_s}\sum_{i\neq j} J_i J_j\, \hat{n}_i\hat{n}_j. \tag{2.33}$$

Here we can clearly see and expect an interplay between a coherent delocalization

controlled by t_0, a local repulsion controlled by U_i^{eff} and a collective density interaction controlled by $g_{\text{eff}} J_i J_j$.

Eq. (2.33) is the EBHM with density interaction. Now, the spatial profile of the coefficients J_j determines which collective combination of densities the cavity is coupled to. Given that the coefficients $J_j = u_c^*(\mathbf{R}_j) u_p(\mathbf{R}_j)$ depend mode functions evaluated at each site of the lattice, then their spatial structures is fixed by the optical geometry: angles, wavelength and amplitude of the pump.

A particularly relevant case is the diffraction minima: when the pump beam is transversal to the cavity axis (at $90°$). In this case, the spatial profile of $u_c^*(\mathbf{r}) u_p(\mathbf{r})$ alters the sign site by site, imposing the staggered structure

$$J_j = J_D \, (-1)^j, \tag{2.34}$$

with J_D real [45]. This alternation imprints a sublattice structure on the system: the odd sites (O), with $J_j = +J_D$, and the even sites (E), with $J_j = -J_D$. The collective density operator transforms to

$$\hat{D} = J_D \sum_{\nu} \left(\hat{n}_{O,\nu} - \hat{n}_{E,\nu} \right), \tag{2.35}$$

measuring the difference in population between the two sublattices. Then the full cavity term is described by

$$\hat{H}_{\text{cav}}^{(D)} = \frac{g_{\text{eff}}}{N_s} |J_D|^2 \left(\sum_{\nu} \hat{n}_{O,\nu} - \hat{n}_{E,\nu} \right)^2, \tag{2.36}$$

This is the extension we will be referring to as the density coupling (J_D) model, studied in detail on the Refs. [45, 46, 50].

A schematic depiction of the experimental array for this model is presented in Fig. 2.1.

2.3 Bond coupling (J_B)

We have shown the derivation a density coupling model. Now it's time to consider a complementary situation, when the optical geometry is such that the light couples to the coherence between neighbouring sites, that is, the lattice bonds. This is a regime qualitatively different because it modifies the effective hopping interaction, allowing the stabilization of bond order phases, such as superfluid dimers and supersolid dimers, which will be discussed on Chapter 3.

Again, the derivation begins with the general Hamiltonian

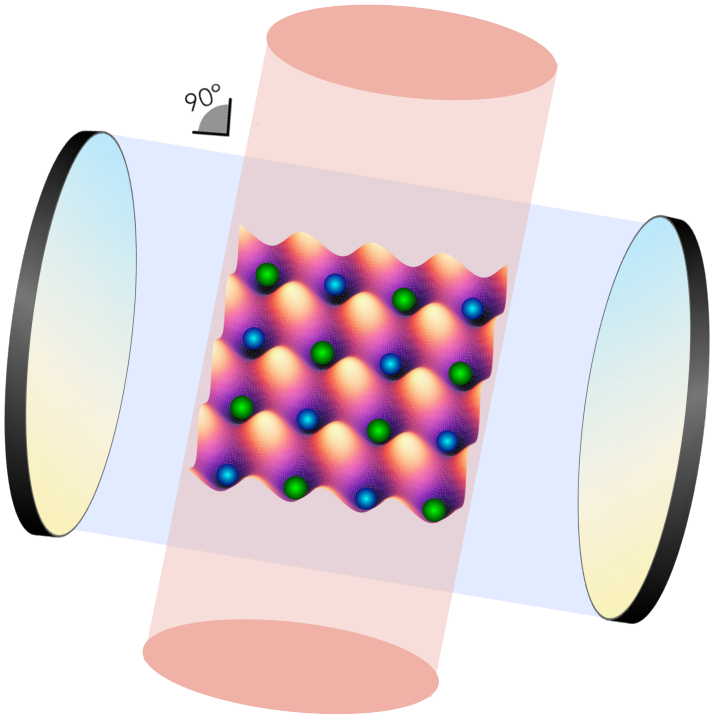

Figure 2.1. Optical geometry for the J_D EBHM.

$$\hat{H}_{\text{eff}} = \hat{H}_b + \frac{g_{\text{eff}}}{2N_s}\left(\hat{F}^\dagger\hat{F} + \hat{F}\hat{F}^\dagger\right), \qquad \hat{F} = \hat{D} + \hat{B}. \tag{2.37}$$

Now we are looking for an optical geometry in which the dominant contribution is $\hat{B}_{pc}$, i.e.

$$|J_{ij}^{pc}| \gg |J_{jj}^{pc}|, \qquad i \neq j, \tag{2.38}$$

so that $\hat{F}_{pc} \approx \hat{B}_{pc}$.

This condition is reached when the product $u_c^*(\mathbf{r})\, u_p(\mathbf{r})$ has its maxima in between the lattice sites, that is, at the midpoints of the bonds, where the Wannier functions overlap. In practice, this is achieved by choosing the functions in such a way that the pump field nodes land on the lattice sites. In 1D, a choice that satisfies this is $u_c(\mathbf{r}) = \text{const.}$ and $u_p(\mathbf{r}) = \sin(\pi r/a)$, where a is the lattice separation length [51]. With this choice, the density integral $J_{jj}^{pc} = \int w^2(\mathbf{r} - \mathbf{R}_j)|u_c^*||u_p|\, d^3r$ is zero by symmetry, while the bond integral is non-zero and controlled.

The resulting bond coefficients alternate sign between consecutive neighbours,

$$J_{ij}^{pc} = \pm J_B, \tag{2.39}$$

with $J_B \simeq 0.05$ for an optical potential with $V_0 \approx 5\, E_R$ in 1D [45]. This pattern

imprints a four-mode spatial structure on the system, as will be explained later.

Taking just one cavity and one pump beam, and considering the latter approximation $\hat{F} \approx \hat{B}$, the effective Hamiltonian is

$$\hat{H}_{\text{eff}}^{(B)} \simeq \hat{H}_b + \frac{g_{\text{eff}}}{2N_s}\left(\hat{B}^\dagger\hat{B} + \hat{B}\hat{B}^\dagger\right), \qquad \hat{B} = \sum_{\langle i,j\rangle} J_{ij}\,\hat{K}_{ij}, \tag{2.40}$$

where we can define the hermitic bond operator

$$\hat{K}_{ij} \equiv \hat{b}_i^\dagger\hat{b}_j + \hat{b}_j^\dagger\hat{b}_i, \tag{2.41}$$

and g_{eff} is given by Eq. (2.24). Given that, then the cavity term simplifies as

$$\hat{H}_{\text{cav}}^{(B)} = \frac{g_{\text{eff}}}{N_s}\,\hat{B}^2 = \frac{g_{\text{eff}}}{N_s}\left(\sum_{\langle i,j\rangle} J_{ij}\,\hat{K}_{ij}\right)^2. \tag{2.42}$$

In order to understand the physics contained in (2.42), we can expand the square, separating each diagonal ($\langle i,j\rangle = \langle k,l\rangle$) and crossed ($\langle i,j\rangle \neq \langle k,l\rangle$) contributions:

$$\hat{B}^2 = \sum_{\langle i,j\rangle} J_{ij}^2\,\hat{K}_{ij}^2 + \sum_{\langle i,j\rangle\neq\langle k,l\rangle} J_{ij}J_{kl}\,\hat{K}_{ij}\hat{K}_{kl}. \tag{2.43}$$

As a first step we expand $\hat{K}_{ij}^2$ explicitly. Using the definition (2.41) and expanding

$$\hat{K}_{ij}^2 = (\hat{b}_i^\dagger\hat{b}_j)^2 + (\hat{b}_j^\dagger\hat{b}_i)^2 + \hat{b}_i^\dagger\hat{b}_j\hat{b}_j^\dagger\hat{b}_i + \hat{b}_j^\dagger\hat{b}_i\hat{b}_i^\dagger\hat{b}_j. \tag{2.44}$$

We can use the canonical commutation relations for the last two terms; for the bosonic operators $[\hat{b}_i, \hat{b}_j^\dagger] = \delta_{ij}$. For $i \neq j$, they commute, so that

$$\hat{b}_i^\dagger\hat{b}_j\hat{b}_j^\dagger\hat{b}_i = \hat{b}_i^\dagger(\hat{n}_j+1)\hat{b}_i = (\hat{n}_j+1)\hat{n}_i, \tag{2.45}$$

$$\hat{b}_j^\dagger\hat{b}_i\hat{b}_i^\dagger\hat{b}_j = \hat{b}_j^\dagger(\hat{n}_i+1)\hat{b}_j = (\hat{n}_i+1)\hat{n}_j. \tag{2.46}$$

Substituting in (2.44):

$$\hat{K}_{ij}^2 = (\hat{b}_i^\dagger)^2\hat{b}_j^2 + (\hat{b}_j^\dagger)^2\hat{b}_i^2 + 2\hat{n}_i\hat{n}_j + \hat{n}_i + \hat{n}_j. \tag{2.47}$$

Let's stop for a moment to explain the physical interpretation of the contributions. In order, we have: a pair-tunneling, a density-density contribution, and linear terms (can be absorbed as a shift in μ).

Repeating the procedure for the J_D case, we can separate the diagonal and crossed

contributions in $\hat{B}^2$, using (2.47) in (2.43)

$$\hat{H}_{\text{eff}}^{(B)} = \hat{H}_b + \frac{g_{\text{eff}}}{N_s} \sum_{\langle i,j \rangle} J_{ij}^2 \left[(\hat{b}_i^\dagger)^2 \hat{b}_j^2 + (\hat{b}_j^\dagger)^2 \hat{b}_i^2 + 2\hat{n}_i \hat{n}_j + \hat{n}_i + \hat{n}_j \right] + \frac{g_{\text{eff}}}{N_s} \sum_{\langle i,j \rangle \neq \langle k,l \rangle} J_{ij} J_{kl} \, \hat{K}_{ij} \hat{K}_{kl}. \tag{2.48}$$

With the alternate structure of (2.39), the lattice bonds may be divided into different modes according to the sign of J_{ij}. We define the bond operator for each mode as

$$\hat{S}_\varphi \equiv \sum_{\langle i,j \rangle \in \varphi} \hat{K}_{ij}, \tag{2.49}$$

so that

$$\hat{B} = \sum_\varphi J_{B,\varphi} \, \hat{S}_\varphi. \tag{2.50}$$

For the same regime discussed in the previous section, with diffraction minima (cavity axis and pump laser beam are at $90°$), then the alternating pattern of the coefficients$J_{ij} = (-1)^{i+1} J_B$ impose a four site periodicity in the lattice. This requires to introduce four modes $\xi = 1, 2, 3, 4$ to represent the four families of equivalent sites, with the periodic condition $\xi + 4 \equiv \xi$ [45]. The effective Hamiltonian is then decomposed into four contributions, one for each mode

$$\hat{H}_{\text{eff}}^{(B)} = \sum_{\xi=1}^{4} \hat{H}_\xi^{\text{eff}}. \tag{2.51}$$

2.4 Multicomponent density coupling

The two previous sections considered optical geometries that induced a two-mode structure to the system. Even and Odd sites, for the J_D model; four families of sites for the J_B model. For both cases, the spatial periodicity of the light field was $R = 2$. A natural extension consist in asking what could occur when choosing a pump angle with another value($\neq 90°$), such that the spatial projection $u_c^*(\mathbf{r})\, u_p(\mathbf{r})$ acquires a periodicity with $R > 2$ spatial modes [45, 50].

This is a significantly richer scenario for the phase diagram. The interplay between R spatial modes generates an energy landscape with new possibilities of symmetry breaking, including multicomponent density waves (DW) and supersolid (SS). The derivation is a generalization of the one for $R = 2$, so the treatment can be done under the same framework.

For the purpose of this work, let's consider the density coupling regime, where $\hat{B} \approx 0$, so that

$$\hat{F} \simeq \hat{D} = \sum_j J_{jj}\, \hat{n}_j, \qquad J_{jj} \approx u_c^*(\mathbf{R}_j)\, u_p(\mathbf{R}_j). \tag{2.52}$$

The novelty respect to the Section 2.2 is that the product of the modes $u_c^*(\mathbf{R}_j)\, u_p(\mathbf{R}_j)$ does not only have a two-value alternation, but R different phase values periodically along the lattice. Specifically, for the travelling wave beams, the projection of the differential wave vector $\mathbf{k}_p - \mathbf{k}_c$ along the lattice axis $\hat{\mathbf{e}}$, leading to

$$J_{jj} = J_D\, e^{i(\mathbf{k}_p - \mathbf{k}_c)\cdot \mathbf{R}_j}. \tag{2.53}$$

the condition of commensurability with the lattice requires

$$(\mathbf{k}_p - \mathbf{k}_c) \cdot \hat{\mathbf{e}} \cdot a = \frac{2\pi}{R}, \tag{2.54}$$

with a the lattice spacing, and $R \in \mathbb{Z}^+$. When this condition is satisfied, the lattice sites are grouped in R families or spatial modes $\xi = 1, \ldots, R$, each with N_s/R sites. All sites of the same family couples with the light with the same amplitude and phase. Geometrically, the condition (2.54) fixed the angle of the pump beam respect with the cavity axis

$$\cos\theta_p = \cos\theta_c - \frac{\lambda}{a} \cdot \frac{1}{R}, \tag{2.55}$$

where $\theta_{c,p}$ are the angles for the wave vectors for the cavity and the pump respect with the lattice axis, and λ is the wavelength of the light [45]. Simply adjusting the pump angles, the number of spatial modes R is controlled and, consequently, the effective interaction structure.

For a general value R, the collective density operator takes the form

$$\hat{D} = J_D \sum_{\xi=1}^{R} e^{i\theta_\xi}\, \hat{N}_\xi, \qquad \hat{N}_\xi = \sum_{j\in\xi} \hat{n}_j, \tag{2.56}$$

where $\theta_\xi = 2\pi(\xi - 1)/R$ is the relative phase of each mode ξ and $\hat{N}_\xi$ is the number operator for that mode.

For the most inmediate extension, $R = 3$, the geometric condition is

$$(\mathbf{k}_p - \mathbf{k}_c) \cdot \hat{\mathbf{e}} \cdot r_j = \frac{2\pi}{3}\, j, \tag{2.57}$$

so that the three modes have the phases $\theta = 0, 2\pi/3, 4\pi/3$ and the collective operator

is

$$\hat{D} = J_D \left(\hat{N}_1 + e^{i\frac{2\pi}{3}} \hat{N}_2 + e^{i\frac{4\pi}{3}} \hat{N}_3 \right). \tag{2.58}$$

The physical interpretation is direct, as the cavity measures the difference in population between the three sublattices with their corresponding phase weights. When the three sublattices have the same population ($\rho_1 = \rho_2 = \rho_3$), the operator $\hat{D}$ is zero and the cavity does not scatter light; when there is density imbalance between modes, $|\langle \hat{D} \rangle| \neq 0$ and the cavity backaction is maximized.

The term induced by the cavity is $\hat{H}^{(D)}_{\text{cav}} = \frac{g_{\text{eff}}}{N_s} \hat{D}^\dagger \hat{D}$. Given that $\hat{D}$ is not Hermitic for $R \geq 3$, because of the complex phases θ_ξ, it is necessary to evaluate $\hat{D}^\dagger \hat{D}$ explicitly

$$\begin{aligned} \hat{D}^\dagger \hat{D} &= |J_D|^2 \left(\hat{N}_1 + e^{-i\frac{2\pi}{3}} \hat{N}_2 + e^{-i\frac{4\pi}{3}} \hat{N}_3 \right) \left(\hat{N}_1 + e^{i\frac{2\pi}{3}} \hat{N}_2 + e^{i\frac{4\pi}{3}} \hat{N}_3 \right) \\ &= |J_D|^2 \left[\hat{N}_1^2 + \hat{N}_2^2 + \hat{N}_3^2 - \hat{N}_1\hat{N}_2 - \hat{N}_2\hat{N}_3 - \hat{N}_1\hat{N}_3 \right], \end{aligned} \tag{2.59}$$

where we've used the fact $e^{i2\pi/3} + e^{-i2\pi/3} = -1$ and the hermicity of $\hat{N}_\xi$. The result of (2.59) has a clear structure: the diagonal terms $\hat{N}_\xi^2$ are a renormalization for the onsite interaction and the chemical potential for each mode, while the crossed terms $\hat{N}_\xi \hat{N}_{\xi'}$ introduce a repulsive interaction for different modes, i.e. the system prefers the state where different modes have different populations, favouring DW by $g_{\text{eff}} < 0$.

This $\hat{H}^{(D)}_{\text{cav}}$ is added to the BHM to form the EBHM that we call the multicomponent density coupling model.

Chapter 3

Quantum phases for extended models

The EBHM's derived in the previous chapter describe strongly correlated bosons in optical lattices with cavity-induced collective coupling. The main characteristic of this collective modes is that it generates global long-range interactions but with a tunable spatial structure determined by the optical geometry [44, 44, 45]. This aspect, while conserving the local or short-range physics, mainly the MI-SF transition, also naturally admits the emergence of additional phases of density or bond orders, typical for non-local extensions [6, 42].

The purpose of this chapter is, on Section 3.1, to stablish the definitions for the relevant quantum phases for this EBHM's, comment on the observables and order parameters necessary to their identification. Then on Section 3.2 is to describe how this phases may be identified experimentally with ultracold atoms experiments, linking the order parameters with optical signals and other standard atomic characterization techniques [44, 44]. Finally, we'll discuss the role of the EE as a measure of correlations for each phase.

3.1 MI, SF, DW, SS and dimerization

We will define each many-body quantum phase relevant for the EBHM's studied in this work, specifying the order parameters characterizing each one, the structure of the many-body state that describes them, and how are they modified or generated by the presence of light-matter coupling.

Mott insulator (MI)

The Mott quantum phase is incompressible and localized, present in the BHM for $U/t_0 \gg 1$ with commensurate filling [6, 2]. Its definition is based in two simultaneous conditions. The first is the absence of phase coherence. The superfluid order parameter is zero everywhere

$$\psi_i \equiv \langle \hat{b}_i \rangle = 0. \tag{3.1}$$

The second is incompressibility. The compressibility of a system, defined as

$$\kappa = \frac{\partial \langle \hat{n} \rangle}{\partial \mu}, \tag{3.2}$$

is zero for the thermodynamic limit ($T = 0$), reflecting the existence of a finite particle-hole energy gap Δ_{MI}. This gap separates the ground-state and the first excitation, and is the reason for why the density by site is fixed. For the BHM, within a mean-field description, the MI gap with filling n_0 in the limit $t_0 \to 0$ is $\Delta_{\mathrm{MI}} = U$ for $n_0 = 1$ [6].

The many-body state for the MI in the limit $t_0 = 0$ is a Fock state with exact occupation of n_0 by site.

$$|\Psi_{\mathrm{MI}}\rangle = \bigotimes_i |n_0\rangle_i, \tag{3.3}$$

which is a product state without quantum site correlations. The particle fluctuations by site are exponentially suppressed with U/t_0,

$$(\Delta n_i)^2 \equiv \langle \hat{n}_i^2 \rangle - \langle \hat{n}_i \rangle^2 \to 0 \quad \text{para } t_0/U \to 0, \tag{3.4}$$

implying that the MI is essentially a classical state from the entanglement point of view. Meaning its bipartite entanglement entropy is zero, $S_{\mathrm{EE}}^{\mathrm{MI}} = 0$, independent of the partition. For a small finite t_0, the MI acquires perturbative corrections mixing the Fock state $|n_0\rangle$ with the particle-hole states $|n_0 \pm 1\rangle$, generating a small but finite entanglement, growing as the system approaches the MI-SF transition [52].

The fluctuations are related with the compressibility by

$$\kappa = \frac{(\Delta \hat{n}_i)^2 N_s}{k_B T}. \tag{3.5}$$

In the presence of a cavity, the MI persist when the local processes dominate, but the Mott lobes are typically renormalized by the cavity-induced interactions. For the J_D model (Section 2.2, the renormalization for the chemical potential $\mu_\xi = \mu \pm 2g_{\mathrm{eff}}|J_D|^2\rho$ shift the Mott lobes, while the renormalization of the local interaction $U_\xi = U + 2g_{\mathrm{eff}}|J_D|^2/N_s$ modifies the width of the Mott lobes [45].

A schematic depiction of the phase is presented in Fig.3.1.

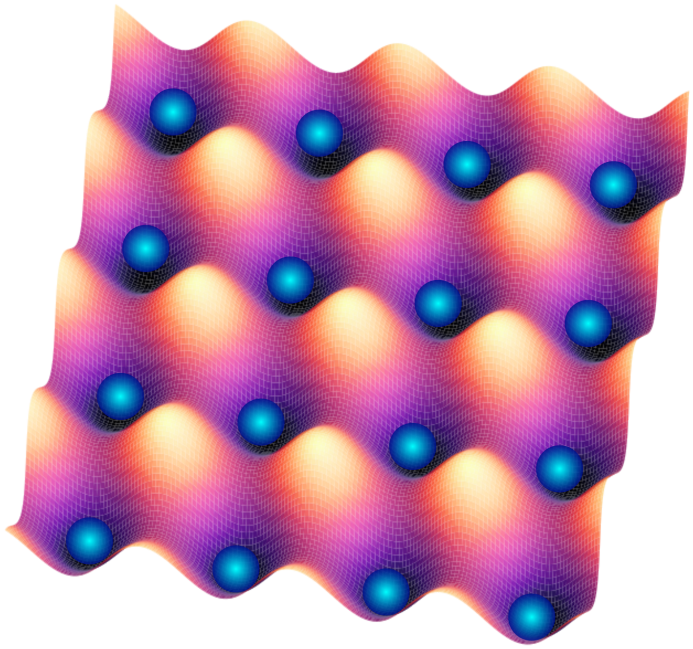

Figure 3.1. MI configuration. Fixed particle number per site.

Superfluid (SF)

The superfluid phase is delocalized and coherent, present in the BHM for a sufficiently large t_0/U [6]. It is characterized by a finite superfluid parameter

$$\psi_i = \langle \hat{b}_i \rangle \neq 0, \tag{3.6}$$

indicating the spontaneous breaking of the $U(1)$ symmetry, related to particle number conservation. Microscopically, the SF corresponds to the Bose-Einstein condensation of the atoms into the zero-momentum mode of the lowest energy band. Taking the limit $U \to 0$, the many-body state is exactly a coherent state for each site,

$$|\Psi_{\mathrm{SF}}\rangle = \bigotimes_i |\phi\rangle_i, \qquad |\phi\rangle_i = e^{-|\phi|^2/2} \sum_{n=0}^{\infty} \frac{\phi^n}{\sqrt{n!}} |n\rangle_i, \tag{3.7}$$

with $\phi = \langle \hat{b} \rangle$ and Poisson distribution for the Fock states, $p_n = |\phi|^{2n} e^{-|\phi|^2}/n!$ [53]. The correlations in the SF slowly decay with distance, described by the correlation function for one body

$$g^{(1)}(r) = \langle \hat{b}_i^\dagger \hat{b}_{i+r} \rangle \tag{3.8}$$

that goes to a constant value for $d \geq 2$, and algebraically decays for 1D [54]. Additionally, the SF phase has finite compressibility $\kappa > 0$, gapless excitations (Goldstone modes associated with the symmetry breaking $U(1)$) and maximum number fluctuations,

$(\Delta n_i)^2 = |\phi|^2 = \rho$.

From an entanglement perspective, the SF state has a bipartite entanglement entropy that grows logarithmically with the size of the system in 1D, $S \sim \frac{1}{3} \ln N_s$ [55, 56]. This logarithmic law is a correction to the area law, and its characteristic for gapless phases in 1D.

In the presence of a cavity, the SF may acquire additional structures, but for sufficiently large t_0/U, it still exist.

A schematic representation of the phase is presented in Fig.3.2.

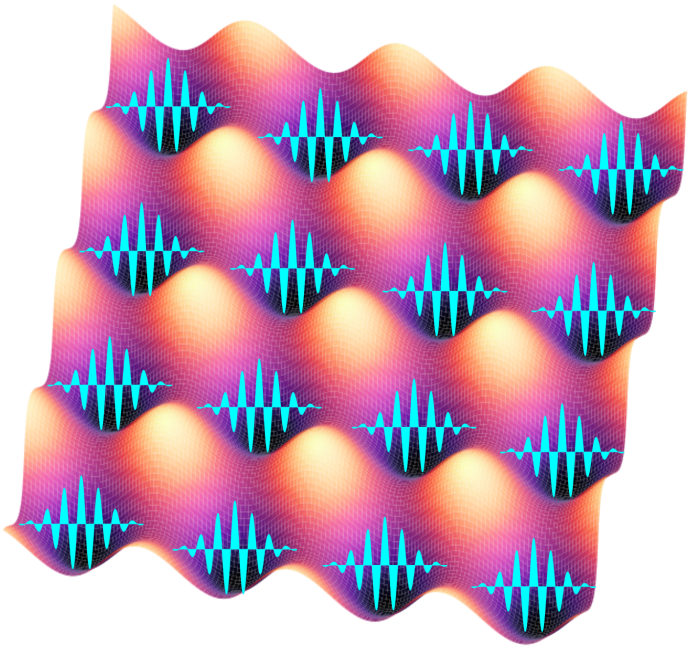

Figure 3.2. SF configuration. The particles are delocalized.

Density wave (DW)

The DW phase is an insulating state that breaks the translational symmetry of the lattice trough a periodic atomic density pattern. In the most general form, it is characterized by

$$\langle \hat{n}_i \rangle = \rho + \delta n \, \cos(\mathbf{Q} \cdot \mathbf{R}_i + \varphi), \tag{3.9}$$

where $\mathbf{Q}$ is the order vector, ρ is the average density, $\delta n > 0$ is the amplitude of modulation and φ the arbitrary phase reflecting the degeneracy of the ordering. For the two-sublattice models ($R = 2$), the order vector is $\mathbf{Q} = \pi/a$ (in 1D), corresponding

to an even-odd density alternation, and the natural order parameter is

$$\mathcal{O}_{\mathrm{DW}}^2 = \frac{1}{N_s^2}\left(\sum_i (-1)^i \langle \hat{n}_i \rangle\right)^2 = \frac{(N_E - N_O)^2}{N_s^2}, \tag{3.10}$$

where $N_{E,O}$ are the total occupations for each sublattice. This parameter is non-zero ($\mathcal{O}_{\mathrm{DW}} \neq 0$) if and only if there is a density imbalance between sublattices, and it is zero for the MI and SF, where $\rho_O = \rho_E = \rho$.

As the DW is an insulator, it follow $\psi_i = 0$, $\kappa = 0$, and presents an energy gap, understood as a generalized Mott gap. In the context of EBHM's with cavities, the DW emerges naturally for $g_{\mathrm{eff}} < 0$, as the cavity term favours energetically the maximization of $|\langle \hat{D} \rangle|^2 \propto (N_E - N_O)^2$, pushing the system to an imbalanced configuration [45].

A schematic representation of the phase is presented in Fig.3.3.

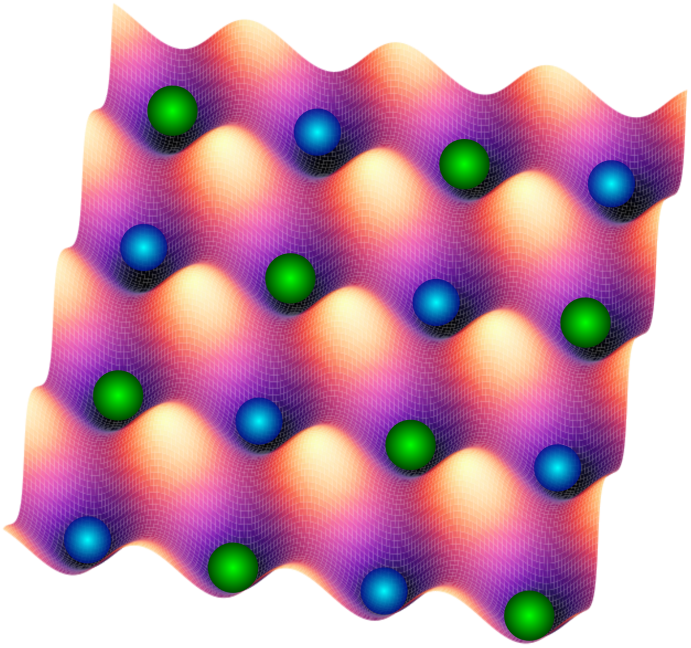

Figure 3.3. DW configuration. Different colors represent different densities. Fixed density per family (O/E).

Supersolid (SS)

The supersolid phase combines simultaneously superfluid and density orders[57]

$$\psi \neq 0 \qquad \text{y} \qquad \mathcal{O}_{\mathrm{DW}} \neq 0. \tag{3.11}$$

This implies that the system presents a global phase coherence while having a spatial density modulation. The SS typically appears as an intermediate phase between SF

and DW, as both order parameters smoothly change and coexist in that region [58, 45].

The existence of SS on bosonic lattice systems with short-range interactions have been object of controversy in the past [57, 59]. In the cavity-mediated EBHM's the global interaction stabilizes the SS robustly [45].

A schematic depiction of the phase is presented in Fig.3.4.

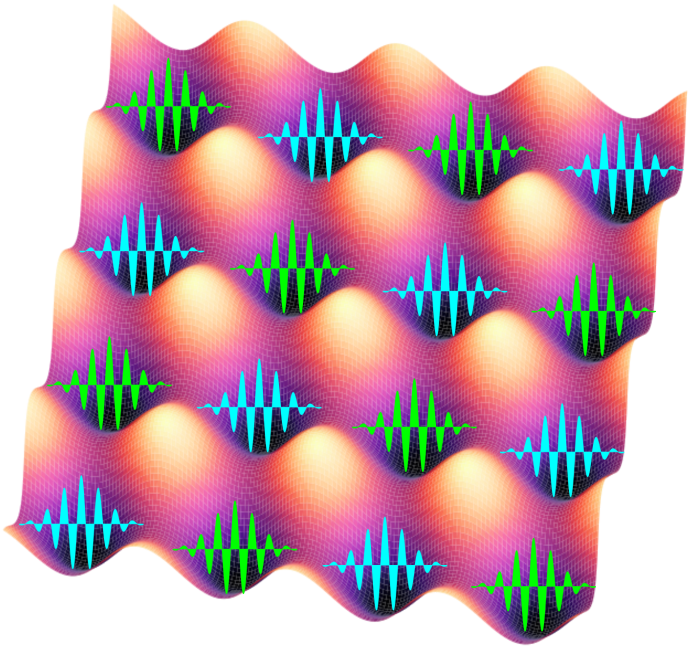

Figure 3.4. SS configuration. Different colors represent different densities. Waves of the same color correspond to the same wave function. This phase is a combination of a density pattern with delocalization.

Superfluid dimer (SFD) and supersolid dimer (SSD)

The dimerized phases are characteristic for the J_B model, and don't have an analogue in purely density coupled models. They emerge from the self organization of the superfluid parameter in response of the cavity-induced interactions over the inter-site coherences. The relevant parameter to inspect dimerization is the Bond order parameter

$$\mathcal{O}_B^2 = \frac{1}{N_b^2}\left(\sum_{\langle i,j\rangle} \eta_{\langle i,j\rangle} \langle \hat{K}_{ij}\rangle\right)^2, \tag{3.12}$$

with the number of bonds N_b, $\hat{K}_{ij} = \hat{b}_i^\dagger \hat{b}_j + \hat{b}_j^\dagger \hat{b}_i$ the inter-site coherence operator, and $\eta_{\langle i,j\rangle} = \pm 1$ a factor reflecting the modulation induced by light. In 1D, $\eta_{\langle i,i+1\rangle} = (-1)^i$

and (3.12) reduces to

$$\mathcal{O}_B^2 = \frac{1}{N_b^2}\left(\sum_j (-1)^j \langle \hat{K}_{j,j+1}\rangle\right)^2 . \tag{3.13}$$

The SFD phase is defined by

$$\psi_\xi \neq 0, \qquad \mathcal{O}_B \neq 0, \qquad \mathcal{O}_{\mathrm{DW}} = 0, \tag{3.14}$$

meaning the system is a SF with a spatial modulation on the phase of its order parameter ψ_ξ, but with no density imbalance. More concretely, the neighbouring sites order parameters differ by a phase $\Delta\phi \neq 0, \pi$, with the pattern

$$\psi_\xi = |\psi|\, e^{i\phi_\xi}, \qquad \phi_{\xi+1} - \phi_\xi = \Delta\phi \cdot (-1)^\xi, \tag{3.15}$$

generating a dimer pattern where adjacent sites share the same phase, separated by a jump $\Delta\phi$ for consecutive dimers. This spatial modulation is analogous to the FFLO/LOFF state in superconductors[60, 61]. This is specially interesting from the perspective of quantum simulation. In the other hand, the SSD phase is the extension of the SFD that includes density imbalance

$$\psi_\xi \neq 0, \qquad \mathcal{O}_B \neq 0, \qquad \mathcal{O}_{\mathrm{DW}} \neq 0. \tag{3.16}$$

For this state, both sites of one specific dimer have the same mean occupation, but consecutive dimers differ, both in phase and density.

To understand dimerization, it is useful to define the dimer phase difference parameter

$$\Delta\phi = \arg(\psi_\xi^* \psi_{\xi+1}), \tag{3.17}$$

which is $\Delta\phi \neq 0$ for SFD and $\Delta\phi = 0$ for SSD.

Summary

The Table 3.1 shows a summary for the order parameters that characterize each phase and on which of the models presented in the Chapter 2 can appear.

The entanglement properties for each phase constitute the central object of study of this work, and will be analysed deeply on Chapters 4 and 6.

3.2 Experimental signatures

The quantum phases described in Sec. 3.1 (SF, MI, DW, SS, SFD and SSD) are, in principle, observable to ultracold atoms in optical cavities experimental platforms.

Phase	$\Sigma\psi$	$\mathcal{O}_{\mathrm{DW}}$	$\mathcal{O}_B$	$\Delta\phi$	Models
MI	0	0	0	0	All
SF	$\neq 0$	0	0	0	All
DW	0	$\neq 0$	0	0	J_D
SS	$\neq 0$	$\neq 0$	0	0	J_D
SFD	$\neq 0$	0	$\neq 0$	$\neq 0$	J_B
SSD	$\neq 0$	$\neq 0$	$\neq 0$	$\neq 0$	J_B

Table 3.1. Order parameters for each quantum phase present in the EBHMs of interest.

The distinctive advantage of using this platforms compared to other implementations of EBHM's is that they offer a natural and non-destructive diagnosis, which is the light escaping the cavity. Under dispersive conditions, the field inside the cavity is slaved to the collective quantum state of the matter through the operator $\hat{F}$, so that the detected photon flux in the exterior has codified information of the bond or density observables [44]. This optical diagnosis can be complemented with other standard techniques for the characterization of quantum gases, such as time of flight expansion (TOF), Bragg spectroscopy and quantum gas microscopy; all of them providing valuable information about the phase coherence, incompressibility and spatial density patterns [3].

The main result to connect the atomic quantum state with the optical signal is the equation relating the field inside the cavity with the collective operator $\hat{F}$, obtained through the adiabatic elimination process (see Section 2.1)

$$\hat{a} \propto \frac{\hat{F}}{\sqrt{N_s}(\Delta_{pc} + i\kappa)}. \tag{3.18}$$

From (3.18) we directly get the relations between the fields and the observables

$$\langle \hat{a} \rangle \propto \langle \hat{F} \rangle, \qquad \langle \hat{a}^\dagger \hat{a} \rangle \propto \langle \hat{F}^\dagger \hat{F} \rangle. \tag{3.19}$$

Hence, the flux of the photons leaking through the cavity, proportional to $\kappa\langle \hat{a}^\dagger \hat{a} \rangle$, is a measure of $\langle \hat{F}^\dagger \hat{F} \rangle$. The homodyne detention allows the reconstruction of the quadrature $\langle \hat{a} \rangle$ in both amplitude and phase, while the heterodyne detection gives access to the complex amplitude of the field [44]. This measurement is non-destructive, meaning that the atomic state is not projected onto the individual Fock states, but the system evolves conditioned to the optical register history.

For the density coupling (J_D) model, the collective operator is just $\hat{D} \propto (\hat{N}_O - \hat{N}_E)$,

so that

$$\langle \hat{a}^\dagger \hat{a} \rangle \propto \langle (\hat{N}_O - \hat{N}_E)^2 \rangle = N_s^2 \, (\Delta\rho)^2 + \langle \delta(\hat{N}_O - \hat{N}_E)^2 \rangle, \tag{3.20}$$

where $\Delta\rho = (\rho_O - \rho_E)/2$ is the density imbalance, and order parameter for DW, and the second term includes the quantum fluctuations. This means that for MI and SF ($\Delta\rho = 0$) the photon flux is just the fluctuations, while for DW and SS ($\Delta\rho \neq 0$)the flux grows with the lattice size, allowing the signal to be distinguished from the background fluctuations [62, 45].

This photon flux as a function of the model parameters $(U, zt_0, \mu, g_{\text{eff}} N_s)$ can trace the contours of the phase diagrams. At the phase boundaries MI-DW and DW-SS, the flux exhibits a discontinuity, signalling the phase transition. This methodology has been used successfully on experiments from Landig et al.. [47] and Klinder et al. [49] where the SF-SS and SS-MI frontiers have been mapped.

Now, for the Bond coupling (J_B) model, the collective operator is just $\hat{B} = \sum_{\langle i,j \rangle} J_{ij} \hat{K}_{ij}$, so that

$$\langle \hat{a}^\dagger \hat{a} \rangle \propto \langle \hat{B}^2 \rangle, \qquad \langle \hat{a} \rangle \propto \langle \hat{B} \rangle. \tag{3.21}$$

For the SF, $\langle \hat{B} \rangle \propto z N_s |\psi|^2 \neq 0$, but with $\Delta\rho = 0$. For the SFD, the alternation of J_{ij} produces the modulation of the bond coherence, which is reflected on the complex amplitude of $\langle \hat{a} \rangle$. Again, the homodyne detention reveals the amplitude and phase of the bond modulation [45]. For both superfluid phases, the signal $\langle \hat{a}^\dagger \hat{a} \rangle = 0$ is then zero, but their dependence with the parameters is different. For SFD the signal grows with $|g_{\text{eff}}|$, but for SS there is a competence between the bond and density signals.

Finally, for the multicomponent J_D ($R = 3$) model, the collective operator has a complex structure: $\hat{D} = J_D(\hat{N}_1 + e^{i2\pi/3}\hat{N}_2 + e^{i4\pi/3}\hat{N}_3)$. As discussed for 3.20, the number of photons, proportional to $|\langle \hat{D} \rangle|^2$ is non-zero only if the density imbalance is zero, for this case between the three modes. However, in order to determine which of the six degenerate DW configurations is realized on the system, it is necessary to access the complex amplitude $\langle \hat{a} \rangle \propto \langle \hat{D} \rangle$, containing that information about which modes have more or less density. This requires a Heterodyne detection of the cavity field [44, 45].

And as we said at the beginning of this section, accessing the spatially resolved information of the system requires standard diagnosis techniques.

Time of flight expansion (TOF)

The TOF involves turning off all the potentials and allowing the gas expand freely during a time t_{TOF}. The absorption image obtained after the expansion is proportional

to the distribution of momentum $n(\mathbf{k})$ of the trapped atomic cloud [3]

$$n_{\mathrm{TOF}}(\mathbf{r}) \propto n\left(\mathbf{k} = \frac{m\mathbf{r}}{\hbar t_{\mathrm{TOF}}}\right). \tag{3.22}$$

And this distribution of momentum is directly related to the correlation function for one body

$$n(\mathbf{k}) = \frac{1}{N_s}\sum_{i,j} e^{i\mathbf{k}\cdot(\mathbf{R}_i-\mathbf{R}_j)}\langle \hat{b}_i^\dagger \hat{b}_j\rangle = |\tilde{w}(\mathbf{k})|^2 \tilde{g}^{(1)}(\mathbf{k}), \tag{3.23}$$

here $\tilde{w}(\mathbf{k})$ and $\tilde{g}^{(1)}(\mathbf{k})$ are the Fourier transforms of the Wannier function and the one-body correlations, respectively. The different quantum phases are distinguished by their TOF image:

- MI phase:$\langle \hat{b}_i^\dagger \hat{b}_j\rangle \approx 0$ for $i \neq j$. So $n(\mathbf{k})$ is approximately uniform, with no interference peaks [2, 16].
- SF phase: $\langle \hat{b}_i^\dagger \hat{b}_j\rangle \neq 0$ for $i \neq j$. So $n(\mathbf{k})$ exhibits great interference peaks in the vectors $\mathbf{k} = \mathbf{G}$ of the reciprocal lattice, which are the signature of the $\mathbf{k} = 0$ mode of a Bose-Einstein condensate [16].
- DW and SS phases. the spatial modulation of the density with the vector $\mathbf{Q}$ introduces additional peaks to $n(\mathbf{k})$ at the positions $\mathbf{k} = \mathbf{Q} + \mathbf{G}$, which coexist with the previous (or absence of) peaks for the SF and MI phases [3].
- SFD phase. The phase modulation of the order parameter with period $4a$ introduces extra peaks on $n(\mathbf{k})$ at the vectors $\mathbf{k} = \pi/(2a) + \mathbf{G}$. This is the TOF signature for dimerization [46].

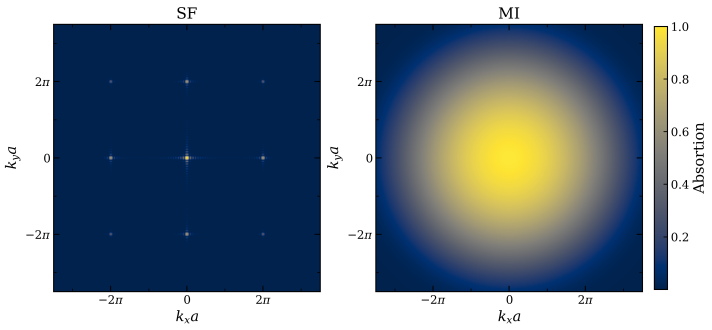

Figure 3.5. A simulation of the TOF absortion image for SF and MI phases.

Bragg spectroscopy

This allows to measure $S(\mathbf{k}, \omega)$ (the dynamical structure factor) reflecting collective excitations on the system [64]. For phases with density order, the structure factor

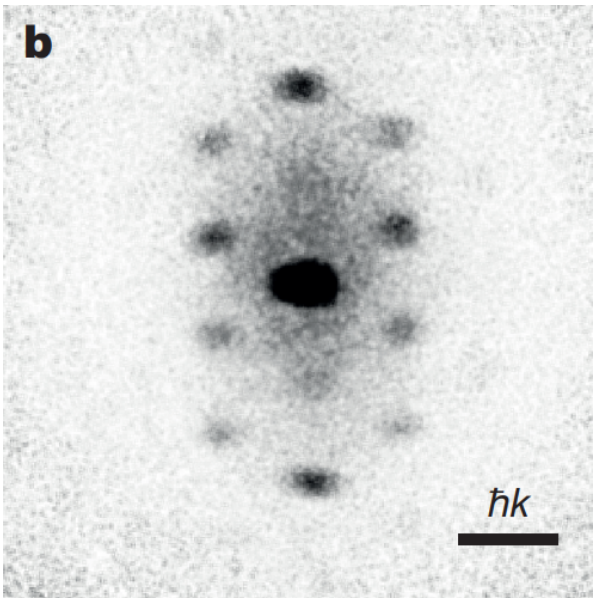

Figure 3.6. Absortion image of the distribution of momentum in the SS phase. The additional atomic momentum modes are induced by the scattering of photons from the pump to the modes of the cavity [63].

$$S(\mathbf{Q}) = \frac{1}{N_s} \sum_{i,j} e^{i\mathbf{Q}\cdot(\mathbf{R}_i - \mathbf{R}_j)} \langle \hat{n}_i \hat{n}_j \rangle \tag{3.24}$$

exhibits a peak at the vector $\mathbf{Q}$, whose intensity is proportional to $|\mathcal{O}_{\mathrm{DW}}|^2$, serving as a direct measure of the order parameter for DW. The Bragg spectroscopy is specially useful to determine this vector $\mathbf{Q}$ and hence identify the periodicity of the density order (R=2,3,...) without site resolution [3].

Quantum gas microscopy

When available, the quantum gas microscopy [17, 18] allows to measure $\langle \hat{n}_i \rangle$ with single-site resolution, offering the most direct imaging of the state of the system. For the our relevant models, the most relevant observations are:

- Density distribution $\langle \hat{n}_i \rangle$. It allows to identify the occupation and can measure $\mathcal{O}_{\mathrm{DW}}$ directly.
- Density correlations $\langle \hat{n}_i \hat{n}_j \rangle - \langle \hat{n}_i \rangle \langle \hat{n}_j \rangle$. Distinguishes quantum correlations with classical fluctuations, accessible through image correlations in microscopy experiments.
- Local fluctuations $(\Delta n_i)^2 = \langle \hat{n}_i^2 \rangle - \langle \hat{n}_i \rangle^2$. Possible to map with single-site resolution, giving information about the local compressibility and identifying the state on different regions of the system.

- Bond coherence $\langle \hat{K}_{ij} \rangle = \langle \hat{b}_i^\dagger \hat{b}_j + \hat{b}_j^\dagger \hat{b}_i \rangle$. It can be derived from measurements of the correlation function for one body.

Chapter 4

Entanglement Entropy

Quantum entanglement is a manifestation of the quantum nature of composite systems. A pure state of a system can't be necessarily described a product state of its parts. Historically, this idea appears since the discussion of the EPR [65] and the terminology introduced by Schrödinger [66], but it relevance goes beyond, as the entanglement has become a crucial tool to characterize quantum phases and transitions for systems with many-body interactions [67, 52, 68].

For ultracold bosonic lattices, in particular the BHM and its extensions, the EE fulfils the role of a parameter for quantum phase diagnosis and a probe for quantum criticality. Those characteristics make this quantity central for the study of phases for systems with global interactions, for example, induced by optical cavities [48, 69].

In the introduction we provided a short overview for the entanglement entropy, now in this chapter we will go deeper on the topic. On Section 4.1, the formal definitions necessary to quantify the entanglement for bipartite systems, introducing the reduced density matrix and relevant forms of entropies such as Rényi and von Neumann. Then, on Section 4.2 we will discuss the area law and its corrections on the context of BHM's. Finally, on Section 4.3 we explain the role of the EE as an order parameter. The specific calculation methods are presented later in Chapter 5.

4.1 Definitions and bipartite systems

Consider a quantum system bipartitioned into two subsystems A and B. The Hilbert space is then the external product

$$\mathcal{H} = \mathcal{H}_A \otimes \mathcal{H}_B. \tag{4.1}$$

Let $|\Psi\rangle \in \mathcal{H}$ be a pure state. with orthonormal basis $\{|a\rangle\}$ of $\mathcal{H}_A$ and $\{|b\rangle\}$ of $\mathcal{H}_B$, it can be expressed as

$$|\Psi\rangle = \sum_{a,b} C_{ab}\ |a\rangle \otimes |b\rangle\,. \tag{4.2}$$

The state $|\Psi\rangle$ is called separable if there exist $|\psi_A\rangle \in \mathcal{H}_A$ and $|\psi_B\rangle \in \mathcal{H}_B$ such that

$$|\Psi\rangle = |\psi_A\rangle \otimes |\psi_B\rangle \,. \tag{4.3}$$

In the opposite case, the state is said to be entangled (see Fig. 4.1).

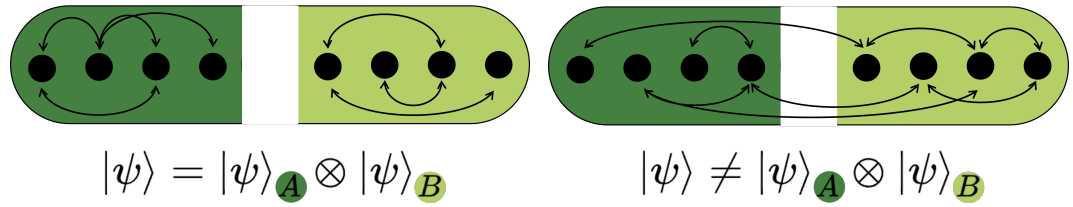

Figure 4.1. Diagram of the bipartite system for (a) separable and (b) entangled states. The arrows indicate interconnected sites.

A paradigmatic example illustrating this difference is a two $\frac{1}{2}$-spin system. The state $|\Psi_{\text{sep}}\rangle = |\uparrow\rangle \otimes |\downarrow\rangle$ is separable, and describes two particles with well defined properties individually. Instead, the Bell state

$$|\Psi_{\text{Bell}}\rangle = \frac{1}{\sqrt{2}} \left(|\uparrow\rangle \otimes |\downarrow\rangle - |\downarrow\rangle \otimes |\uparrow\rangle\right) \tag{4.4}$$

is maximally entangled. None of the two spins are individually defined and the correlations between the two are intrinsically quantum [70].

A quantum state is most generally described by the density matrix ρ, satisfying

$$\hat{\rho}^\dagger = \hat{\rho}, \qquad \text{Tr}(\hat{\rho}) = 1, \qquad \hat{\rho} \geq 0. \tag{4.5}$$

A pure state $|\Psi\rangle$, has a density matrix

$$\hat{\rho} = |\Psi\rangle \langle\Psi| \,. \tag{4.6}$$

For a mixed state described by a statistical ensemble $\{p_\alpha, |\Psi_\alpha\rangle\}$, with $p_\alpha \geq 0$ and $\sum_\alpha p_\alpha = 1$

$$\hat{\rho} = \sum_\alpha p_\alpha \, |\Psi_\alpha\rangle \langle\Psi_\alpha| \,. \tag{4.7}$$

One can distinguish a pure and a mixed state through the purity

$$\text{Tr}(\hat{\rho}^2) = \begin{cases} 1, & \text{pure state,} \\ < 1, & \text{mixed state.} \end{cases} \tag{4.8}$$

Physically, the purity measures how much "diagonal" is a state in some basis.

To quantify the entanglement of subsystem A with subsystem B from a pure state of a local system, we introduce the reduced density matrix of A, defined as:

$$\hat{\rho}_A = \mathrm{Tr}_B\, \hat{\rho}_{AB}. \tag{4.9}$$

The partial trace is the operation defined as the sum over the states of the orthonormal basis of B

$$\hat{\rho}_A = \sum_b \langle b|\, \hat{\rho}_{AB}\, |b\rangle\,, \tag{4.10}$$

Element by element,considering $\hat{\rho}_{AB} = |a_i\rangle\langle a_j| \otimes |b_i\rangle\langle b_j|$, the trace is computed as

$$\begin{aligned}\mathrm{Tr}_B\left[|a_i\rangle\langle a_j| \otimes |b_i\rangle\langle b_j|\right] &= |a_i\rangle\langle a_j|\ \mathrm{Tr}\left[|b_i\rangle\langle b_j|\right] \\ &= |a_i\rangle\langle a_j|\ \langle b_j|b_i\rangle \\ &= \delta_{ij}\ |a_i\rangle\langle a_j|\,. \end{aligned} \tag{4.11}$$

One essential property of the reduced density matrix is that, even if $\hat{\rho}_{AB}$ describes a pure state, $\hat{\rho}_A$ may result in a mixed state. This is a surprising manifestation of the quantum nature, a system in a pure state may contain statistically mixed subsystems. This occurs because, when tracing over B, we loose information about the correlations between the two parts, and this reflects as a mixture on $\hat{\rho}_A$. The more entangled the system, the more mixed $\hat{\rho}_A$ will be [70, 71].

For all bipartite pure state, there exist a quantum representation manifesting the entanglement structure, called the Schmidt decomposition. The theorem guarantees that any $|\Psi\rangle$ living in a bipartitioned Hilbert space can be written as

$$|\Psi\rangle = \sum_{n=1}^{\chi} \sqrt{\lambda_n}\ |u_n\rangle_A \otimes |v_n\rangle_B\,, \qquad \lambda_n \geq 0, \qquad \sum_n \lambda_n = 1, \tag{4.12}$$

where $\{|u_n\rangle\}$ y $\{|v_n\rangle\}$ are orthonormal basis of $\mathcal{H}_A$ and $\mathcal{H}_B$, respectively. $\chi \leq \min(\dim(A), \dim(B))$ is called the Schmidt range. λ_n are the Schmidt coefficients. The decomposition is obtained by taking the coefficient matrix C of (4.2) and applying the singular value decomposition (SVD) [70].

This decomposition has important consequences. First, the reduced density matrix becomes diagonal in this basis

$$\hat{\rho}_A = \sum_{n=1}^{\chi} \lambda_n\ |u_n\rangle\langle u_n|\,, \qquad \hat{\rho}_B = \sum_{n=1}^{\chi} \lambda_n\ |v_n\rangle\langle v_n|\,. \tag{4.13}$$

Implying that the spectrum of $\hat{\rho}_A$ and $\hat{\rho}_B$ coincide, meaning

$$S(\hat{\rho}_A) = S(\hat{\rho}_B), \tag{4.14}$$

We can also extract information from the value of χ. For separable states $\chi = 1$, while $\chi > 1$ is an indication of entanglement [72].

Von Neumann entropy

The most natural and physically meaningful quantification of entanglement is the von Neumann (vN) entropy, with definition

$$S(\hat{\rho}) = -\mathrm{Tr}\left(\hat{\rho} \ln \hat{\rho}\right). \tag{4.15}$$

For a pure global state, the EE associated with the bipartition $A|B$ is defined as

$$S_A = S(\hat{\rho}_A) = -\mathrm{Tr}_A\left(\hat{\rho}_A \ln \hat{\rho}_A\right). \tag{4.16}$$

In terms of the Schmidt coefficients, it takes the form

$$S_A = -\sum_{n=1}^{\chi} \lambda_n \ln \lambda_n, \tag{4.17}$$

which is an identical form of the Shannon entropy of the $\{\lambda_n\}$ distribution [73]. This gives a physical interpretation for the EE, quantifying how broad is the distribution of the Schmidt coefficients. In other words, how many effective modes contribute to the state.

Some fundamental properties of the von Neumman entropy are the following:

$$S_A = 0 \quad \Longleftrightarrow \quad |\Psi\rangle \text{ is separable.} \tag{4.18}$$

$$S_A = S_B \quad \text{for pure states} \tag{4.19}$$

$$S_A \leq \ln \min(d_A, d_B) \quad \text{equal for maximally entangled} \tag{4.20}$$

$$S(\hat{\rho}_{AB}) \leq S_A + S_B \quad \text{equal if} \quad \hat{\rho}_{AB} = \hat{\rho}_A \otimes \hat{\rho}_B \tag{4.21}$$

Rényi entropy

In a more general way, the family of Rényi entropies is defined as

$$S_\alpha(\hat{\rho}) = \frac{1}{1-\alpha} \ln \mathrm{Tr}\left(\hat{\rho}^\alpha\right), \qquad \alpha > 0, \quad \alpha \neq 1. \tag{4.22}$$

When $\alpha \to 1$ we obtain again the vN entropy

$$\lim_{\alpha \to 1} S_\alpha(\hat{\rho}) = S(\hat{\rho}). \tag{4.23}$$

Another relevant case is the Rényi entropy for $\alpha = 2$, directly related to the purity

$$S_2(\hat{\rho}) = -\ln \mathrm{Tr}(\hat{\rho}^2). \tag{4.24}$$

This quantity is specially relevant experimentally, because it can be directly measured in quantum simulations through protocols based on interference of two copies of the system, or through randomized measurements [74, 75, 76]. This protocols have been already implemented for ultracold atoms [74] and ion traps [75]. This opens the possibility to test and measure theoretical predictions of entanglement.

Both the Rényi and von Neumann entropy share the same qualitative behaviour.

Bipartitions for BHM's

In lattice models, a spatial bipartition is a natural choice, choosing the set of sites dividing two regions A and B. For a system with N particles, the Hilbert space can be decomposed as

$$\mathcal{H} = \bigoplus_{n_A=0}^{N} \mathcal{H}_A^{(n_A)} \otimes \mathcal{H}_B^{(N-n_A)}. \tag{4.25}$$

where n_A is the particle number in subsystem A.

This structure implies that the reduced density matrix $\hat{\rho}_A$ is block diagonal. This property becomes essential for numerical and analytical purposes.

4.2 Area Law and corrections

For many-body systems, another important property of the entanglement is that the EE does not grow arbitrarily with the size of the system, but rather satisfying a geometrical restriction known as the area law [52, 77, 78].

Let us consider a state $|\Psi\rangle$ for a quantum system defined in a d-dimensional lattice,

and let A be a spatial region with a frontier ∂A and characteristic lineal size L. For a broad family of local systems, with interactions of short range, the following is satisfied

$$S_A \sim \alpha \, |\partial A|, \tag{4.26}$$

where $|\partial A|$ is the area of the frontier between A and B, and α is a coefficient dependent of the microscopic parameters of the Hamiltonian.

The physical origin of the law is that, for systems with short-range correlations and local interactions (with correlation length ξ), the quantum correlations between A and B are dominated by the neighbouring sites near the frontier and the number of those pairs of sites scales with the area. Generally, the ground-state of any local Hamiltonian with a gap in 1D strictly satisfies the area law[79]. This is the reason behind the validity of methods like DMRG or MPS for 1D gapped systems[72, 35].

When the system is gapless, there's a divergence in the correlation length ξ and the argument doesn't apply anymore. Therefore, the EE may exhibit corrections to the area law of the form [80, 81]):

$$S_A = \alpha \, |\partial A| + \beta \, \ln L + \gamma + \mathcal{O}(L^{-1}), \tag{4.27}$$

Physically, when $\beta \neq 0$, the system exhibits gapless degrees of freedom or entanglement with long range. γ is the topological entanglement term, $\gamma \neq 0$ means that the system is topologically protected, i.e., the ground-state has a global entanglement, invariant under any local unitary transformation.

4.3 Entanglement entropy: an order parameter

Traditionally, quantum phases are distinguished through local order parameters like the superfluid order parameter $\psi = \langle \hat{b} \rangle$ or the magnetization $\langle \hat{\sigma}^z \rangle$. This characterization, formalized by Landau, has been successful to describe quantum phase transitions [14]. However, there are fundamental limitations. First, there are phases with topological order (FQHE, topological liquid spin), with no local order parameter, but with non-trivial quantum structure[82, 80]; there exist phase transitions sharing the order parameter, but differing in subtle aspects (e.g. spin liquids transitions, deconfinement transitions); for highly correlated many-body systems, long-range correlations are sometimes hard to manifest locally.

In this context, the EE offers a non-local and purely quantum characterization complementing the local order parameters[67, 52]. Many advantages include universality laws like the area law [52], the sensitivity through the singularities at the critical

points [48, 56] and the genuine non-locality.

In general, the numerical calculation of the EE for many-body systems is computationally expensive, as it requires to compute the reduced density matrix $\hat{\rho}_A$, whose size grows exponentially with system size. Therefore, approximation or specialized methods may be necessary (see Chapter 5).

Chapter 5

Solving Methods

5.1 Exact Diagonalization

Exact diagonalization (ED) is the most fundamental computational method to study quantum many-body systems. It is conceptually straightforward: given a Hamiltonian $\hat{H}$ defined over a Hilbert space of finite dimension $\mathcal{H}$, the ED consist in constructing explicitly the matrix representing $\hat{H}$ in an appropriate basis, and solve the eigenproblem to find its eigenvectors and eigenvalues through typical linear algebra numerical methods.

For the BHM, with N_s sites and N bosons, the Hilbert space is constructed through the Fock occupation states

$$|\mathbf{n}\rangle = |n_1, n_2, \ldots, n_{N_s}\rangle, \tag{5.1}$$

Where $n_i \geq 0$ is the particle number at site i, subject to the restriction to the total particle number $\sum_{i=1}^{N_s} n_i = N$. The dimension for this system is

$$\dim(\mathcal{H}) = \frac{(N + N_s - 1)!}{N!(N_s - 1)!}, \tag{5.2}$$

which grows combinatorially with the system size, being the main limitation of the method.

In practice, the occupation by site is truncated to a maximum of $n_{\max}$, so $n_i \in \{0, 1, \ldots, n_{\max}\}$. This approximation is controlled because for systems with $U/J \gg 1$ (MI phase), the probability of high occupations is exponentially small, hence $n_{\max} = n_0 + 3$, where n_0 is the mean occupation, tends to be sufficient.

Once we have enumerated the states of the basis $\{|\mathbf{n}_k\rangle\}_{k=1}^{\mathcal{D}}$, the matrix elements are given by

$$H_{kl} = \langle \mathbf{n}_k | \hat{H} | \mathbf{n}_l \rangle. \tag{5.3}$$

For the standard Bose-Hubbard Hamiltonian.

$$\hat{H}_{\text{BH}} = -t_0 \sum_{\langle i,j \rangle} \left(\hat{b}_i^\dagger \hat{b}_j + \text{h.c.} \right) + \frac{U}{2} \sum_i \hat{n}_i(\hat{n}_i - 1) - \mu \sum_i \hat{n}_i. \tag{5.4}$$

Given that we only allow hopping to neighbouring sites, each state is linked to a small subset of states (proportional to $N_s \cdot n_{\max}$), which makes it useful to use sparse linear algebra approaches such as the Lanczos algorithm, particularly efficient for symmetric matrices.

The most common way to enumerate the basis is by the lexicographic ordering, resulting in a symmetric matrix for the BHM, going from the state $|N, 0, \ldots, 0\rangle$ to $|0, \ldots, 0, N\rangle$. Following Zhang's work, the procedure is as follows: Consider two vectors $|n_1, n_2, \ldots, n_{N_s}\rangle$ and $\left|n'_1, n'_2, \ldots, n'_{N_s}\right\rangle$. There exists an index $1 \leq k \leq N_s - 1$ such that all occupations before site k are identical for both vectors. That is,

$$n_i = n'_i \quad \forall\, i \text{ with } 1 \leq i \leq k-1,$$

while $n_k \neq n'_k$.

For example, for the vectors $|131100\rangle$ and $|131010\rangle$ the index is $k = 4$, since $n_4 \neq n'_4$ and all preceding entries coincide.

We say that $|n_1, n_2, \ldots, n_{N_s}\rangle$ is greater than $\left|n'_1, n'_2, \ldots, n'_{N_s}\right\rangle$ if $n_k > n'_k$, and smaller otherwise. In this way, we define a lexicographic ordering as illustrated in Table 5.1.

v	n_1	n_2	n_3
1	3	0	0
2	2	1	0
3	2	0	1
4	1	2	0
5	1	1	1
6	1	0	2
7	0	3	0
8	0	2	1
9	0	1	2
10	0	0	3

Table 5.1. Example of lexicographic ordering for a basis with $N = N_s = 3$.

The construction of this ordering, starting from the vector $|n_1, n_2, \ldots, n_{N_s}\rangle$ with $n_{N_s} < N$, proceeds as follows:

If $n_i = 0 \quad \forall\, i$ with $k+1 \leq i \leq M-1$, the following vector $\left|n'_1, n'_2, \ldots, n'_{N_s}\right\rangle$ is defined by

- $n'_i = n_i \quad \forall\, i$ with $1 \leq i \leq k-1$,
- $n'_k = n_k - 1$,
- $n'_{k+1} = N - \sum_{i=1}^{k} n'_i$, and $n'_i = 0$ for $i \geq k+2$.

As a result we obtain the sparsity pattern of Fig. 5.1.

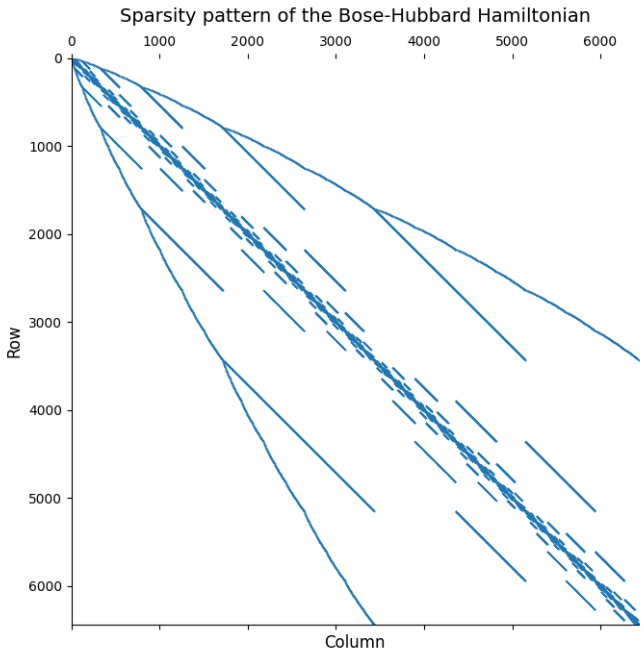

Figure 5.1. The plot shows the non-zero elements of the BHM matrix with $N = N_s = 8$. The matrix is mostly zero (sparse).

Computing entanglement entropy

Once the ground state $|\psi_0\rangle$ is obtained, the bipartite von Newmann EE considering the bipartition $A \cup B$ can be computed from the reduced density $\hat{\rho}^A$, using

$$S(\hat{\rho}^A) = -\mathrm{Tr}[\hat{\rho}^A \ln \hat{\rho}^A] \tag{5.5}$$

The first step is to fix the physical parameters $(N_s, N, U, t_0, J_D, J_B, g_{\text{eff}})$ for a given desired configuration of the system, for N_s sites and N particles.

Then perform the lexicographic ordering of the Fock basis to construct the Hamiltonian and solve the eigenproblem.

Then we can express the density matrix of the global state:

$$\hat{\rho}^{AB} = |\psi_0\rangle \langle\psi_0| , \tag{5.6}$$

Then we need to define a bipartition for the system. Given that the EBHM's define an E/O sublattice structure, it is natural to select an even-odd bipartition. Once the bipartition is defined, we need to carefully map the elements to the reduced basis $\hat{\rho}^{AB} \to \hat{\rho}^A$. Operationally, this is the partial tracing over B. And we obtain $\hat{\rho}^A$, the reduced density matrix, which can be diagonalized to be factorized into

$$\hat{\rho}^A = W_{\rho^A}\, D_{\rho^A}\, W_{\rho^A}^{-1}, \tag{5.7}$$

where D_{ρ^A} is the diagonal eigenvalues matrix containing $\{\lambda_\alpha\}$. With this decomposition we can compute the logarithm of the matrix as

$$\ln \hat{\rho}^A = W_{\rho^A}\, \ln D_{\rho^A}\, W_{\rho^A}^{-1}, \tag{5.8}$$

and finally we can obtain the entanglement entropy with the trace

$$S(\hat{\rho}^A) = -\mathrm{Tr}\left[\hat{\rho}^A\, \ln \hat{\rho}^A\right] = -\sum_\alpha \lambda_\alpha\, \ln \lambda_\alpha. \tag{5.9}$$

As it can be seen, this expression is equivalent to the Schmidt decomposition explained on Chapter 4.

This calculation is exact, which makes the ED a reference for the following EE calculation methods.

5.2 Mean-field treatment

The MF treatment constitutes another widely used approximation for the study of phases in the BHM, as it reduces the many-body scenario to an effective local one, keeping the local quantum structure. Its main advantage is the analytic and numerical tractability, even for large systems, at the expense of neglecting the inter-site correlations beyond the mean-field level.

Consider the standard Bose-Hubbard (BH) with hopping t, local interaction U and chemical potential μ:

$$\hat{H}_{\mathrm{BH}} = -t \sum_{\langle ij \rangle} (\hat{b}_i^\dagger \hat{b}_j + \mathrm{H.c.}) + \sum_i \left[\frac{U}{2}\, \hat{n}_i(\hat{n}_i - 1) - \mu\, \hat{n}_i \right]. \tag{5.10}$$

In the mean-field (MF) scheme, following the Gutzwiller ansantz, the total state is approximated into a product os states over the lattice sites:

$$|\Psi_{\mathrm{MF},\alpha}\rangle = \bigotimes_i |\psi_\alpha\rangle_i\,, \qquad |\psi_\alpha\rangle_i = \sum_{n=0}^{n_{\max}} f_{i,n}^{(\alpha)}\, |n\rangle_i\,, \tag{5.11}$$

where the coefficients $f_{i,n}^{(\alpha)}$ are the complex amplitudes satisfying the normalization $|f_{i,n}^{(\alpha)}|^2 = 1$. The key idea of the MF is to decouple the hopping term, eliminating the quantum fluctuations between sites. In order to do that, we write the annihilation operator as $\hat{b}_i = \langle \hat{b}_i \rangle + \delta \hat{b}_i$ and we neglect the quadratic term on the fluctuations $\delta \hat{b}_i^\dagger \delta \hat{b}_j$,

leading to

$$\hat{b}_i^\dagger \hat{b}_j \approx \psi_i^* \hat{b}_j + \hat{b}_i^\dagger \psi_j - \psi_i^* \psi_j, \tag{5.12}$$

$\psi_i = \langle \hat{b}_i \rangle$ being the superfluid parameter on site i. For the extended cases where sublattice modes appear (even sites E and odd sites O), the effective mean-field Hamiltonian is decomposed into two single-site contributions, one for each sublattice, as we will explain later in detail. For the homogeneous case ($\psi_i = \psi$) the resulting Hamiltonian gets decomposed into a sum of local Hamiltonians:

$$\frac{\hat{H}_{\mathrm{MF}}}{N_s} = -zt\left(\phi\,\hat{b}^\dagger + \phi^* \hat{b} - |\phi|^2\right) + \frac{U}{2}\,\hat{n}(\hat{n}-1) - \mu\,\hat{n}, \tag{5.13}$$

where z is the coordination number for the lattice. The parameter $\psi = \langle \hat{b} \rangle$ behaves as the following: $\psi = 0$ in the MI phase, and $\psi \neq 0$ in the SF phase. Typically ψ is found self-consistently. The diagonalization of 5.13 produces local eigenvectors $\{|\psi_\alpha\rangle\}_{\alpha=0}^{n_{\max}}$ and eigenvalues $\{\varepsilon_\alpha\}$, constituting a "natural" basis to reintroducing the correlations via the slave boson approach, as will be discussed in Section 5.3.

Alternative in presence of multiple local minima: global optimization

As stated, for the standard BHM in the mean-field scheme, $\psi = \langle \psi_0 | \hat{b} | \psi_0 \rangle$ is typically found self-consistently, robustly converging to the global ground state. However, the extended Bose-Hubbard models considered for this work present an energetic landscape with multiple local minima in the order parameter space. This originates from the coupling of different spatial modes mediated by the light field, introducing competence between different density and coherence configurations. In this context, the self-consistent iteration may converge to a local minima that does not correspond to the true ground-state.

To resolve this limitation, the MF problem is reformulated as a global optimization problem over the Gutzwiller coefficients. Following the scheme proposed by Caballero-Benítez et al. [45], for a system with two spatial modes (odd sites O and even sites E), both induced by light, the MF state is written as a product state of both subspaces:

$$|\Psi\rangle_b = |\Psi_O\rangle_b \otimes |\Psi_E\rangle_b\,, \qquad |\Psi_\xi\rangle_b = \sum_{n=0}^{n_{\max}} \alpha_n^\xi\, |n\rangle_\xi\,, \tag{5.14}$$

with $\xi \in \{O, E\}$ and subject to the normalization $\sum_n |\alpha_n^\xi|^2 = 1$. The order parameters are obtained through a self-consistent calculation using:

$$\psi_{O/E} = \langle \Psi_{O/E} | \hat{b} | \Psi_{O/E} \rangle, \qquad \rho_{O/E} = \langle \Psi_{O/E} | \hat{n} | \Psi_{O/E} \rangle. \tag{5.15}$$

Then the ground energy is obtained as the global minima of the expectation value of the Hamiltonian over the set of admissible Gutzwiller amplitudes:

$$E_0 = \min_{\{\alpha^O\},\{\alpha^E\}} \langle \hat{H}^b_{\text{eff}} \rangle, \tag{5.16}$$

subject to the self-consistent conditions for ψ and ρ, and the normalization condition for each mode. In practice, this optimization is performed via global minimization algorithms (e.g. gradient methods with multiple starting conditions), evaluating the energy functional in a sufficiently large grid for the parameters space to identify the absolute minimum. This approach guarantees that the obtained solutions corresponds to the true ground state.

5.2.1 Mean-Field applied to the EBHM's

Density coupling (J_D)

Following Section 2.2, we end up with the effective Hamiltonian.

$$\hat{H}^b_{\text{eff}} = \hat{H}_{\text{BH}} + \frac{g_{\text{eff}}}{N_s}|J_D|^2 \left(\sum_\nu \hat{n}_{O,\nu} - \hat{n}_{E,\nu} \right)^2, \tag{5.17}$$

to which the mean-field approach is applicable, resulting in the following mean-field effective Hamiltonian with sublattice decomposition

$$\hat{H}^b_{\text{eff}} \approx \hat{H}^O_{\text{eff}} + \hat{H}^E_{\text{eff}}, \tag{5.18}$$

with

$$\hat{H}^\xi_{\text{eff}} = \frac{N_s}{2} \left[-zt_0\hat{\beta} - \mu_\xi \hat{n}_\xi + \frac{U_\xi}{2}\hat{n}_\xi(\hat{n}_\xi - 1) - g_{\text{eff}}|J_D|^2\rho_\xi\hat{n}_\xi - g_{\text{eff}}c_{D,\xi} \right], \tag{5.19}$$

where the chemical potential and the onsite repulsion are renormalized due to the light-matter coupling:

$$\mu_{O/E} = \mu \pm 2\rho g_{\text{eff}}|J_D|^2 \tag{5.20}$$

$$U_{O/E} = U + 2g_{\text{eff}}|J_D|^2/N_s. \tag{5.21}$$

and

$$C_{D,o/e} = (\pm N_s|J_D|^2\Delta\rho\rho_{o/e})/2 - (|J_D|^2\rho^2_{o/e})/2 \tag{5.22}$$

Here $\rho = (\rho_O + \rho_E)/2$ is the average density and $\hat{\beta} = \psi^*_O\hat{b}_E + \psi^*_E\hat{b}_O + \psi_O\hat{b}^\dagger_E + \psi_E\hat{b}^\dagger_O - (\psi^*_O\psi_E + \text{c.c.})$ the MF hopping operator.

For this model, we get three relevant order parameters: the superfluid order parameter, the average density, and the density imbalance.

5.2.2 MI limit

Some analytic results can be found for the BHM using this MF formulation. Using Eq.5.13, for $t/U \ll 1$, then $\psi \to 0$, and the MF Hamiltonian is reduced to

$$\hat{H}_{\mathrm{MF}} = \frac{U}{2}\,\hat{n}(\hat{n}-1) - \mu\,\hat{n}, \tag{5.23}$$

which is already diagonal in the Fock basis. Its eigenvalues result

$$E(n) = \frac{U}{2}\,n(n-1) - \mu n. \tag{5.24}$$

Minimizing Eq. 5.24 for integer filling, we get that the occupation number for the ground-state is

$$n_0 = \left\lfloor \frac{\mu}{U} \right\rfloor + 1, \qquad \mu \geq 0, \tag{5.25}$$

$$n_0 = 0, \qquad \mu < 0. \tag{5.26}$$

Thus, the local coefficients of the ground state are $f^{(0)}_{i,n} = \delta_{n,n_0}$ and the Gutwiller ansatz exactly reproduces the many-body Mott state

$$|\Psi_{\mathrm{MF},0}\rangle = \bigotimes_i |n_0\rangle_i\,, \tag{5.27}$$

this is a product state without entanglement between sites. This reflects the fact that, in the MI phase, the EE for a system bipartition is expected to be zero.

5.2.3 SF limit

Now, taking the opposite limit $U/t \to 0$, the BHM MF Hamiltonians reduced to free-hopping lattice problem. For this case, the ground-state is exactly a Bose-Einstein condensate within the lowest band approximation. In a homogeneous lattice this corresponds to the state with $\mathbf{k} = 0$. On a MF level, this state is exactly described by a coherent state on each site,

$$|\psi_{\mathrm{SF}}\rangle_i = e^{-|\phi|^2/2} \sum_{n=0}^{\infty} \frac{\phi^n}{\sqrt{n!}}\,|n\rangle_i \equiv |\phi\rangle_i\,, \tag{5.28}$$

with $\phi = \langle \hat{b} \rangle \neq 0$ [53]. The corresponding many-body state, given the Gutzwiller ansatz, is

$$|\Psi_{\mathrm{SF}}\rangle = \bigotimes_i |\phi\rangle_i \,, \tag{5.29}$$

satisfying the Gutzwiller equation with Poisson coefficients given by

$$f_n^{(0)} = e^{-|\phi|^2/2} \frac{\phi^n}{\sqrt{n!}}. \tag{5.30}$$

For this state, the energy by site is

$$\frac{E_{\mathrm{SF}}}{N_s} = -zt|\phi|^2, \tag{5.31}$$

minimized with fixed density $|\phi|^2 = \rho = N/N_s$ by the chemical potential $\mu = -zt$ (minimal energy condition in the free band). The fluctuations are maximized and Poisson-like:

$$\langle \hat{n} \rangle = |\phi|^2, \qquad \langle (\Delta \hat{n})^2 \rangle = |\phi|^2, \tag{5.32}$$

which reflects the well-defined nature of the condensate: the coherent state maximized the particle fluctuations while minimizing the phase uncertainty.

For the regime of weak interaction ($U/zt \ll 1$) the coherent state is still a good approximation, with perturbative corrections around U/zt progressively reducing the number fluctuations. As U/zt increases, the Gutzwiller state incorporates more Fock components and the coefficient distribution moves further away from the Poissonian, until it reaches $U/zt \gtrsim (U/zt)_c$, when the system enters the MI phase with $\phi = 0$.

5.3 Slave Bosons approach: re-introducing fluctuations on mean-field

The mean-field treatment of Section 5.2 captures an accurate description of the phase diagram for the BHM and its extensions, but as discussed, this is a local approximation incapable of capturing the quantum correlations between sites that give rise to a finite entanglement. The slave bosons method (SB) allows to go beyond, reintroducing the quantum fluctuations as harmonic excitations around the mean-field (MF) solutions [83, 84, 48]. The main appeal of this treatment is that it reduces the strongly interacting BH Hamiltonian to a quadratic form for all the phases of the diagram, including the critical points, which opens the door to an exact computation of the entanglement properties through the covariant matrices formalism [85, 86].

In this section we will develop the step-by-step method, first for the standard BHM,

then for the EBH J_D model.

5.3.1 SB for the BHM

As described in Section 5.2, the diagonalization of the MF single-site Hamiltonian

$$\frac{\hat{H}_{\mathrm{MF}}}{N_s} = -zt\left(\phi\,\hat{b}^\dagger + \phi^*\hat{b}\right) + \frac{U}{2}\hat{n}(\hat{n}-1) - \mu\hat{n} \tag{5.33}$$

produces a complete set of local eigenstates $\{|\psi_\alpha\rangle\}_{\alpha=0}^{n_{\max}}$ with eigenvalues $\{\varepsilon_\alpha\}$, where $|\psi_0\rangle$ is the ground state and $n_{\max}$ the truncation of the local Fock space. Each eigenstate may be expressed in the Fock basis as

$$|\psi_\alpha\rangle = \sum_{n=0}^{n_{\max}} f_n^{(\alpha)}\,|n\rangle, \tag{5.34}$$

where the coefficients $f_n^{(\alpha)}$ form a unitary matrix $W_{\alpha n} = f_n^{(\alpha)}$ diagonalizing $\hat{H}_{\mathrm{MF}}$. The MF many-body state is the product

$$|\Psi_{\mathrm{MF}}\rangle = \prod_i \left[\sum_{n=0}^{n_{\max}} \frac{f_n^{(0)}}{\sqrt{n!}}(\hat{b}_i^\dagger)^n\right]|0\rangle. \tag{5.35}$$

All the content of the MF is encoded on the coefficients $f_n^{(0)}$ of the local ground state. The superfluid order parameter is $\phi = \sum_n \sqrt{n}\, f_n^{(0)} f_{n-1}^{(0)*}$, zero for MI and non-zero for SF. The excited eigenstates constitute the natural basis on which the quantum fluctuations are going to be constructed.

The key idea of the SB technique is to extend the local Hilbert space by defining $(n_{\max}+1)$ fictitious bosonic particles annihilated and created by $\hat{\beta}_{i,n}$ and $\hat{\beta}_{i,n}^\dagger$. These are called SB or Schwinger bosons operators, subject to the hardcore restriction

$$\sum_{n=0}^{n_{\max}} \hat{\beta}_{i,n}^\dagger \hat{\beta}_{i,n} = 1, \tag{5.36}$$

guaranteeing that the local state is just one Fock state at a time [48, 83], avoiding double counting. Under this representation, each Fock state $|n\rangle$ is created from a slave boson through a fictitious vacuum $|n\rangle_i = \hat{\beta}_{i,n}^\dagger|0_{\mathrm{SB}}\rangle$. Then the original bosonic operator is reconstructed as

$$\hat{b}_i = \sum_{n=0}^{n_{\max}-1} \sqrt{n+1}\;\hat{\beta}_{i,n}^\dagger\,\hat{\beta}_{i,n+1}. \tag{5.37}$$

In general, a local operator $\hat{O}_i$ is written under this representation as

$$\hat{O}_i = \sum_{\alpha,\beta} \hat{\gamma}_{i,\alpha}^\dagger\, O_{\alpha\beta}\,\hat{\gamma}_{i,\beta}, \qquad O_{\alpha\beta} = \langle\psi_\alpha|\hat{O}|\psi_\beta\rangle, \tag{5.38}$$

where we have introduced the rotated SB operators $\hat{\gamma}_{i,\alpha}$ defined as

$$\hat{\beta}_{i,n} = \sum_{\alpha} f_n^{(\alpha)}\, \hat{\gamma}_{i,\alpha}, \qquad \hat{\gamma}_{i,\alpha} = \sum_{n} f_n^{(\alpha)*}\, \hat{\beta}_{i,n}. \tag{5.39}$$

Given this definition, the rotated operators $\hat{\gamma}_{i,\alpha}$ are the slave bosons in the MF eigenbasis, i.e. each MF excited state is created from the vacuum $\hat{\gamma}^\dagger_{i,\alpha}|0_{\mathrm{SB}}\rangle = |\psi_\alpha\rangle_i$.

Having defined this operators, we perform an approximation, "condensing" the $\hat{\gamma}_{i,0}$ bosons (MF ground state), and treating the excitations as weak fluctuations. formally:

$$\hat{\gamma}^{(\dagger)}_{i,0} \approx 1, \qquad \langle \hat{\gamma}^\dagger_{i,\alpha}\hat{\gamma}_{i,\alpha}\rangle \ll 1 \quad \text{para } \alpha > 0. \tag{5.40}$$

and implementing (5.36) we end up with

$$\hat{\gamma}^{(\dagger)}_{i,0} \approx \sqrt{1 - \sum_{\alpha>0} \hat{\gamma}^\dagger_{i,\alpha}\hat{\gamma}_{i,\alpha}} \approx 1 - \frac{1}{2}\sum_{\alpha>0} \hat{\gamma}^\dagger_{i,\alpha}\hat{\gamma}_{i,\alpha} + \mathcal{O}(\gamma^4). \tag{5.41}$$

With this substitution, the bosonic operator (5.37) is expanded as

$$\hat{b}^\dagger_i \approx \tilde{F}_{00}\left(1 - \sum_{\alpha>0} \hat{\gamma}^\dagger_{i,\alpha}\hat{\gamma}_{i,\alpha}\right) + \sum_{\alpha>0}\left(\tilde{F}_{0\alpha}\,\hat{\gamma}_{i,\alpha} + \hat{\gamma}^\dagger_{i,\alpha}\tilde{F}_{\alpha 0}\right) + \mathcal{O}(\gamma^2), \tag{5.42}$$

where we define the matrix elements

$$\tilde{F}_{\alpha\beta} = \langle \psi_\alpha | \hat{b}^\dagger | \psi_\beta \rangle. \tag{5.43}$$

Notice that$\tilde{F}_{00} = \phi$, zero for MI and non-zero for SF. Analogously, we also define

$$\tilde{G}_{\alpha\beta} = \langle \psi_\alpha | \tfrac{U}{2}\hat{n}(\hat{n}-1) - \mu\hat{n} | \psi_\beta \rangle. \tag{5.44}$$

Using (5.42) on the BH Hamiltonian (5.10), we get [48]

$$\hat{H} = H^{(0)} + \hat{H}^{(1)} + \hat{H}^{(2)} + \mathcal{O}(\gamma^3), \tag{5.45}$$

where:

$H^{(0)}$ is a shift.

$\hat{H}^{(1)} = \sum_i \sum_{\alpha>0}\left[\hat{\gamma}^\dagger_{i,0}\langle\psi_0|\hat{H}_{\mathrm{MF}}|\psi_\alpha\rangle\hat{\gamma}_{i,\alpha} + \mathrm{h.c.}\right]$ is zero due to the definition of $|\psi_\alpha\rangle$ as eigenstate of $\hat{H}_{\mathrm{MF}}$, and the orthogonality of the basis.

$\hat{H}^{(2)}$ is the quadratic Hamiltonian describing all the fluctuations. It is composed of

the following contributions:

$$\hat{H}_{\text{site}} = \sum_{i} \sum_{\alpha,\beta>0} \hat{\gamma}^{\dagger}_{i,\alpha} A^{(0)}_{\alpha\beta} \hat{\gamma}_{i,\beta}, \tag{5.46}$$

$$\hat{H}_{\text{hop}} = \sum_{\langle i,j\rangle} \sum_{\alpha,\beta>0} \hat{\gamma}^{\dagger}_{i,\alpha} A^{(1)}_{\alpha\beta} \hat{\gamma}_{j,\beta}, \tag{5.47}$$

$$\hat{H}_{\text{pairs}} = \frac{1}{2} \sum_{\langle i,j\rangle} \sum_{\alpha,\beta>0} \left(\hat{\gamma}_{i,\alpha} B_{\alpha\beta} \hat{\gamma}_{j,\beta} + \text{h.c.}\right), \tag{5.48}$$

Using the matrices defined as

$$A^{(0)}_{\alpha\beta} = \delta_{\alpha\beta}(\varepsilon_\alpha - \varepsilon_0), \tag{5.49}$$

$$A^{(1)}_{\alpha\beta} = -t_0 \left(\tilde{F}_{\alpha 0}\tilde{F}^{*}_{0\beta} + \tilde{F}_{0\beta}\tilde{F}^{*}_{0\alpha}\right), \tag{5.50}$$

$$B_{\alpha\beta} = -t_0 \left(\tilde{F}_{0\alpha}\tilde{F}^{*}_{0\beta} + \tilde{F}_{0\beta}\tilde{F}^{*}_{0\alpha}\right). \tag{5.51}$$

Term by term, (5.46) contains the MF excitation gaps, (5.47) describes the propagation of the fluctuations between neighbours, and (5.48) describes the creation-annihilation of two excitations in neighbouring sites (this are the anomalous processes giving rise to entanglement).

Then it is useful to use the momentum representation for the Hamiltonian. For the homogeneous model, this transformation is $\hat{\gamma}_{i,\alpha} = V^{-1/2} \sum_{\mathbf{k}} e^{i\mathbf{k}\cdot\mathbf{R}_i} \hat{\gamma}_{\mathbf{k},\alpha}$, with$V = N_s$ the number of sites. Then the Hamiltonian, now quadratic, reads [48]

$$\hat{H}^{(2)} = \frac{1}{2} \sum_{\mathbf{k}} \begin{pmatrix} \hat{\boldsymbol{\gamma}}^{\dagger}_{\mathbf{k}} & \hat{\boldsymbol{\gamma}}_{-\mathbf{k}} \end{pmatrix} \mathcal{H}_{\mathbf{k}} \begin{pmatrix} \hat{\boldsymbol{\gamma}}_{\mathbf{k}} \\ \hat{\boldsymbol{\gamma}}^{\dagger}_{-\mathbf{k}} \end{pmatrix} + \text{cte}, \tag{5.52}$$

Notice that the $\alpha = 0$ have been elliminated by consdensation, and we have defined the vector containing all the rotated operators $\hat{\boldsymbol{\gamma}}_{\mathbf{k}} = (\hat{\gamma}_{\mathbf{k},1}, \hat{\gamma}_{\mathbf{k},2}, \ldots, \hat{\gamma}_{\mathbf{k},n_{\max}})^T$. And the $\mathcal{H}_{\mathbf{k}}$ matrix has a block structure

$$\mathcal{H}_{\mathbf{k}} = \begin{pmatrix} \mathbf{A}_{\mathbf{k}} & \mathbf{B}_{\mathbf{k}} \\ \mathbf{B}^{*}_{\mathbf{k}} & \mathbf{A}^{*}_{\mathbf{k}} \end{pmatrix}, \tag{5.53}$$

with the elements

$$\mathbf{A}_{\mathbf{k}} = A^{(0)} + z\eta_{\mathbf{k}} A^{(1)}, \qquad \mathbf{B}_{\mathbf{k}} = z\eta_{\mathbf{k}} B, \tag{5.54}$$

where the lattice form factor is $\eta_{\mathbf{k}} = \frac{1}{z}\sum_{\boldsymbol{\delta}} e^{i\mathbf{k}\cdot\boldsymbol{\delta}}$ ($\boldsymbol{\delta}$ covers all z neighbours of each site). If the lattice has dimension d and is a hypercube, then $\eta_{\mathbf{k}} = \frac{1}{d}\sum_{i=1}^{d} \cos(k_i a)$.

Then we can perform Bogoliubov diagonalization by finding the matrix $P_{\mathbf{k}}$ diago-

nalizing $\Upsilon\mathcal{H}_{\mathbf{k}}$, with

$$\Upsilon = \begin{pmatrix} \mathbf{1}_{n_{\max}} & 0 \\ 0 & -\mathbf{1}_{n_{\max}} \end{pmatrix}, \tag{5.55}$$

preserving the commutation relations for bosons ($P_{\mathbf{k}}^{\dagger}\Upsilon P_{\mathbf{k}} = \Upsilon$) [87]. This gives the diagonal form

$$\hat{H}^{(2)} = \sum_{\mathbf{k}} \sum_{\alpha=1}^{n_{\max}} \omega_{\mathbf{k},\alpha}\, \hat{\lambda}_{\mathbf{k},\alpha}^{\dagger} \hat{\lambda}_{\mathbf{k},\alpha} + \text{cte}, \tag{5.56}$$

from which we can extract the quasiparticle excitation spectrum $\omega_{\mathbf{k},\alpha}$ and the quasiparticle Bogoliubov operators $\hat{\lambda}_{\mathbf{k},\alpha}$.

Entanglement entropy from the slave bosons solution

The most crucial property of this SB approach is that we get a resulting Hamiltonian that is quadratic (5.56). By Wick's theorem, the ground-state of such a Hamiltonian has a gaussian distribution, and the reduced density matrix $\hat{\rho}_A$ (considering bipartition $A|B$) is also gaussian [85]. This allow to completely reconstruct $\hat{\rho}_A$ using the two-point correlations.

Consider the bipartition $A|B$ for the system (A can be, for example, half a torus defined by $L_A \times 2L_A$). For A, we define a correlation matrix as

$$C_A = [\mathbf{C}_{\mathbf{r},\mathbf{r}'}]_{\mathbf{r},\mathbf{r}'\in A}\,, \qquad \mathbf{C}_{\mathbf{r},\mathbf{r}'} = \langle\Psi_0| \begin{pmatrix} \hat{\gamma}_{\mathbf{r}} \\ \hat{\gamma}_{\mathbf{r}}^{\dagger} \end{pmatrix} \begin{pmatrix} \hat{\gamma}_{\mathbf{r}'}^{\dagger} & \hat{\gamma}_{\mathbf{r}'} \end{pmatrix} |\Psi_0\rangle, \tag{5.57}$$

where $|\Psi_0\rangle$ is the quasiparticle vacuum (ground-state of $\hat{H}^{(2)}$). The matrix $\mathbf{C}_{\mathbf{r},\mathbf{r}'}$, can be computed from a Bogoliubov transformation

$$\mathbf{C}_{\mathbf{k}} = P_{\mathbf{k}}\, \mathcal{P}\, P_{\mathbf{k}}^{\dagger}, \qquad \mathcal{P} = \begin{pmatrix} \mathbf{1} & 0 \\ 0 & 0 \end{pmatrix}. \tag{5.58}$$

The spectrum of entanglement is obtained by diagonalizing C_A through the Bogoliubov transformation

$$U_A^{\dagger} \begin{pmatrix} -\mathbf{1} - C^* & F \\ -F^* & C \end{pmatrix} U_A = \begin{pmatrix} \text{diag}(-1 - f_k) & 0 \\ 0 & \text{diag}(f_k) \end{pmatrix}, \tag{5.59}$$

where $f_k = 1/(e^{\omega_k^{(A)}} - 1)$ is the Bose-Einstein distribution with fictitious temperature $T = 1$ [48, 85].

The von Neumann EE is then obtained as the thermal entropy of the quasiparticle gas using the entanglement spectrum

$$S_{\mathrm{vN}} = \sum_k [(1+f_k)\ln(1+f_k) - f_k \ln f_k] \tag{5.60}$$

Considerations for the SF

For a superfluid, the excitation spectrum exhibits a gapless Goldstone mode $\omega_{\mathbf{k}} \propto |\mathbf{k}|$, which produces a divergence $1/|\mathbf{k}|$ in the population of slave bosons. For $d \geq 2$ the integral $\int k^{d-1}dk/k$ actually converges, so the divergence is an artefact of the finite size. However, we still need a special treatment for the $\mathbf{k} = 0$ mode [48, 88].

One strategy is adding a small size-dependent perturbative term . [48, 88]

$$\hat{H} \to \hat{H} - h(L)\sum_i (\hat{b}_i + \hat{b}_i^\dagger), \qquad h(L) \sim L^{-\kappa}, \tag{5.61}$$

using $\kappa = 2d$ creates a gap $\propto \sqrt{h}$ in the Goldstone mode. With this, we are able to fix the divergence of the zero mode.

But one simpler naive strategy is to just skip the $\mathbf{k} = 0$ point in the calculation.

5.3.2 SB for the J_D ($R = 2$) EBHM

The SB method is also applicable to the density coupling EBHM following almost the same steps, with one fundamental modification: the MF solutions have two inequivalent modes (even E and odd O sites)[69].

As described in Section 5.2, the MF solution for the J_D produces two local eigenvectors, one for each sublattice (E/O):

$$|\psi_{O,\alpha}\rangle = \sum_n f_{O,n}^{(\alpha)}|n\rangle, \qquad |\psi_{E,\alpha}\rangle = \sum_n f_{E,n}^{(\alpha)}|n\rangle, \tag{5.62}$$

with eigenvalues $\varepsilon_{O,\alpha}$ and $\varepsilon_{E,\alpha}$, respectively. The order parameters for each sublattice are $\psi_{O/E} = \langle\hat{b}\rangle_{O/E}$ and $\rho_{O/E} = \langle\hat{n}\rangle_{O/E}$.

Then local matrix elements are defined for each sublattice $\xi \in \{O, E\}$

$$b_{\xi,\alpha\beta} = \langle\psi_{\xi,\alpha}|\hat{b}|\psi_{\xi,\beta}\rangle, \qquad n_{\xi,\alpha\beta} = \langle\psi_{\xi,\alpha}|\hat{n}|\psi_{\xi,\beta}\rangle. \tag{5.63}$$

The SB operators are introduced separately for each sublattice, $\hat{\gamma}_{\mathbf{r},\alpha}$ with $\mathbf{r} \in O$ or $\mathbf{r} \in E$. Following the same procedure of 5.3.1, the same procedure of "condensation" to obtain the quadratic expansion is done, producing $\hat{H} = H^{(0)} + \hat{H}^{(2)} + \mathcal{O}(\gamma^3)$, but now the cavity adds extra contributions to $\hat{H}^{(2)}$ [69]:

First, the standard BHM contributions from Eqs. (5.47)-(5.48), but now the matrix

elements $b_{\xi,\alpha\beta}$ depend on each sublattice ξ.

Then the contribution arising from the light-mediated long-range interactions, coupling the sites of the same sublattices ($E-E$ and $O-O$) and from different sublattices ($E-O$) through the $\hat{D}=J_D\sum_\nu(\hat{n}_{O,\nu}-\hat{n}_{E,\nu})$ operator . This contributions result in the matrices

$$A^{\mathrm{LR}}_{\mathbf{r}\alpha,\mathbf{r}'\beta}=2g_{\mathrm{eff}}|J_D|^2 Z_{\mathbf{r}}Z_{\mathbf{r}'}\,n_{\xi,\alpha 0}\,n_{\xi',0\beta}, \tag{5.64}$$

$$B^{\mathrm{LR}}_{\mathbf{r}\alpha,\mathbf{r}'\beta}=2g_{\mathrm{eff}}|J_D|^2 Z_{\mathbf{r}}Z_{\mathbf{r}'}\,n_{\xi,0\alpha}\,n_{\xi',0\beta}. \tag{5.65}$$

where $Z_{\mathbf{r}}=(-1)^{r_x+r_y}$.

An notable difference compared to the BHM is that the long-range terms (5.64)-(5.65) couple the modes $\mathbf{k}$ with $\mathbf{k}+\boldsymbol{\pi}$. This results in a folding of the Brilloin zone, the $\mathbf{k}$ couples with $\mathbf{k}+\boldsymbol{\pi}$, $-\mathbf{k}$ and $-\mathbf{k}-\boldsymbol{\pi}$ so the Hamiltonian (still quadratic) reads

$$\hat{H}^{(2)}=\frac{1}{4}\sum_{\mathbf{k}\in\mathcal{B}}\hat{\Gamma}^\dagger_{\mathbf{k}}\,\mathcal{H}^{(2)}_{\mathbf{k}}\,\hat{\Gamma}^T_{\mathbf{k}}, \tag{5.66}$$

with the vector defined as

$$\hat{\Gamma}_{\mathbf{k}}=(\hat{\boldsymbol{\gamma}}_{\mathbf{k}},\ \hat{\boldsymbol{\gamma}}_{\mathbf{k}+\boldsymbol{\pi}},\ \hat{\boldsymbol{\gamma}}^\dagger_{-\mathbf{k}},\ \hat{\boldsymbol{\gamma}}^\dagger_{-\mathbf{k}-\boldsymbol{\pi}}). \tag{5.67}$$

The $4n_{\max}\times 4n_{\max}$ matrix $\mathcal{H}^{(2)}_{\mathbf{k}}$

$$\mathcal{H}^{(2)}_{\mathbf{k}}=\begin{pmatrix}\mathbf{A}_{\mathbf{k}} & \mathbf{B}_{\mathbf{k}}\\ \mathbf{B}_{\mathbf{k}} & \mathbf{A}_{\mathbf{k}}\end{pmatrix}. \tag{5.68}$$

The$\mathbf{A}_{\mathbf{k}}$ and $\mathbf{B}_{\mathbf{k}}$ matrices have a 2×2 structure, given by

$$\mathbf{A}_{\mathbf{k}}=\begin{pmatrix}\frac{A^e_{\mathbf{k}}+A^o_{\mathbf{k}}}{2}+\frac{A^{eo}_{\mathbf{k}}+A^{oe}_{\mathbf{k}}}{2} & \frac{A^e_{\mathbf{k}}-A^o_{\mathbf{k}}}{2}-\frac{A^{eo}_{\mathbf{k}}-A^{oe}_{\mathbf{k}}}{2}\\ \frac{A^e_{\mathbf{k}}-A^o_{\mathbf{k}}}{2}+\frac{A^{eo}_{\mathbf{k}}-A^{oe}_{\mathbf{k}}}{2} & \frac{A^e_{\mathbf{k}}+A^o_{\mathbf{k}}}{2}-\frac{A^{eo}_{\mathbf{k}}+A^{oe}_{\mathbf{k}}}{2}\end{pmatrix}, \tag{5.69}$$

with

$$A^e_{k,\alpha\beta}=(E^{MF}_{e,\alpha}-E^{MF}_{e,0})\delta_{\alpha,\beta}+g_{\mathrm{eff}}|J_D|^2\,n_{e,\alpha 0}\,n_{e,0\beta}[\delta_{k,\pi}+\delta_{k,0}] \tag{5.70}$$

$$A^o_{k,\alpha\beta}=(E^{MF}_{o,\alpha}-E^{MF}_{o,0})\delta_{\alpha,\beta}+g_{\mathrm{eff}}|J_D|^2\,n_{o,\alpha 0}\,n_{o,0\beta}[\delta_{k,\pi}+\delta_{k,0}] \tag{5.71}$$

$$A^{eo}_{k,\alpha\beta}=g_{\mathrm{eff}}|J_D|^2\,n_{e,\alpha 0}\,n_{o,0\beta}[\delta_{k,\pi}-\delta_{k,0}]-\frac{tf_k}{N_s}\left(b^\dagger_{o,0\beta}b_{e,\alpha 0}+b^\dagger_{e,\alpha 0}b_{o,0\beta}\right) \tag{5.72}$$

$$A^{oe}_{k,\alpha\beta}=g_{\mathrm{eff}}|J_D|^2\,n_{o,\alpha 0}\,n_{e,0\beta}[\delta_{k,\pi}-\delta_{k,0}]-\frac{tf_k}{N_s}\left(b^\dagger_{e,0\beta}b_{o,\alpha 0}+b^\dagger_{o,\alpha 0}b_{e,0\beta}\right). \tag{5.73}$$

and

$$\mathbf{B_k} = \begin{pmatrix} \frac{B^e_k+B^o_k}{2} + \frac{B^{eo}_k+B^{oe}_k}{2} & \frac{B^e_k-B^o_k}{2} - \frac{B^{eo}_k-B^{oe}_k}{2} \\ \frac{B^e_k-B^o_k}{2} + \frac{B^{eo}_k-B^{oe}_k}{2} & \frac{B^e_k+B^o_k}{2} - \frac{B^{eo}_k+B^{oe}_k}{2} \end{pmatrix} \tag{5.74}$$

with

$$B^e_{k,\alpha\beta} = g_{\text{eff}} |J_D|^2 \, n_{e,0\alpha} \, n_{e,0\beta} [\delta_{k,\pi} + \delta_{k,0}] \tag{5.75}$$

$$B^o_{k,\alpha\beta} = g_{\text{eff}} |J_D|^2 \, n_{o,0\alpha} \, n_{o,0\beta} [\delta_{k,\pi} + \delta_{k,0}] \tag{5.76}$$

$$B^{eo}_{k,\alpha\beta} = g_{\text{eff}} |J_D|^2 \, n_{e,0\alpha} \, n_{o,0\beta} [\delta_{k,\pi} - \delta_{k,0}] - \frac{t f_k}{N_s} \left(b^\dagger_{o,0\beta} b_{e,0\alpha} + b^\dagger_{e,0\alpha} b_{o,0\beta} \right) \tag{5.77}$$

$$B^{oe}_{k,\alpha\beta} = g_{\text{eff}} |J_D|^2 \, n_{o,0\alpha} \, n_{e,0\beta} [\delta_{k,\pi} - \delta_{k,0}] - \frac{t f_k}{N_s} \left(b^\dagger_{e,0\beta} b_{o,0\alpha} + b^\dagger_{o,0\alpha} b_{e,0\beta} \right). \tag{5.78}$$

with $f_{\mathbf{k}} = 2(\cos k_x + \cos k_y)$ the lattice structure factor.

Then the excitation spectrum $\omega_{\mathbf{k},p}$ ($p = 1, \ldots, 2n_{\max}$) is produced by the Bogoliubov diagonalization of (5.66). with this diagonalization the correlation matrix C_A can be constructed. The additional symmetry along the cut $A - B$ allows to decompose C_A in blocks labelled by the moment $k_\parallel$ parallel to the cut.

Chapter 6

Results

On this chapter the numerical results obtained with the approaches discussed on Chapter 5 are presented. First discussing exact diagonalization (ED) for a finite one-dimensional periodic chain. Then the mean-field Gutzwiller results, presenting the phase diagrams for fixed chemical potential μ and for fixed average density ρ.

6.1 Exact diagonalization

The ED was performed for a $1D$ periodic lattice with $N_s = 8$ sites and $N = 8$ bosons. For each relevant set of parameters$(J_D, J_B, g_{\text{eff}})$ we sweep the ratio t_0/U and compute the order parameters necessary to identify the phases discussed in Chapter 3, and then compute the entanglement entropy exactly.

Let $|\psi_0\rangle$ be the normalized ED ground state. The bosonic operators at site i are $\hat{b}_i$ and $\hat{b}_i^\dagger$, and $\hat{n}_i = \hat{b}_i^\dagger \hat{b}_i$. Also, there's a PBC modulo M, so that $i + 1 \equiv 1$ for $i = M$.

The local density and its fluctuations are evaluated at a representative site i as

$$\langle n_i \rangle \equiv \langle \psi_0 | \, \hat{n}_i \, | \psi_0 \rangle \,, \qquad \Delta n_i \equiv \sqrt{\langle \psi_0 | \, \hat{n}_i^2 \, | \psi_0 \rangle - \langle n_i \rangle^2}. \tag{6.1}$$

The superfluid parameter is computed from the nearest-neighbour coherence

$$f_{\text{cond}} \equiv \frac{1}{2N_s} \sum_{i=1}^{N_s} \langle \psi_0 | \, \hat{b}_i^\dagger \hat{b}_{i+1} + \hat{b}_{i+1}^\dagger \hat{b}_i \, | \psi_0 \rangle \,. \tag{6.2}$$

For J_D models we take the collective density operator

$$\hat{D} \equiv \sum_{i=1}^{N_s} (-1)^i \hat{n}_i. \tag{6.3}$$

And the DW parameter is defined as

$$\mathcal{O}_{\text{DW}}^2 \equiv \frac{1}{N_s^2} \langle \hat{D}^2 \rangle = \frac{1}{N_s^2} \langle \psi_0 | \, \hat{D}^2 \, | \psi_0 \rangle \,. \tag{6.4}$$

For J_B models we take the collective bond operator

$$\hat{B} \equiv \sum_{i=1}^{N_s} \left(\hat{b}_i^\dagger \hat{b}_{i+1} + \hat{b}_{i+1}^\dagger \hat{b}_i \right), \tag{6.5}$$

and the bond order parameter

$$\mathcal{O}_{\mathrm{B}} \equiv \frac{1}{N_s^2} \langle \hat{B}^2 \rangle = \frac{1}{N_s^2} \langle \psi_0 | \hat{B}^2 | \psi_0 \rangle . \tag{6.6}$$

Finally, the bipartite von Neumann EE is computed through the pure-state density matrix $\rho = |\psi_0\rangle \langle \psi_0|$. After tracing over subsystem B,

$$\rho_A \equiv \mathrm{Tr}_B \, \rho, \tag{6.7}$$

Then the EE for A is

$$S_A = - \mathrm{Tr}_A \left[\rho_A \ln \rho_A \right]. \tag{6.8}$$

Figure 6.1 shows the Bose-Hubbard result. This case serves as a reference for comparing the EBHM's results shown in Figs. 6.2 and 6.3.

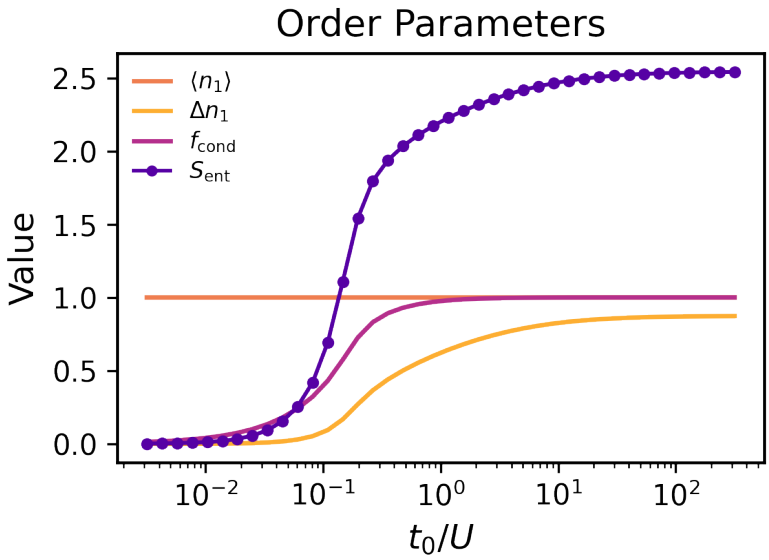

Figure 6.1. ED results for the BHM. For $N = N_s = 8$. Here $g_{\mathrm{eff}} = 0$.

6.2 Mean-field

Now we present the mean-field (MF) results obtained with the Gutzwiller treatment explained in Section 5.2. For diagrams in the $(zt_0/U, \mu)$ plane, the MF Hamiltonian

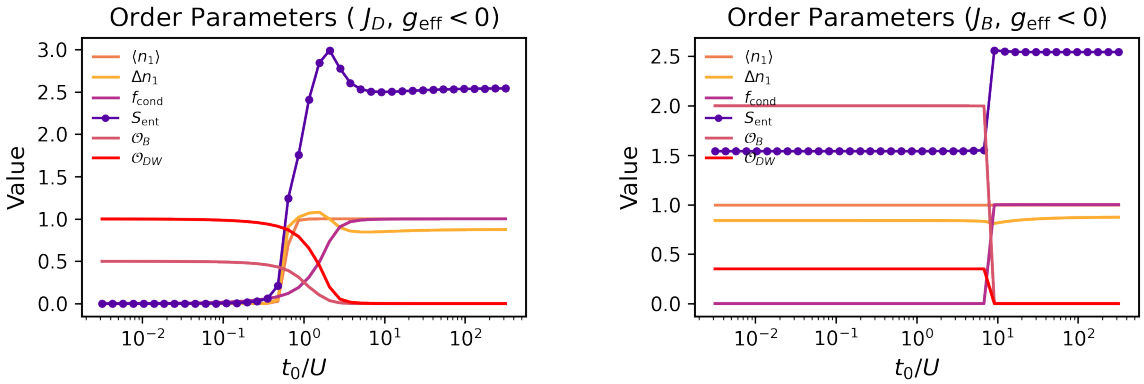

(a) Density model: $J_B = 0$, $g_{\text{eff}} J_D^2 = -4U$.

(b) Bond model: $J_D = 0$, $g_{\text{eff}} J_B^2 = -4U$.

Figure 6.2. ED results for the EBHM with $g_{\text{eff}} < 0$. The panels compare pure density and pure bond couplings. $N = N_s = 8$.

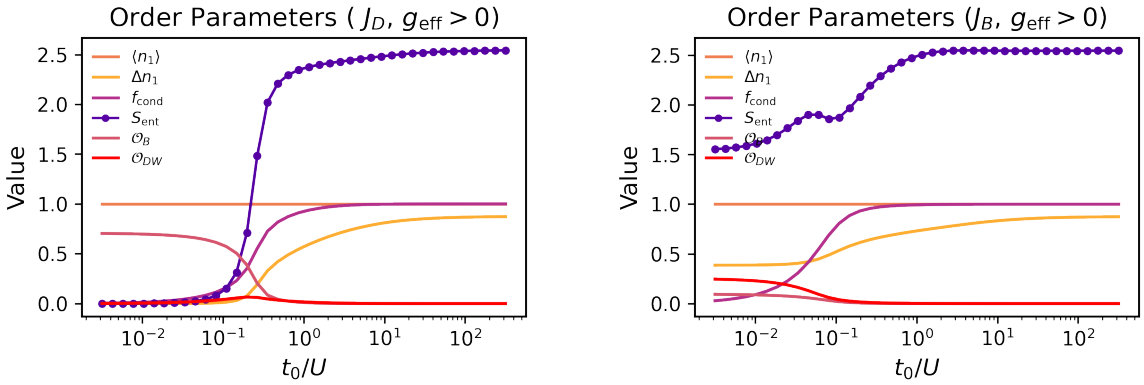

(a) Density model: $J_B = 0$, $g_{\text{eff}} J_D^2 = 4U$.

(b) Bond model: $J_D = 0$, $g_{\text{eff}} J_B^2 = 4U$.

Figure 6.3. ED results for the EBHM with $g_{\text{eff}} > 0$. The panels compare pure density and pure bond couplings. $N = N_s = 8$.

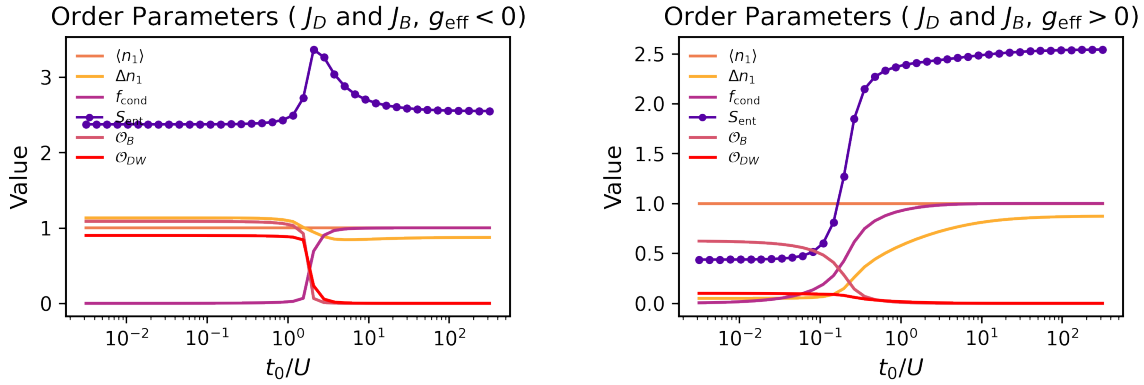

(a) $g_{\text{eff}} J_D^2 = -4U$, $J_B/J_D = 0.25$.

(b) $g_{\text{eff}} J_D^2 = 4U$, $J_B/J_D = 0.25$.

Figure 6.4. ED results for the mixed EBHM with simultaneous density and bond couplings. The panels compare $g_{\text{eff}} < 0$ and $g_{\text{eff}} > 0$. $N = N_s = 8$.

can be solved using self-consistency. For diagrams in the $(zt_0/U, \rho)$ plane, self-consistent iterations can converge to metastable states, so we instead use a variational minimization of the Gutzwiller coefficients and compare balanced and imbalanced solution branches.

Optimization problem

For the systems with even-odd sublattice structure, we use the product-state ansatz

$$|\Psi_{\mathrm{MF}}\rangle = \bigotimes_{i\in O} |\psi_O\rangle \bigotimes_{j\in E} |\psi_E\rangle \,, \tag{6.9}$$

with local states expressed in the Fock basis

$$|\psi_O\rangle = \sum_{n=0}^{n_{\max}} \alpha_n^O \,|n\rangle \,, \qquad |\psi_E\rangle = \sum_{n=0}^{n_{\max}} \alpha_n^E \,|n\rangle \,. \tag{6.10}$$

The coefficients must satisfy

$$\sum_{n=0}^{n_{\max}} |\alpha_n^O|^2 = 1, \qquad \sum_{n=0}^{n_{\max}} |\alpha_n^E|^2 = 1. \tag{6.11}$$

The local parameters are

$$\rho_O \equiv \langle \hat{n} \rangle_O = \langle \psi_O | \, \hat{n} \, | \psi_O \rangle \,, \qquad \rho_E \equiv \langle \hat{n} \rangle_E = \langle \psi_E | \, \hat{n} \, | \psi_E \rangle \,, \tag{6.12}$$

$$\psi_O \equiv \langle \hat{b} \rangle_O = \langle \psi_O | \, \hat{b} \, | \psi_O \rangle \,, \qquad \psi_E \equiv \langle \hat{b} \rangle_E = \langle \psi_E | \, \hat{b} \, | \psi_E \rangle \,. \tag{6.13}$$

We use these parameters to define the density imbalance and the average superfluid order parameters,

$$\Delta\rho \equiv \frac{\rho_O - \rho_E}{2}, \qquad \Sigma\psi \equiv \frac{|\psi_O| + |\psi_E|}{2}. \tag{6.14}$$

For the multicomponent case with $R = 3$, the same notation is generalized to ρ_ξ and ψ_ξ, with $\xi = 1, 2, 3$. We then consider the pairwise density imbalances

$$\Delta\rho_{\xi\eta} \equiv \frac{\rho_\xi - \rho_\eta}{2}. \tag{6.15}$$

Phase diagrams in the (zt_0, μ) plane

At fixed chemical potential, the MF ground state is obtained by iterating the Gutzwiller equations until self-consistency is reached. After convergence, the order parameters $\Sigma\psi$, $\Delta\rho$, and $\Delta\rho_{\xi\eta}$ are computed using Eqs. (6.14) and (6.15). We obtained for the J_D model the results shown in Fig.6.5 and for the multicomponent J_D ($R = 3$) are shown

in Fig.6.6.

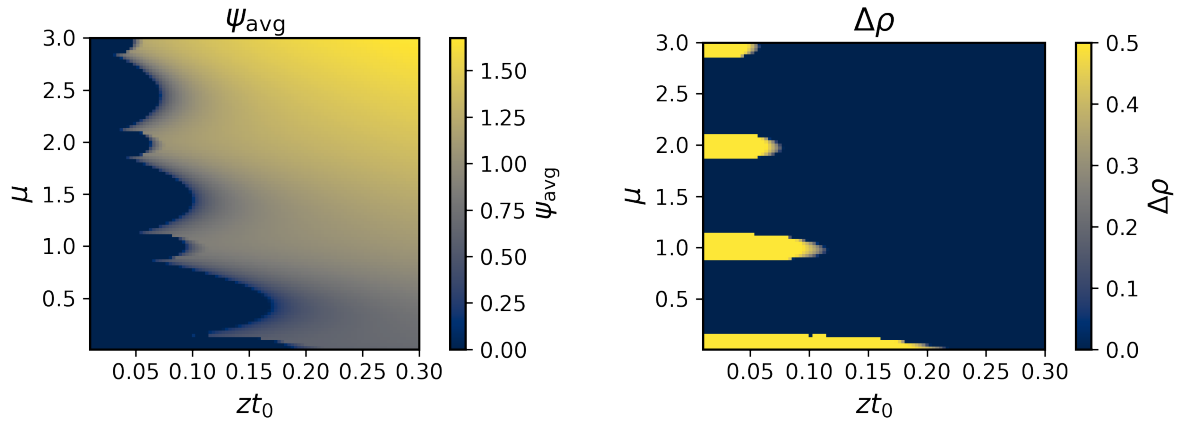

(a) Average superfluid parameter $\Sigma\psi$. **(b)** Density imbalance $\Delta\rho$.

Figure 6.5. Phase diagrams for the J_D EBHM ($R = 2$) in the $(zt_0/U, \mu)$ plane. $J_D = 1$, $g_{\text{eff}} N_s = -0.5U$, $N_s = 100$, $U = 1$, $z = 4$.

Phase diagrams in the (zt_0, ρ) plane

When we want a fixed density ρ, the self-consistent procedure becomes less reliable because the MF energy landscape can contain several local minima. To avoid this, we minimize the Gutzwiller energy variationally at each point $(zt_0/U, \rho)$.

For fixed average density, the variational ground-state energy is written as

$$E_0 = \min_{\{\alpha_n^O, \alpha_n^E\}} \langle \hat{H}_{\text{eff}} \rangle, \tag{6.16}$$

subject to the normalization constraints in Eq. (6.11) and to the density constraint

$$\rho \equiv \frac{\rho_O + \rho_E}{2}. \tag{6.17}$$

All local observables, including $\rho_{O,E}$ and $\psi_{O,E}$, are computed directly from the optimized coefficients.

the two density branches must be compared: Balanced branch($\rho_O = \rho_E = \rho$, or equivalently $\Delta\rho = 0$) and Imbalanced branch ($\Delta\rho \neq 0$, the minimization is initialized with symmetry-breaking configurations).

The physical solution is chosen as

$$E_0 = \min\{E_{\text{bal}}, E_{\text{imb}}\}. \tag{6.18}$$

The corresponding values of $\Sigma\psi$ and $\Delta\rho$ are then computed using the optimal Gutzwiller coefficients.

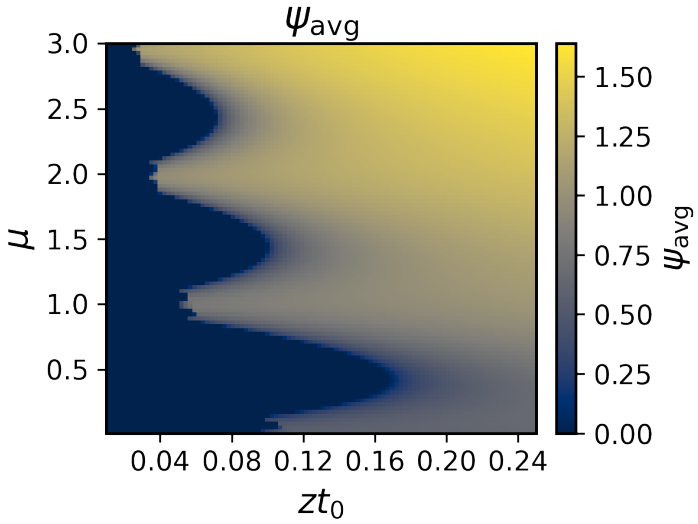

(a) Phase diagram for ψ_{avg}.

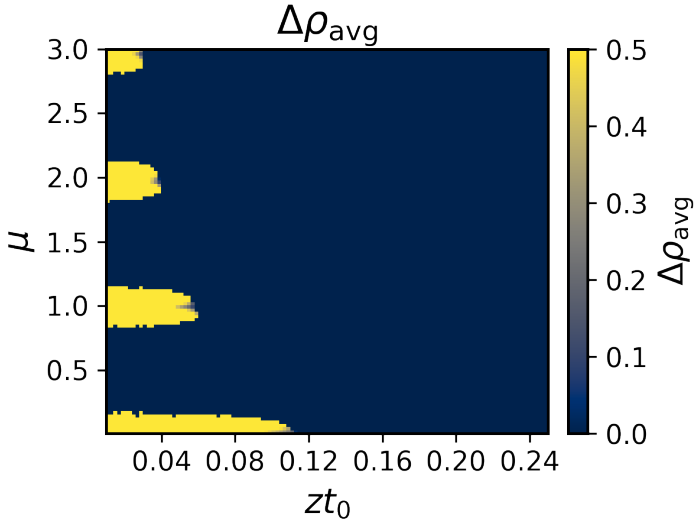

(b) Phase diagram for $\Delta\rho_{\text{avg}}$.

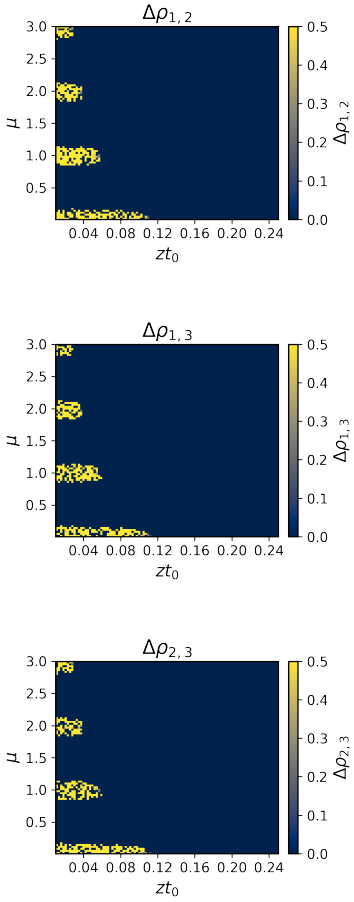

(c) Phase diagram for each $\Delta\rho_{\xi,\eta}$.

Figure 6.6. Mean-field results for the multicomponent ($R = 3$) density-coupled (J_D) EBHM. Left column: average superfluid order parameter ψ_{avg} (top) and average density imbalance $\Delta\rho_{\text{avg}}$ (bottom). Right column: pairwise density imbalances $\Delta\rho_{\xi,\eta}$.

The results for the J_D model using this method are shown in Fig.6.7.

6.3 Slave Bosons Approach

Using the mean-field solution obtained for theJ_D EBHM (Figs. 6.5 and 6.7) we can apply the slave-boson treatment described in Section 5.3.2 to compute the EE. The result is shown in Fig. 6.8. And treating the problem as a global optimization problem over the Gutzwiller coefficients, we were able to obtain the entropy map for a fixed average density. This is shown in Fig. 6.9.

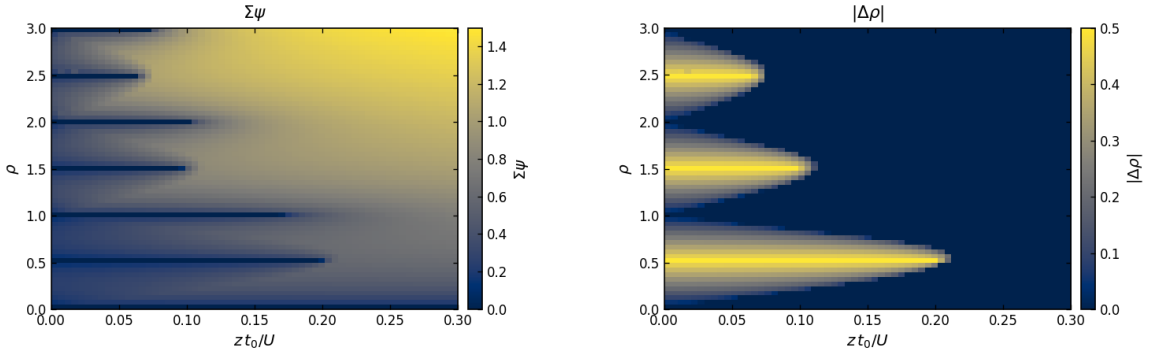

(a) Average superfluid order parameter $\Sigma\psi$.

(b) Density imbalance $\Delta\rho$.

Figure 6.7. Phase diagrams for the J_D EBHM($R = 2$)in the (zt_0, ρ) plane. The results were obtained by variationally optimizing $\alpha_n^{O,E}$. $J_D = 1$, $g_{\text{eff}} N_s = -0.5U$, $N_s = 100$, $U = 1$, $z = 4$.

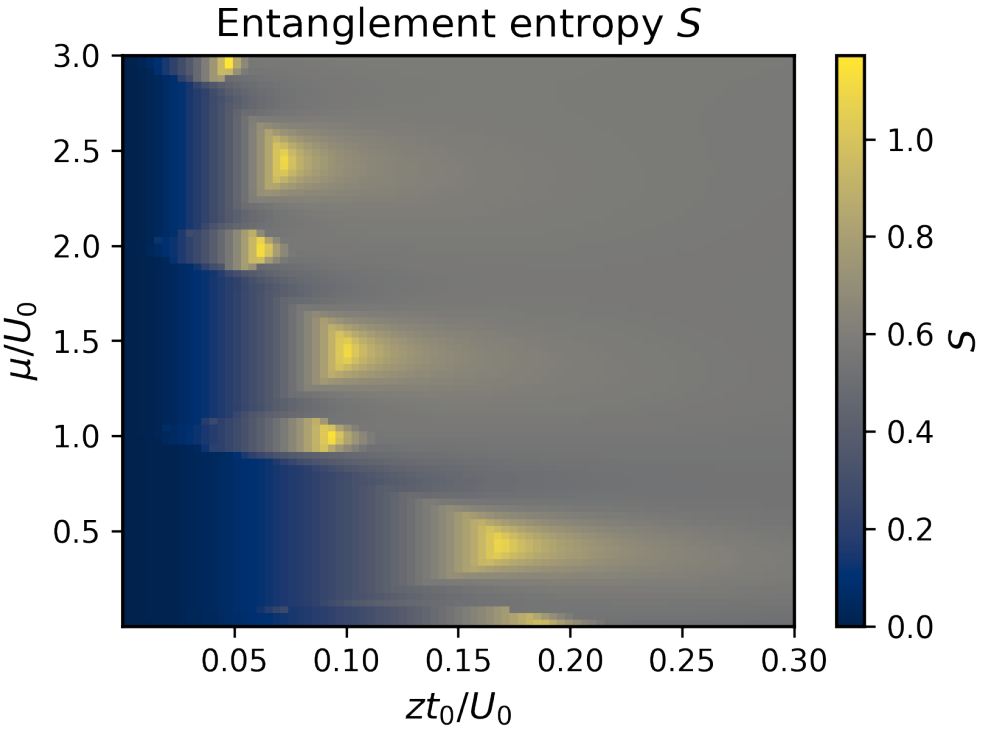

Figure 6.8. Entanglement entropy in the (μ, zt_0) plane for the J_D EBH ($R = 2$) model. Parameters $g_{\text{eff}} N_s = -0.5U$, $N_s = 100$, $J_D = 1.0$, $U = 1$, $z = 4$.

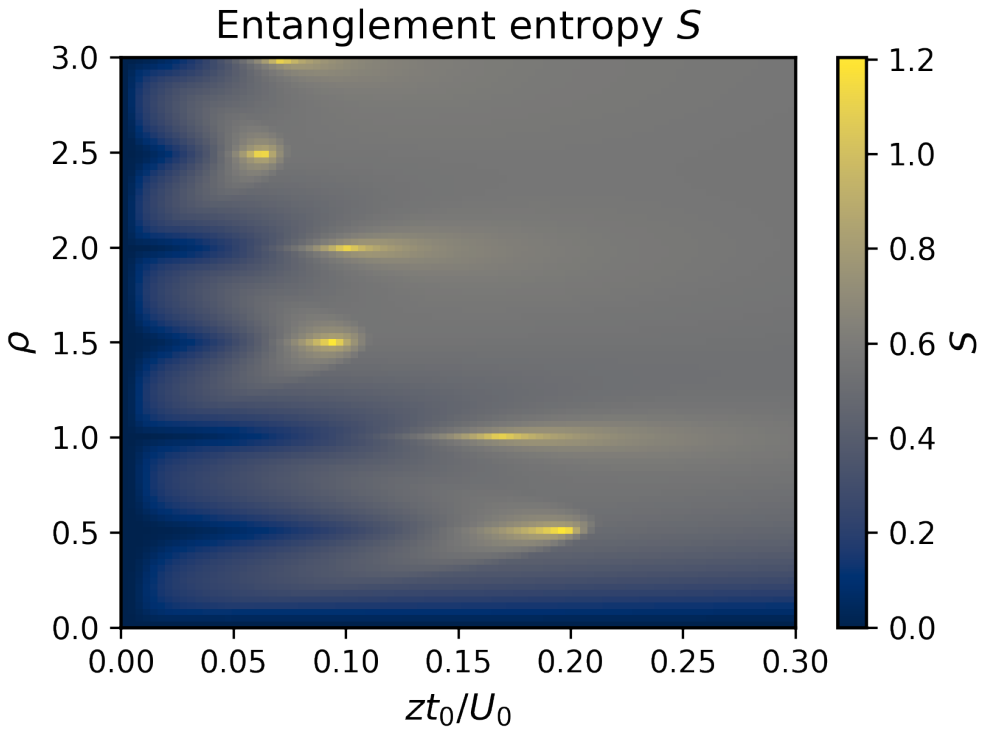

Figure 6.9. Entanglement entropy in the (ρ, zt_0) for the J_D EBH ($R = 2$) model. Parameters $g_{\text{eff}} N_s = -0.5U$, $N_s = 100$, $J_D = 1.0$, $U = 1$, $z = 4$.

Chapter 7

Discussion

7.1 Exact Diagonalization

The ED results presented in Figs. 6.1-6.3 allows to identify the behaviour of entanglement on each phase of the models.

Fig. 6.1 shows the result for the standard BHM, serving as a reference for the rest of the EBHM's, as the behaviour is theoretically understood (see Chapter) 4. Both f_{cond} and S_A exhibit the expected behaviour for the MI-SF transition, starting at zero for the MI phase and growing as the fluctuations Δn_i increase, reaching the saturation values for the SF. Given that the SF limit is a coherent state with Poisson distribution, the saturation limit for the EE is $S_A^{\text{SF}} = \frac{1}{2}\log_2(e\pi N_s/2)$ (see Chapter 4). For $N_s = 8$ it is $S_A^{\text{SF}} \simeq 2.5$. The transition is soft, with no singularities, consistent with a finite system($N_s = 8$) [14].

The monotonous growth of S_A is a clear signature of the BHM, which is expected to change for the models with long-range interactions mediated by cavities.

J_D model

The Figs. 6.2a and 6.3a show the results for the J_D model for both $g_{\text{eff}} < 0$ (DOL) and $g_{\text{eff}} > 0$ (QOL), respectively. The sign produces distinct qualitative modifications to the EE.

For $g_{\text{eff}} < 0$ (Fig. 6.2a), the maximum light scattering favours configurations with density imbalance, stabilizing to a DW for small t_0/U. In this regime $\mathcal{O}_{\text{DW}}^2$ maximizes and the EE is low. For default, we would get $S_A = 1$ in the DW, because the actual groundstate in this regime is two-degenerate, as there is a translational invariance to the system (see Fig. 7.1), so we need to manually add a perturbative term $\hat{H}_{\text{pert}} = \epsilon\hat{D}$ to the EBHM to break the symmetry, resulting in the expected $S_A = 0$. The DW-SS-SF transition manifests as a peak in S_A, signaling the gapless spectrum for the roton mode in the critical point of the $\mathbb{Z}_2$ transition (SF-SS), adding a significant contribution to the EE, as predicted by Sharma et al. [69].

For Para $g_{\text{eff}} > 0$ (Fig. 6.3a, on the contrary, the behaviour is qualitatively similar to a standard BHM, but the transition is shifted. This is due to the QOL effect:

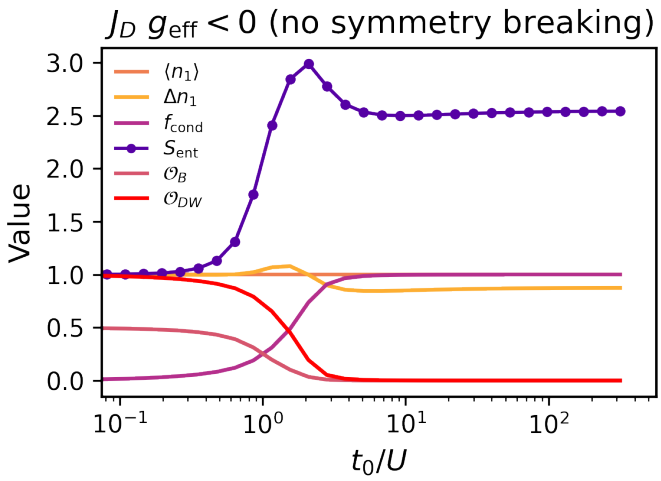

Figure 7.1. ED results for the J_D EBHM with $g_{\text{eff}} < 0$ without adding a perturbative term to break the degeneracy. $J_B = 0$, $g_{\text{eff}} J_D^2 = -4U$ and $N = N_s = 8$.

$U_{\text{eff}} = U + 2g_{\text{eff}}|J_D|^2 > U$, which increases the onsite repulsion. For this sign, the cavity penalizes the density imbalance.

g_{eff} is experimentally tunable through Δ_{pc}, so it allows to produce a desired landscape of entanglement.

J_B model

Analogous results are shown for the J_B model for both $g_{\text{eff}} < 0$ and $g_{\text{eff}} > 0$ in Figs. 6.2b and 6.3b.

For $g_{\text{eff}} < 0$ (DOL) (Fig. 6.2b) , we see the most distinctive behaviour of the EBHM's studied here. The EE remains constant until a critical point is reached and presents a discontinuous jump to another constant. $\mathcal{O}_B$ (red)and f_{cond} exhibit similar discontinuous jumps, while the fluctuations are barely affected. This is typical of a phase transition of first order. At small t_0/U there's dimerization while being an insulator, a phase known as bond insulator (BI),which, together with a density imbalance ($\mathcal{O}_{DW} \neq 0$) define a BI+DW phase. The bond couplings are responsible for the non-zero constant EE.

For the $g_{\text{eff}} > 0$ (QOL) (Fig. 6.3b)the order parameters indicate a DW-SFD-SF transition, starting at small t_0/U with an insulator with a density imbalance (DW). Then, as t_0/U increases, the Bond order coexist with the increase of f_{cond}, defining the SFD. This point is where we see a peak in the EE, then the Bond order is lost causing a small decrease on the EE. And finally following the expected behaviour for a SF reaching the saturation value.

Mixed models ($J_D + J_B$)

It is possible to include both contributions in a mixed system. The results are presented in Figs. 6.4a and 6.4b.

For $g_{\text{eff}} < 0$ (Fig. 6.4a)the behaviour is, as expected, a mixture of the previous cases. With an insulating BI+DW phase, the EE is constant and relatively high. Then at the transition, the coexistence of $\mathcal{O}_B$, $\mathcal{O}_{DW}$ and the increasing f_{cond} define a SSD/SS phase, hence the peak on the EE. Then the system stabilizes to a SF, so the SF decreases to the saturation value.

Finally, for $g_{\text{eff}} < 0$ (Fig. 6.4b) we observe a similar mixed behaviour, but with a transitional SFD phase (instead of a SSD/SS), due to the penalization of the imbalanced states discussed for this regime.

Its relevant to recognize the limitation of the ED method for small systems. $N_s = 8$ is still insufficient to capture the thermodynamic limit.

7.2 Mean-field and slave bosons approach

The entanglement entropy for the J_D model was shown in Fig. 6.8. In order to inspect its behaviour in more detail, we can consider cuts at fixed values of μ, chosen to follow characteristic paths crossings the lobes of the MF diagram.

According to the MF theory for the BHM (see Section 5.2), the critical point occurring at the Mott lobe tips, in terms of the density, is given by

$$\left(\frac{U}{zt}\right)_c = 2\rho + 1 + 2\sqrt{\rho(\rho+1)} \tag{7.1}$$

For $\rho = 1$ this gives $(zt/U)_c \simeq 0.172$. If we inspect the cut $\mu = \sqrt{2} - 1 \simeq 0.41$, shown in Fig. 7.2, corresponding to crossinf the MI(1) lobe, we see the parameters $\Sigma\psi$ and S in agreement with this prediction. The EE indicate maximum fluctuations at the MI-SF transition.

Another relevant path is obtained by fixing $\mu = 1$, shown in Fig. 7.3, corresponding to the DW lobe. The resulting local MF state for this lobe is one of two degenerate configurations: $|\Psi\rangle_O \otimes |\Psi\rangle_E = |1,2\rangle, |2,1\rangle$. This is reflected in the imbalance $\Delta\rho$. The peak of the EE also lies near $zt_0 \simeq 0.13$, in agreement with the theoretical critical point.

These inspection show that the EE provides a sensitive diagnosis for the quantum phase transitions present for this EBHM. For both MI-SF and DW-SS-SF transitions, the maximum of S coincides with the region where the other order parameters begin to change. This behavior is repeated and consistent along all the phase diagram.

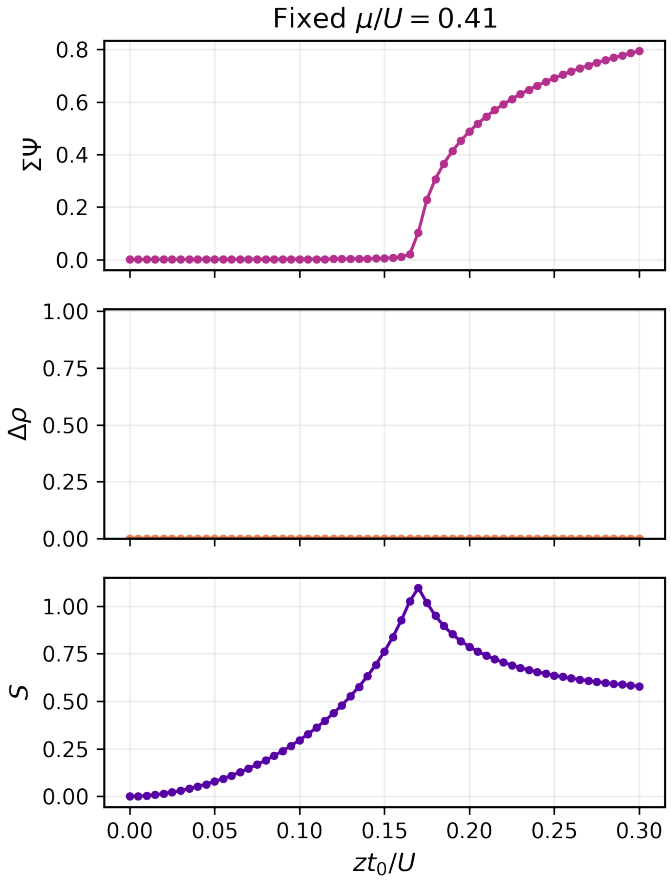

Figure 7.2. Cut of Fig. 6.8 for fixed $\mu = \sqrt{2} - 1$ (First MI lobe). The order parameters $\Sigma\psi$, $\Delta\rho$ and S are compared. Parameters $g_{\text{eff}} N_s = -0.5$, $N_s = 100$, $J_D = 1.0$, $z = 4$.

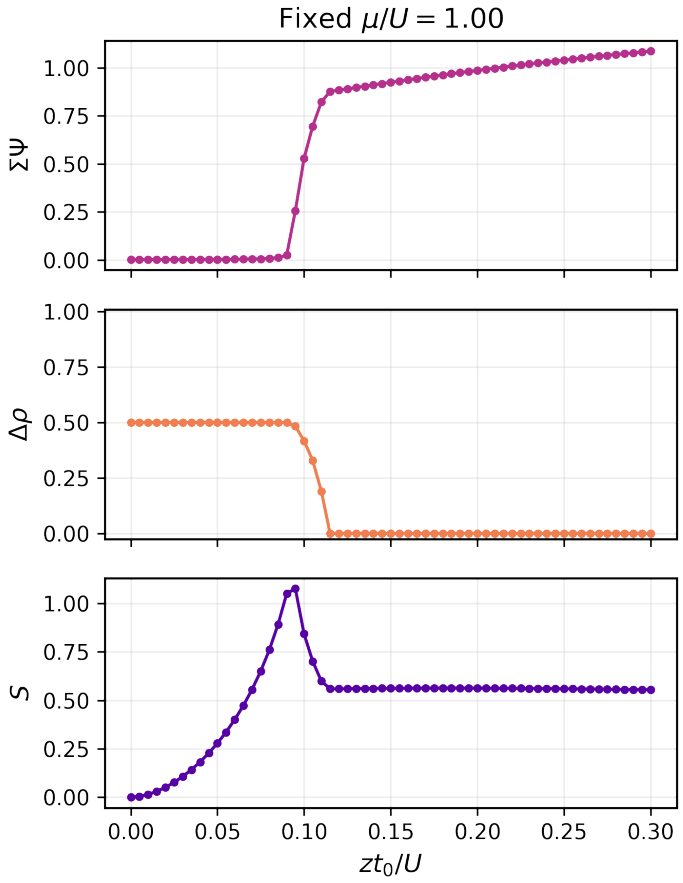

Figure 7.3. Cut of Fig. 6.8 for fixed $\mu = 1$ (First DW lobe). The order parameters $\Sigma\psi$, $\Delta\rho$ and S are compared. Parameters $g_{\text{eff}}N_s = -0.5$, $N_s = 100$, $J_D = 1.0$, $z = 4$.

Chapter 8

Conclusions

In this thesis, we've implemented the slave-boson approach for the EBHM introduced by Caballero-Benitez [45], focusing in the J_D, where the light-induced global interactions become effectively a density coupling producing an even/odd sublattice structure. The implementation followed the methodology proposed by Sharma et al. [69], where the slave-bosons work as a tool to reintroduce the fluctuations using the mean-field solutions.

As a consistency check, the EBHM's were studied both through exact diagonalization and within the mean-field approximation. We've managed to reconstruct their corresponding phase diagrams, all producing results in agreement with the known order parameters previously reported in the literature, giving validation to the numerical and analytical framework developed in this thesis. The main result, the EE calculation for the J_D model, is also consistent with the previous work of Sharma et al.

The bipartite entanglement entropy S_A was shown to be a powerful tool to diagnose the quantum phases and transitions of extended models with global interactions, indicating the location of the transitions and the internal structure of the phases.

The main contribution has been the construction of a unified and practical methodology to treat related models. The cross validation of the results obtained for the J_D model provides confidence to the obtained results for small systems of the J_B, $J_D + J_B$ and multicomponent J_D models, and doing it for a fixed average density ρ using a variational approach to solve the mean-field Hamiltonians (Fig. 8.1). Hence, the natural continuation for this research would be to develop the same formalism for such EBHM's.

Another promising direction for future work is to study the dynamical aspects of this models, specifically under quenches, ramps or time-dependency over the interaction parameters. Previous studies suggest the appearance of hysteresis, metastability or irreversibility behaviour. All this phenomena would therefore be interesting to investigate under the context of entanglement.

Overall, Bose-Hubbard models with light-mediated synthetic long-range interactions present rich phase diagrams, characterizable through their bipartite entanglement entropy using the powerful slave-boson approach around the mean-field

solutions.

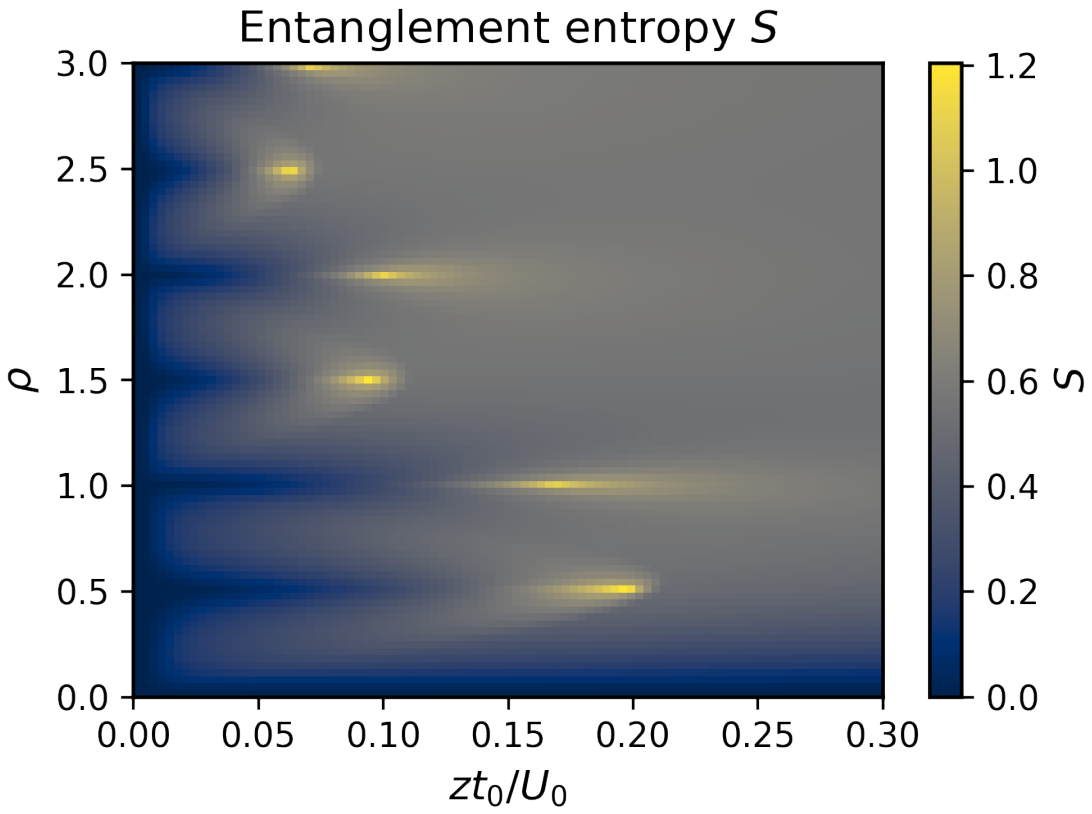

Figure 8.1. Entanglement entropy in the (ρ, zt_0) for the J_D EBH ($R = 2$) model. Parameters $g_{\text{eff}} N_s = -0.5U$, $N_s = 100$, $J_D = 1.0$, $U = 1$, $z = 4$.

Bibliography

[1] J. Hubbard. "Electron Correlations in Narrow Energy Bands". In: *Proceedings of the Royal Society of London Series A* 276.1365 (Nov. 1963), pp. 238–257. DOI: 10.1098/rspa.1963.0204.

[2] D. Jaksch et al. "Cold Bosonic Atoms in Optical Lattices". In: *Phys. Rev. Lett.* 81 (15 Oct. 1998), pp. 3108–3111. DOI: 10.1103/PhysRevLett.81.3108.

[3] Immanuel Bloch, Jean Dalibard, and Wilhelm Zwerger. "Many-body physics with ultracold gases". In: *Rev. Mod. Phys.* 80 (3 July 2008), pp. 885–964. DOI: 10.1103/RevModPhys.80.885.

[4] Maciej Lewenstein et al. "Ultracold atomic gases in optical lattices: mimicking condensed matter physics and beyond". In: *Advances in Physics* 56.2 (2007), pp. 243–379. DOI: 10.1080/00018730701223200.

[5] H. A. Gersch and G. C. Knollman. "Quantum Cell Model for Bosons". In: *Phys. Rev.* 129.2 (Jan. 1963), pp. 959–967. DOI: 10.1103/PhysRev.129.959.

[6] Matthew P. A. Fisher et al. "Boson localization and the superfluid-insulator transition". In: *Phys. Rev. B* 40 (1 July 1989), pp. 546–570. DOI: 10.1103/PhysRevB.40.546.

[7] Oliver Morsch and Markus Oberthaler. "Dynamics of Bose-Einstein condensates in optical lattices". In: *Rev. Mod. Phys.* 78 (1 Feb. 2006), pp. 179–215. DOI: 10.1103/RevModPhys.78.179.

[8] Cheng Chin et al. "Feshbach resonances in ultracold gases". In: *Rev. Mod. Phys.* 82 (2 Apr. 2010), pp. 1225–1286. DOI: 10.1103/RevModPhys.82.1225.

[9] Wilhelm Zwerger. "Mott–Hubbard transition of cold atoms in optical lattices". In: *Journal of Optics B: Quantum and Semiclassical Optics* 5.2 (Apr. 2003), S9. DOI: 10.1088/1464-4266/5/2/352.

[10] B. Capogrosso-Sansone, N. V. Prokof'ev, and B. V. Svistunov. "Phase diagram and thermodynamics of the three-dimensional Bose-Hubbard model". In: *Phys. Rev. B* 75 (13 Apr. 2007), p. 134302. DOI: 10.1103/PhysRevB.75.134302.

[11] Barbara Capogrosso-Sansone et al. "Monte Carlo study of the two-dimensional Bose-Hubbard model". In: *Phys. Rev. A* 77 (1 Jan. 2008), p. 015602. DOI: 10.1103/PhysRevA.77.015602.

[12] K. Sheshadri et al. "Superfluid and Insulating Phases in an Interacting-Boson Model: Mean-Field Theory and the RPA". In: *Europhysics Letters* 22.4 (May 1993), p. 257. DOI: 10.1209/0295-5075/22/4/004.

[13] J. K. Freericks and Mark Jarrell. "Iterated perturbation theory for the attractive Holstein and Hubbard models". In: *Phys. Rev. B* 50 (10 Sept. 1994), pp. 6939–6953. DOI: 10.1103/PhysRevB.50.6939.

[14] S. Sachdev and an O'Reilly Media Company Safari. *Quantum Phase Transitions, Second Edition*. Cambridge University Press, 2011. URL: https://books.google.com.mx/books?id=j7NKzQEACAAJ.

[15] D. van Oosten, P. van der Straten, and H. T. C. Stoof. "Quantum phases in an optical lattice". In: *Phys. Rev. A* 63 (5 Apr. 2001), p. 053601. DOI: 10.1103/PhysRevA.63.053601. URL: https://link.aps.org/doi/10.1103/PhysRevA.63.053601.

[16] M. Greiner et al. "Quantum phase transition from a superfluid to a Mott insulator in an ultracold gas of atoms". In: *Physica B: Condensed Matter* 329-333 (2003). Proceedings of the 23rd International Conference on Low Temperature Physics, pp. 11–12. ISSN: 0921-4526. DOI: https://doi.org/10.1016/S0921-4526(02)01872-0. URL: https://www.sciencedirect.com/science/article/pii/S0921452602018720.

[17] Waseem Bakr et al. "A quantum gas microscope for detecting single atoms in a Hubbard-regime optical lattice". In: 462.7269 (Nov. 2009), pp. 74–77. DOI: 10.1038/nature08482. arXiv: 0908.0174 [cond-mat.quant-gas].

[18] Jacob Sherson et al. "Single-Atom Resolved Fluorescence Imaging of an Atomic Mott Insulator". In: *Nature* 467 (Sept. 2010), pp. 68–72. DOI: 10.1038/nature09378.

[19] André Eckardt. "Colloquium: Atomic quantum gases in periodically driven optical lattices". In: *Rev. Mod. Phys.* 89 (1 Mar. 2017), p. 011004. DOI: 10.1103/RevModPhys.89.011004.

[20] N. Goldman and J. Dalibard. "Periodically Driven Quantum Systems: Effective Hamiltonians and Engineered Gauge Fields". In: *Phys. Rev. X* 4 (3 Sept. 2014), p. 031027. DOI: 10.1103/PhysRevX.4.031027. URL: https://link.aps.org/doi/10.1103/PhysRevX.4.031027.

[21] Artur Widera et al. "Coherent Collisional Spin Dynamics in Optical Lattices". In: *Phys. Rev. Lett.* 95 (19 Nov. 2005), p. 190405. DOI: 10.1103/PhysRevLett.95.190405. URL: https://link.aps.org/doi/10.1103/PhysRevLett.95.190405.

[22] Greiner et al. "Collapse and Revival of the Matter Wave Field of a Bose-Einstein Condensate". In: *Nature* 419 (Sept. 2002), pp. 51–55. DOI: 10.1038/nature00968.

[23] Stefan Kuhr. "Quantum-gas microscopes: a new tool for cold-atom quantum simulators". In: *National Science Review* 3.2 (June 2016), pp. 170–172. ISSN: 2095-5138. DOI: 10.1093/nsr/nww023.

[24] M Endres et al. "Observation of Correlated Particle-Hole Pairs and String Order in Low-Dimensional Mott Insulators". In: *Science (New York, N.Y.)* 334 (Oct. 2011), pp. 200–3. DOI: 10.1126/science.1209284.

[25] Konstantin V. Krutitsky. "Ultracold bosons with short-range interaction in regular optical lattices". In: *Physics Reports* 607 (2016). Ultracold bosons with short-range interaction in regular optical lattices, pp. 1–101. ISSN: 0370-1573. DOI: https://doi.org/10.1016/j.physrep.2015.10.004.

[26] J. K. Freericks and H. Monien. "Strong-coupling expansions for the pure and disordered Bose-Hubbard model". In: *Phys. Rev. B* 53 (5 Feb. 1996), pp. 2691–2700. DOI: 10.1103/PhysRevB.53.2691. URL: https://link.aps.org/doi/10.1103/PhysRevB.53.2691.

[27] N. Elstner and Hartmut Monien. "Dynamics and Thermodynamics of the Bose-Hubbard model". In: *Physical Review B* 59 (July 1998). DOI: 10.1103/PhysRevB.59.12184.

[28] N.V Prokofev, B.V Svistunov, and I.S Tupitsyn. ""Worm" algorithm in quantum Monte Carlo simulations". In: *Physics Letters A* 238.4 (1998), pp. 253–257. ISSN: 0375-9601. DOI: https://doi.org/10.1016/S0375-9601(97)00957-2.

[29] Olav F. Syljuasen and Anders W. Sandvik. "Quantum Monte Carlo with directed loops". In: *Phys. Rev. E* 66 (4 Oct. 2002), p. 046701. DOI: 10.1103/PhysRevE.66.046701.

[30] Jens Kisker and Heiko Rieger. "Bose-glass and Mott-insulator phase in the disordered boson Hubbard model". In: *Phys. Rev. B* 55 (18 May 1997), R11981–R11984. DOI: 10.1103/PhysRevB.55.R11981.

[31] Peter Anders et al. "Dynamical Mean Field Solution of the Bose-Hubbard Model". In: *Phys. Rev. Lett.* 105 (9 Aug. 2010), p. 096402. DOI: 10.1103/PhysRevLett.105.096402.

[32] Steven R. White. "Density matrix formulation for quantum renormalization groups". In: *Phys. Rev. Lett.* 69 (19 Nov. 1992), pp. 2863–2866. DOI: 10.1103/PhysRevLett.69.2863.

[33] Ulrich Schollwöck. "The density-matrix renormalization group in the age of matrix product states". In: *Annals of Physics* 326.1 (2011). January 2011 Special Issue, pp. 96–192. ISSN: 0003-4916. DOI: https://doi.org/10.1016/j.aop.2010.09.012.

[34] A J Daley et al. "Time-dependent density-matrix renormalization-group using adaptive effective Hilbert spaces". In: *Journal of Statistical Mechanics: Theory and Experiment* 2004.04 (Apr. 2004), P04005. DOI: 10.1088/1742-5468/2004/04/P04005.

[35] David Perez-Garcia et al. *PEPS as unique ground states of local Hamiltonians*. 2007. arXiv: 0707.2260 [quant-ph]. URL: https://arxiv.org/abs/0707.2260.

[36] Román Orús. "A practical introduction to tensor networks: Matrix product states and projected entangled pair states". In: *Annals of Physics* 349 (2014),

pp. 117–158. ISSN: 0003-4916. DOI: https://doi.org/10.1016/j.aop.2014.06.013. URL: https://www.sciencedirect.com/science/article/pii/S0003491614001596.

[37] P Buonsante, R Franzosi, and V Penna. "Persistence of mean-field features in the energy spectrum of small arrays of Bose–Einstein condensates". In: *Journal of Physics B: Atomic, Molecular and Optical Physics* 37.7 (Mar. 2004), S229. DOI: 10.1088/0953-4075/37/7/067.

[38] Daisuke Yamamoto, Akiko Masaki, and Ippei Danshita. "Quantum phases of hardcore bosons with long-range interactions on a square lattice". In: *Phys. Rev. B* 86 (5 Sept. 2012), p. 054516. DOI: 10.1103/PhysRevB.86.054516. URL: https://link.aps.org/doi/10.1103/PhysRevB.86.054516.

[39] K. Byczuk. "Dynamical Mean-Field Theory for Correlated Lattice Fermions". In: *Condensed Matter Physics in the Prime of 21st Century: Phenomena*. Ed. by Janusz Jedrzejewski. 2008, pp. 1–33. DOI: 10.1142/9789812709455_0001.

[40] Wen-Jun Hu and Ning-Hua Tong. "Dynamical mean-field theory for the Bose-Hubbard model". In: *Phys. Rev. B* 80 (24 Dec. 2009), p. 245110. DOI: 10.1103/PhysRevB.80.245110. URL: https://link.aps.org/doi/10.1103/PhysRevB.80.245110.

[41] L M Sieberer, M Buchhold, and S Diehl. "Keldysh field theory for driven open quantum systems". In: *Reports on Progress in Physics* 79.9 (Sept. 2016), p. 096001. DOI: 10.1088/0034-4885/79/9/096001. URL: https://doi.org/10.1088/0034-4885/79/9/096001.

[42] Omjyoti Dutta et al. "Non-standard Hubbard models in optical lattices: a review". In: *Reports on Progress in Physics* 78.6 (May 2015), p. 066001. DOI: 10.1088/0034-4885/78/6/066001.

[43] Titas Chanda et al. "Recent progress on quantum simulations of non-standard Bose–Hubbard models". In: *Reports on Progress in Physics* 88.4 (Apr. 2025), p. 044501. DOI: 10.1088/1361-6633/adc3a7.

[44] Igor B. Mekhov, Christoph Maschler, and Helmut Ritsch. "Light scattering from ultracold atoms in optical lattices as an optical probe of quantum statistics". In: *Phys. Rev. A* 76 (5 Nov. 2007), p. 053618. DOI: 10.1103/PhysRevA.76.053618.

[45] Santiago F. Caballero-Benitez, Gabriel Mazzucchi, and Igor B. Mekhov. "Quantum simulators based on the global collective light-matter interaction". In: *Phys. Rev. A* 93 (6 June 2016), p. 063632. DOI: 10.1103/PhysRevA.93.063632. URL: https://link.aps.org/doi/10.1103/PhysRevA.93.063632.

[46] Santiago Caballero-Benitez and I. Mekhov. "Bond Order via Light-Induced Synthetic Many-body Interactions of Ultracold Atoms in Optical Lattices". In: (Apr. 2016). DOI: 10.48550/arXiv.1604.02563.

[47] R. Landig et al. “Quantum phases from competing short- and long-range interactions in an optical lattice”. In: *Nature* 532 (2016), pp. 476–479. DOI: 10.1038/nature17409. URL: https://doi.org/10.1038/nature17409.

[48] Irénée Frérot and Tommaso Roscilde. “Entanglement Entropy across the Superfluid-Insulator Transition: A Signature of Bosonic Criticality”. In: *Phys. Rev. Lett.* 116 (19 May 2016), p. 190401. DOI: 10.1103/PhysRevLett.116.190401. URL: https://link.aps.org/doi/10.1103/PhysRevLett.116.190401.

[49] J. Klinder et al. “Observation of a Superradiant Mott Insulator in the Dicke-Hubbard Model”. In: *Phys. Rev. Lett.* 115 (23 Dec. 2015), p. 230403. DOI: 10.1103/PhysRevLett.115.230403. URL: https://link.aps.org/doi/10.1103/PhysRevLett.115.230403.

[50] Santiago F. Caballero-Benitez and Igor B. Mekhov. “Quantum Optical Lattices for Emergent Many-Body Phases of Ultracold Atoms”. In: *Phys. Rev. Lett.* 115 (24 Dec. 2015), p. 243604. DOI: 10.1103/PhysRevLett.115.243604. URL: https://link.aps.org/doi/10.1103/PhysRevLett.115.243604.

[51] W. Kozlowski, S. F. Caballero-Benitez, and I. B. Mekhov. “Probing matter-field and atom-number correlations in optical lattices by global nondestructive addressing”. In: *Phys. Rev. A* 92 (1 July 2015), p. 013613. DOI: 10.1103/PhysRevA.92.013613. URL: https://link.aps.org/doi/10.1103/PhysRevA.92.013613.

[52] J. Eisert, M. Cramer, and M. B. Plenio. “Colloquium: Area laws for the entanglement entropy”. In: *Rev. Mod. Phys.* 82 (1 Feb. 2010), pp. 277–306. DOI: 10.1103/RevModPhys.82.277. URL: https://link.aps.org/doi/10.1103/RevModPhys.82.277.

[53] A. M. Perelomov. *Generalized coherent states and their applications / A. Perelomov.* eng. Texts and monographs in physics. Berlin ; Springer-Verlag, 1986. ISBN: 0387159126. URL: http://swbplus.bsz-bw.de/bsz012105503cov.htm.

[54] Thierry Giamarchi. *Quantum Physics in One Dimension*. Oxford University Press, Dec. 2003. ISBN: 9780198525004. DOI: 10.1093/acprof:oso/9780198525004.001.0001. URL: https://doi.org/10.1093/acprof:oso/9780198525004.001.0001.

[55] Pasquale Calabrese and John Cardy. “Entanglement entropy and quantum field theory”. In: *Journal of Statistical Mechanics: Theory and Experiment* 2004.06 (June 2004), P06002. DOI: 10.1088/1742-5468/2004/06/P06002. URL: https://doi.org/10.1088/1742-5468/2004/06/P06002.

[56] G. Vidal et al. “Entanglement in Quantum Critical Phenomena”. In: *Phys. Rev. Lett.* 90 (22 June 2003), p. 227902. DOI: 10.1103/PhysRevLett.90.227902. URL: https://link.aps.org/doi/10.1103/PhysRevLett.90.227902.

[57] Massimo Boninsegni and Nikolay V. Prokof’ev. “Colloquium: Supersolids: What and where are they?” In: *Rev. Mod. Phys.* 84 (2 May 2012), pp. 759–776. DOI:

10.1103/RevModPhys.84.759. URL: https://link.aps.org/doi/10.1103/RevModPhys.84.759.

[58] M. Iskin. "Route to supersolidity for the extended Bose-Hubbard model". In: *Phys. Rev. A* 83 (5 May 2011), 051606(R). DOI: 10.1103/PhysRevA.83.051606. URL: https://link.aps.org/doi/10.1103/PhysRevA.83.051606.

[59] V. W. Scarola and S. Das Sarma. "Quantum Phases of the Extended Bose-Hubbard Hamiltonian: Possibility of a Supersolid State of Cold Atoms in Optical Lattices". In: *Phys. Rev. Lett.* 95 (3 July 2005), p. 033003. DOI: 10.1103/PhysRevLett.95.033003.

[60] Peter Fulde and Richard Ferrell. "Superconductivity in a Strong Spin-Exchange Field". In: *Phys. Rev.* 135 (3A Aug. 1964), A550–A563. DOI: 10.1103/PhysRev.135.A550.

[61] Anatoly I. Larkin and Yu. N. Ovchinnikov. "Quasiclassical Method in the Theory of Superconductivity". In: *Journal of Experimental and Theoretical Physics* (1969). URL: https://api.semanticscholar.org/CorpusID:117608877.

[62] I. Mekhov, C. Maschler, and H. Ritsch. "Probing quantum phases of ultracold atoms in optical lattices by transmission spectra in cavity quantum electrodynamics". In: *Nature Physics* 3 (2007), pp. 319–323. DOI: 10.1038/nphys571. URL: https://doi.org/10.1038/nphys571.

[63] Julien Léonard et al. "Supersolid formation in a quantum gas breaking a continuous translational symmetry". In: *Nature* 543 (Mar. 2017), pp. 87–90. DOI: 10.1038/nature21067. URL: https://doi.org/10.1038/nature21067.

[64] J. Stenger et al. "Bragg Spectroscopy of a Bose-Einstein Condensate". In: *Phys. Rev. Lett.* 82 (23 June 1999), pp. 4569–4573. DOI: 10.1103/PhysRevLett.82.4569. URL: https://link.aps.org/doi/10.1103/PhysRevLett.82.4569.

[65] A. Einstein, B. Podolsky, and N. Rosen. "Can Quantum-Mechanical Description of Physical Reality Be Considered Complete?" In: *Phys. Rev.* 47 (10 May 1935), pp. 777–780. DOI: 10.1103/PhysRev.47.777. URL: https://link.aps.org/doi/10.1103/PhysRev.47.777.

[66] E. Schrödinger. "Die gegenwärtige Situation in der Quantenmechanik". In: *Naturwissenschaften* 23 (1935), pp. 807–812. DOI: 10.1007/BF01491891. URL: https://doi.org/10.1007/BF01491891.

[67] Luigi Amico et al. "Entanglement in many-body systems". In: *Rev. Mod. Phys.* 80 (2 May 2008), pp. 517–576. DOI: 10.1103/RevModPhys.80.517. URL: https://link.aps.org/doi/10.1103/RevModPhys.80.517.

[68] Nicolas Laflorencie. "Quantum entanglement in condensed matter systems". In: *Physics Reports* 646 (2016). Quantum entanglement in condensed matter systems, pp. 1–59. ISSN: 0370-1573. DOI: https://doi.org/10.1016/j.physrep.

2016.06.008. URL: https://www.sciencedirect.com/science/article/pii/S0370157316301582.

[69] Shraddha Sharma et al. "Quantum Critical Behavior of Entanglement in Lattice Bosons with Cavity-Mediated Long-Range Interactions". In: *Phys. Rev. Lett.* 129 (14 Sept. 2022), p. 143001. DOI: 10.1103/PhysRevLett.129.143001. URL: https://link.aps.org/doi/10.1103/PhysRevLett.129.143001.

[70] Michael A. Nielsen and Isaac L. Chuang. *Quantum Computation and Quantum Information: 10th Anniversary Edition*. Cambridge University Press, 2010.

[71] Ryszard Horodecki et al. "Quantum entanglement". In: *Rev. Mod. Phys.* 81 (2 June 2009), pp. 865–942. DOI: 10.1103/RevModPhys.81.865. URL: https://link.aps.org/doi/10.1103/RevModPhys.81.865.

[72] Ulrich Schollwock. "The density-matrix renormalization group in the age of matrix product states". In: *Annals of Physics* 326.1 (2011). January 2011 Special Issue, pp. 96–192. ISSN: 0003-4916. DOI: https://doi.org/10.1016/j.aop.2010.09.012. URL: https://www.sciencedirect.com/science/article/pii/S0003491610001752.

[73] C. E. Shannon. "A Mathematical Theory of Communication". In: *Bell System Technical Journal* 27.3 (1948), pp. 379–423. DOI: https://doi.org/10.1002/j.1538-7305.1948.tb01338.x. eprint: https://onlinelibrary.wiley.com/doi/pdf/10.1002/j.1538-7305.1948.tb01338.x.

[74] R. Islam et al. "Measuring entanglement entropy in a quantum many-body system". In: *Nature* 528 (2015), pp. 77–83. DOI: 10.1038/nature15750.

[75] Tiff Brydges et al. "Probing Rényi entanglement entropy via randomized measurements". In: *Science* 364.6437 (2019), pp. 260–263. DOI: 10.1126/science.aau4963.

[76] A. Elben et al. "Rényi Entropies from Random Quenches in Atomic Hubbard and Spin Models". In: *Phys. Rev. Lett.* 120 (5 Feb. 2018), p. 050406. DOI: 10.1103/PhysRevLett.120.050406.

[77] Luca Bombelli et al. "Quantum source of entropy for black holes". In: *Phys. Rev. D* 34 (2 July 1986), pp. 373–383. DOI: 10.1103/PhysRevD.34.373.

[78] Mark Srednicki. "Entropy and area". In: *Phys. Rev. Lett.* 71 (5 Aug. 1993), pp. 666–669. DOI: 10.1103/PhysRevLett.71.666. URL: https://link.aps.org/doi/10.1103/PhysRevLett.71.666.

[79] M B Hastings. "An area law for one-dimensional quantum systems". In: *Journal of Statistical Mechanics: Theory and Experiment* 2007.08 (Aug. 2007), P08024. DOI: 10.1088/1742-5468/2007/08/P08024. URL: https://doi.org/10.1088/1742-5468/2007/08/P08024.

[80] Alexei Kitaev and John Preskill. "Topological Entanglement Entropy". In: *Phys. Rev. Lett.* 96 (11 Mar. 2006), p. 110404. DOI: 10.1103/PhysRevLett.96.110404. URL: https://link.aps.org/doi/10.1103/PhysRevLett.96.110404.

[81] Michael Levin and Xiao-Gang Wen. "Detecting Topological Order in a Ground State Wave Function". In: *Phys. Rev. Lett.* 96 (11 Mar. 2006), p. 110405. DOI: 10.1103/PhysRevLett.96.110405. URL: https://link.aps.org/doi/10.1103/PhysRevLett.96.110405.

[82] X. G. WEN. "TOPOLOGICAL ORDERS IN RIGID STATES". In: *International Journal of Modern Physics B* 04.02 (1990), pp. 239–271. DOI: 10.1142/S0217979290000139. eprint: https://doi.org/10.1142/S0217979290000139. URL: https://doi.org/10.1142/S0217979290000139.

[83] Raymond Fresard. *Slave Boson Formulation for Interacting Boson Systems and the Superfluid-Insulator Transition*. 1994. arXiv: cond-mat/9405053 [cond-mat]. URL: https://arxiv.org/abs/cond-mat/9405053.

[84] Ehud Altman and Assa Auerbach. "Oscillating Superfluidity of Bosons in Optical Lattices". In: *Phys. Rev. Lett.* 89 (25 Dec. 2002), p. 250404. DOI: 10.1103/PhysRevLett.89.250404. URL: https://link.aps.org/doi/10.1103/PhysRevLett.89.250404.

[85] Ingo Peschel and Viktor Eisler. "Reduced density matrices and entanglement entropy in free lattice models". In: *Journal of Physics A: Mathematical and Theoretical* 42.50 (Dec. 2009), p. 504003. DOI: 10.1088/1751-8113/42/50/504003. URL: https://doi.org/10.1088/1751-8113/42/50/504003.

[86] Alonso Botero and Benni Reznik. "Spatial structures and localization of vacuum entanglement in the linear harmonic chain". In: *Phys. Rev. A* 70 (5 Nov. 2004), p. 052329. DOI: 10.1103/PhysRevA.70.052329.

[87] S.R.P.G. Ripka, J.P. Blaizot, and G. Ripka. *Quantum Theory of Finite Systems*. MIT Press, 1986. ISBN: 9780262022149. URL: https://books.google.com.mx/books?id=s_xlQgAACAAJ.

[88] H. Francis Song et al. "Entanglement entropy of the two-dimensional Heisenberg antiferromagnet". In: *Phys. Rev. B* 83 (22 June 2011), p. 224410. DOI: 10.1103/PhysRevB.83.224410. URL: https://link.aps.org/doi/10.1103/PhysRevB.83.224410.